Surface Waxes in Grapevine as Target for Resistance Breeding

Zur Erlangung des akademischen Grades eines

DOKTORS DER NATURWISSENSCHAFTEN

(Dr. rer. nat.)

von der KIT-Fakultät für Chemie und Biowissenschaften

des Karlsruher Instituts für Technologie (KIT)

genehmigte

DISSERTATION

von

Xinshuang Ge

aus

Shandong, China

Dekan: Prof. Dr. Reinhard Fischer

Referent: Prof. Dr. Peter Nick

Korreferent: Prof. Dr. Jörg Kämper

Tag der mündlichen Prüfung: 10.02.2021

Die vorliegende Dissertation wurde am Botanischen Institut des Karlsruhe Instituts für Technologie (KIT), Botanisches Institut, Lehrstuhl 1 für Molekulare Zellbiologie, im Zeitraum von Oktober 2016 bis Januar 2021 angefertigt.

Hiermit erkläre ich, dass ich die vorliegende Dissertation, abgesehen von der Benutzung der angegebenen Hilfsmittel, selbständig verfasst habe.

Alle Stellen, die gemäß Wortlaut oder Inhalt aus anderen Arbeiten entnommen sind, wurden durch Angabe der Quelle als Entlehnungen kenntlich gemacht.

Diese Dissertation liegt in gleicher oder ähnlicher Form keiner anderen Prüfungsbehörde vor.

Zudem erkläre ich, dass ich mich beim Anfertigen dieser Arbeit an die Regeln zur Sicherung guter wissenschaftlicher Praxis des KIT gehalten habe, einschließlich der Abgabe und Archivierung der Primärdaten, und dass die elektronische Version mit der schriftlichen übereinstimmt.

Karlsruhe, im Januar 2021

Xinshuang Ge

Acknowledgments

I would like to express my heartfelt thanks to all the people who help and support me to complete doctoral study in Germany.

Firstly, I extend my sincerest gratitude to Prof. Dr. Peter Nick for providing the chance that I could study in botanical institute I and enjoy the life in Germany. And he gives a great deal of constructive suggestions for the project and instructions for doing the scientific research.

I would like to express my sincere appreciation to Prof. Dr. Jörg Kämper for being my co-examiner.

I would like to take this opportunity to express my sincere gratitude to Dr. Birgit Hetzer and Breutmann Gunilla (Max Rubner Institute, Karlsruhe, Germany). We worked together to investigate the surface waxes morphology by cryo-SEM in the European wild grapevine accession and also analyze the phenotypes of transgenic *Arabidopsis* lines.

I would like to thank Dr. Christine Tisch, Dr. Ruth Walter and Dr.rer.nat. Andreas Kortekamp (Dienstleistungszentrum Ländlicher Raum Rheinpfalz, Neustadt, Germany) for providing the chance to finish the experiment of the Powdery Mildew infection in the leaf discs of three genotypes and sharing the data of Powdery Mildew infection severity and frequency in

the plants.

I also would like to thank Patrick Schindele in the botanical institute II for providing the method of *Arabidopsis* transformation and teaching me how to do it properly.

My special thanks to Dr. Michael Riemann as the group leader for discussing together about the molecular biology, providing suggestions and revising my thesis.

Thanks for all the people in botanical institute I. My especial thanks to Sabine Purper, Nadja Wunsch, Ernst Heene Dr. Qiong Liu, Dr. Xiaolu Xu, Dr.Fan Bai, Dr. Peijie Gong, Dr. Ruipu Wang, Dr. Xue Peng, Dr. Gangliang Tang, Dr. Pingyin Guan, Gero Kaeser, Wenjing Shi, Christian Metzger and Xuan Liu from whom I got unselfish help and support.

I also express my sincere thanks to my family and my friends. With their listening and support, I could pass through the hard time.

Finally, I would also thank CSC scholarship for financial support.

Abbreviations

ABC transporters: ATP binding cassette transporters

ACC: Acetyl-CoA carboxylase

BiFC: bimolecular fluorescence complementation

BSTFA-TMCS:

[*N*,*O*-bis(trimethylsilyl)trifluoroacetamide):trimethylchlorosilane

Cryo-SEM: Cryo-scanning electron microscopy

CTAB: cetyltrimethylammonium bromide

DMIs: demethylation inhibiting fungicides

ECR: trans-2, 3-enoyl-CoA reductase

ER: endoplasmic reticulum

FAE: fatty acids elongase

FATB: acyl-ACP thioesterase

FAR: fatty acyl-CoA reductase

FAS: fatty acid synthase

GC/MS: mass spectrometry-gas chromatography

HCD: β-Hydroxy acyl-CoA dehydratase

HR: hypersensitive response

KCR: β-Ketoacyl-CoA reductase

KCS: β-Ketoacyl-CoA synthase

LACS: long-chain-acyl-CoA synthetases

LTPs: lipid transporter proteins

PM*:* plasma membrane

ROS: reactive oxygen species

VLCFAs: very long chain fatty acids

XRD: X-ray powder diffraction

Contents

Acknowledgments ..... **I**

Abbreviations ..... **III**

Contents ..... **V**

Zusammenfassung **1**

Abstract **3**

1. Introduction **5**

1.1 Powdery Mildew, a devastating disease in viticulture 5
1.2 The symptoms of Powdery Mildew 5
1.3 The life cycle of Powdery Mildew 6
1.4 Management of grapevine Powdery Mildew 7
1.5 Wax structures 8
1.6 Wax chemical components 10
1.7 The function of surface waxes in the defense against abiotic and biotic stress 11
1.8 The regulation of plant development by the epicuticular waxes 12
1.9 Wax biosynthesis mechanism in *Arabidopsis* 12
1.9.1 De novo fatty acids synthesis 13
1.9.2 VLCFAs formation in the ER 14
1.9.3 The alkane formation pathway of VLCFAs derivation 14
1.9.4 The alcohol formation pathway of VLCFAs derivation 15
1.10 Wax transport 16
1.10.1 Wax precursors go into the ER 16
1.10.2 Transport from the ER to the PM 16
1.10.3 Wax components through the PM into the apoplast 17
1.10.4 Wax components export from the epidermal cell 17
1.11 MYB30 and MYB 106 function in *Arabidopsis* 18
1.12 Scope of the study 19

2. Materials and methods **21**

2.1 Plant material 21
2.2 Cryo-Scanning electron microscopy analysis (cryo-SEM) 21
2.3 Quantification of wax structures 22
2.4 Inoculation with *Erysiphe necator* 23
2.5 Microscopic analysis and staging of *E. necator* development 24
2.6 Grapevine cell culture 25
2.7 *Arabidopsis* mutants and growth conditions 26
2.8 RNA extraction 27
2.9 cDNA synthesis 27
2.10 Quantitative real-time PCR 28
2.11 Cloning the protein-coding regions of MYB30 and MYB106 in Ke114 and Ke35 28

2.12 Construction of plasmids and establishment of transgenic MYB30 and MYB106 lines 29
2.13 Epidermal wax content analysis 30
2.14 Protein interaction between MYB30 and MYB106 31
2.15 Analysis and cloning the promoter of MYB30 and MYB106 32
2.16 Promoter activity assay 33
3. Results 35
3.1 Different types of surface wax structures depend on genotype and on cell differentiation in *Vitis* 35
3.2 The time course of surface wax formation depends on leaf development 36
3.3 The surface wax pattern in the different clades 38
3.4 The correlations for the different clades in surface wax accumulation 39
3.5 The link between surface wax content and Powdery Mildew susceptibility 41
3.6 The stages of Powdery Mildew spores' development on fully expanded leaves 42
3.7 Abundant surface wax can interfere with appressorium formation 44
3.8 The genotypes of Ke114 and Ke35 are close relationship, though the phenotypes are extremely different 46
3.9 Cloning and sequence analysis of MYB106 and MYB30 in the *V. sylvestris* group of Ke114 and Ke35 48
3.10 Two alleles of MYB106 complement the *Arabidopsis myb106* mutant, not only the wax content, but also the over-branched trichome phenotype 52
3.11 Two alleles of MYB30 complement the defective wax accumulation phenotype of *Arabidopsis myb30* mutant 55
3.12 Expression pattern of two alleles of MYB106 and two alleles of MYB30 in Ke114 and Ke35 58
3.13 Subcellular co-localization of two alleles of MYB106 and two alleles of MYB30 58
3.14 MYB106 interacts with MYB30 to regulate the wax formation in the genotypes Ke114 and Ke35 60
3.15 Plant hormones, light and low temperature may regulate MYB106 and MYB30 expression in the cis-acting regulatory elements analysis 62
3.16 Chitosan regulates the promoter of MYB106 and MYB30 activity 64
4. Discussion 66
4.1 Genetic variation of surface wax morphology and development in *V. sylvestris* 66
4.2 Low wax content genotypes are more susceptible to Powdery Mildew 68
4.3 Abundant surface waxes regulate appressorium formation of Powdery Mildew spores 69
4.4 MYB106 and MYB30 are associated with wax biosynthesis pathway in grapevines 70
4.5 The genes' functions of two alleles of MYB106 and two alleles of MYB30 have less differences, separately 72

4.6 MYB106 is more relatively conserved, compared with MYB30 73
4.7 MYB106 and MYB30 are involved in defense regulation 74
4.8 Conclusion 75
4.9 Outlook 77
Appendix 78
References 101

Zusammenfassung

Rund 80% des europäischen Fungizid-Verbrauchs gehen auf den Weinbau zurück. Es werden mehrere Krankheiten bekämpft, die während des 19tn Jahrhunderts eingeschleppt worden sind, wobei unter denen der Echte Mehltau besonders destruktiv ist (Arnold et al 2005). Aufgrund ihrer Struktur und räumlicher Anordnung, liegt die Vermutung nahe, dass die Wachschicht der pflanzlichen Epidermis Einfluss auf die Infektion durch den Mehltau hat (Collinge 2009; Kunst and Samuels 2003). Es wäre möglich, dass sie die Adhäsion an oder die Penetration der Blattoberfläche durch das Appressorium erschwert oder verhindert (Wenping Qiu 2015). Daher ist es von Interesse herauszufinden, ob resistente Pflanzen Unterschiede in den Wachsanlagerungen aufweisen. Gegebenenfalls wären auch die Mechanismen der Wachs-Biosynthese in unserer Weinreben Sammlung zu untersuchen, um damit Strategien zur Generation von neuen, resistenten Weinreben zu erstellen.

In dieser Arbeit konnten wir in unserer Sammlung von Weinreben, die nahe mit unserem Kultur-Wein verwandt sind, drei distinkte Morphologien des Oberflächen-Waches feststellen: als lange, flügelähnlichen Strukturen, als kleine Wachs-Kristalle und als eine Mischform der beiden vorherigen Formen. Die Bildung und Anlagerung von Wachs ist zwar abhängig vom Alter des Blatts, stabilisiert sich jedoch, vollständig geöffneten Blatt. Es

konnte festgestellt werden, dass die Pflanzen-Linien mit geringerem Wachs-Vorkommen empfänglicher für die Infektion mit Echtem Mehltau sind. Zudem konnte der hohe Wachs-Gehalt der Linie Ke114, mit der Linie Ke34 verglichen, Sporen davon abhalten ein Appressorium zu bilden, sondern in der „aberrant stage“ (ausschließlich Hyphen-Wachstum) zu verharren und somit die Mehltau-Infektion verhindern.

Es wurde für weitere Vergleiche das Paar von Genotypen Ke114 und Ke34 gewählt, da diese Linien sich bezüglich des „SNP polygenetic tree“ sehr ähnlich sind und trotzdem signifikante Unterschiede in der Wax-Morphologie und Mehltau-Resistenz aufweisen. Pflanzen dieser Linien exprimierten die Gene MYB106 und MYB30 unterschiedlich, besonders MYB 106 exprimierten in dem zweiten Blatt. Beide Gene konnten den wachsfreien Phänotyp einer *myb106* und *myb30 Arabidosis* Mutante komplementieren. In den untersuchten Linien interagieren MYB106 und MYB30 miteinander, um die Wachs-Biosynthese zu regulieren. Zudem konnte aufgezeigt werden, dass Chitosan, eine der Hauptkomponenten der pilzlichen Zellwand, die Promoter-Aktivität der Transkriptionsfaktoren MYB106 und MYB30 ändert und so Gen-Expressions Level der Pflanze beeinflusst.

Abstract

Viticulture accounts for around 80% of fungicide use in Europe, a demand which is caused by several diseases that have been introduced in the 19th century, especially Powdery Mildew (Arnold, Schnitzler, Douard, Peter, & Gillet, 2005). Owing to the structure and the location of surface wax (Collinge, 2009; L. Kunst & Samuels, 2003), maybe it can block Powdery Mildew penetrating the surface wax and cuticle as well as the adhesion at the leaf surface (Wenping Qiu, 2015). It is important consequently to find out that if there are distinct resistance to the Powdery Mildew in the grape accessions which have wax accumulation differences. Further wax biosynthesis mechanism needs to be investigated in the grapevine collection. That can provide another strategy to create new varieties.

In this study, there were three types of wax morphologies discerned as long wing-like structure, small wax crystals and occurrence long wax wings with small wax crystals together in the wild ancestor of domesticated grapevine collections. Surface waxes formation and accumulation of the genotypes indicated genetic variation and wax contents stabilized at fully expanded leaves. The relationship between wax content and Powdery Mildew resistance was that varieties with low wax abundance were more susceptible to Powdery Mildew. Moreover, the higher wax accumulation of Ke114 genotype, compared with genotype of Ke35, could prevent the Powdery Mildew spores further generating the appressorium, instead, the

aberrant stage ap*(only hyphae growth) appearance, thus influenced the resistance to Powdery Mildew.

we found one pair of Ke114 and Ke35, which were close to each other according to the SNP polygenetic tree, that they had different wax formation and the resistance to the Powdery Mildew. Further the expression levels of MYB106 and MYB30 were also distinguished in the pair, especially MYB106 expression level in the secondary leaf. Both of them could complement the wax-lack phenotype in *myb106* and *myb30 Arabidopsis* mutant background, respectively. MYB 106 and MYB 30 interacted with each other to regulate the wax biosynthesis in the pair. Furthermore, chitosan, as the main component of fungal cell walls could regulate the promoter activity of MYB 106 and MYB 30, further influenced the genes expression level and regulate the wax biosynthesis in the Ke114 and Ke35.

1. Introduction

1.1 Powdery Mildew, a devastating disease in viticulture

The causal agent of Powdery Mildew on grapevines is the fungus *Erysiphe necator*,which is an obligate biotrophic pathogen (David M. Gadoury, Cadle-Davidson, Wilcox, Dry, Seem, et al., 2012; Qiu, Feechan, & Dry, 2015). The disease comes originally from North America and spreads widely in Europe since the 19th century (Lange, 1996). The European cultivated grapevine (*Vitis vinifera*), compared with American varieties, are much more susceptible to Powdery Mildew, so the disease causes large-scale grapevine production decline and fruit quality reduction, which in turn generate significant economic losses (Ellis, 2008; D. M. Gadoury, Seem, Pearson, & Wilcox, 2001).

1.2 The symptoms of Powdery Mildew

Powdery Mildew could infect almost the whole grapevine green tissues (**Fig. 1-1**). In the early stage of infection, there are some small diffuse round white colonies appearing on the adaxial side of leaves and the surface of berries (Sall, 1982). As infection progressed, the entire leaves and berries are covered with grey colonies, further there appear colonies on the abaxial side of leaves. The infected leaves become stunted, show premature senescence and abscission in late stages of the infection. The berries appear misshapen, cracking, rotting and plants show early fruit drop (David M.

Gadoury, Seem, Ficke, & Wilcox, 2003; Jones et al., 2014).

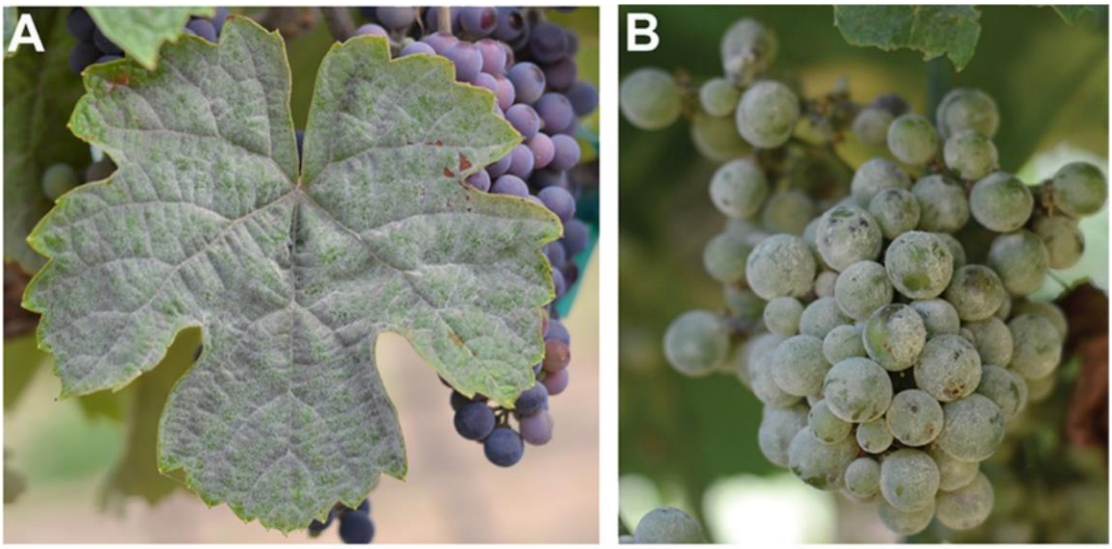

Figure 1-1. The symptoms of Powdery Mildew infected leaf and grape. Figure from (Jones et al., 2014)

1.3 The life cycle of Powdery Mildew

The grapevine leaves and buds are infected by the conidia or ascospores released from the cleistothecia in spring (**Fig. 1-2**). They firstly geminate on the surface of grapevine green tissues and form a specialized infectious structure, the appressorium, to penetrate and invade into the epidermal cells to obtain the nutrients for further development (David M. Gadoury, 1990; Heintz & Blaich, 1990). Then the mycelium covers the entire surface, conidia are generated from the protruding vertically hyphae for propagation after a few warm days. Finally, they start quickly infecting new host tissues through spore distribution by wind. The rapid spread and growth of Powdery Mildew primarily utilize the asexual reproduction cycle. Conidia continuously generate in moderate temperature and a humid environment.

There are two ways for Powdery Mildew to overwinter. The first one is to produce cleistothecia in the late summer (David M. Gadoury, 1990, 1991). They could hang on the bark crevices with hook-shaped ends when they are washed by rains. The other is that the fungus infects the developing buds and overwinter inside. Then they wait for the following spring to propagate (Ellis, 2008; Gemmrich & Seidel, 1996).

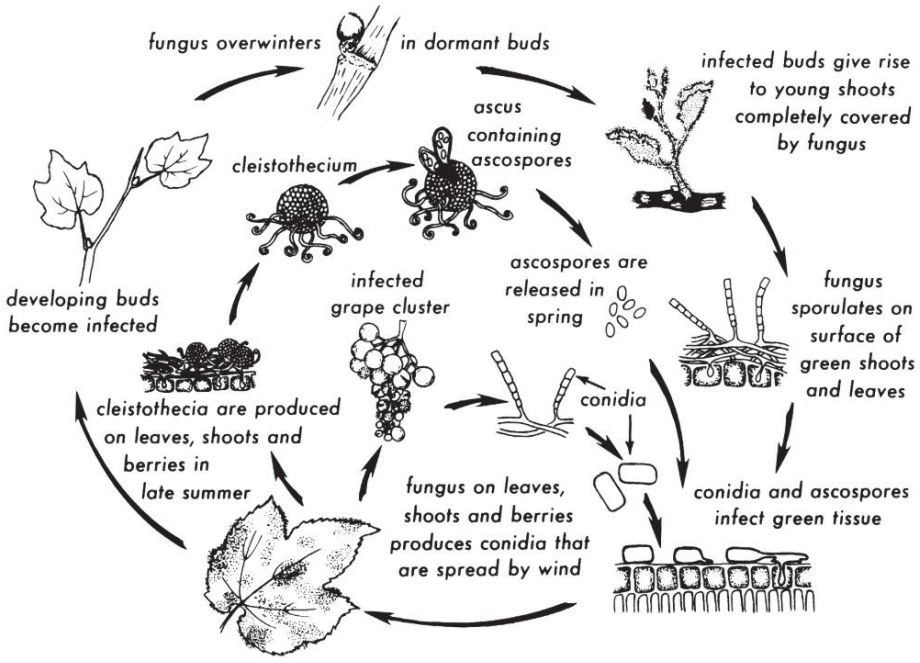

Figure 1-2. The life cycle of Powdery Mildew. Figure from (Ellis, 2008)

1.4 Management of grapevine Powdery Mildew

The selection of resistant grapevine varieties is a reasonable method because the American species are less susceptible to Powdery Mildew (Halleen & Holz, 2017). Further as preventive measures, we can facilitate ventilation and improve the growth conditions by grapevine pruning and training methods (Austin & Wilcox, 2011; Zoecklein, Wolf, Duncan, Judge,

& Cook, 1992). For biological control, mycophagous mites have been investigated that the higher density of them in acarodomatia or leaf domatia, leads to the less Powdery Mildew propagation on foliage and fruits (English-Loeb, Norton, Gadoury, Seem, & Wilcox, 1999, 2007; Norton, English-Loeb, Gadoury, & Seem, 2000). The usage of inorganic fungicides especially sulfur is still common worldwide, because of the effectiveness. For fungicides, the limitations are their impact on environmental pollution and pathogen resistance development (D. M. Gadoury et al., 1994; Russell, 2005). There are some organic fungicides such as sterol demethylation inhibiting fungicides (DMIs) being used, but *Erysiphe necator* has been found to be resistant to these fungicides (Shetty, Narkar, Sawant, & Sawant, 2014).

1.5 Wax structures

Plant surface waxes, as the primary physical plant-environment interaction layers (**Fig. 1-3**), protect the plant tissues from the abiotic and biotic stresses (J. Kim et al., 2013; Lewandowska, Keyl, & Feussner, 2020; X. Wang, Kong, Zhi, & Chang, 2020; Yeats & Rose, 2013).

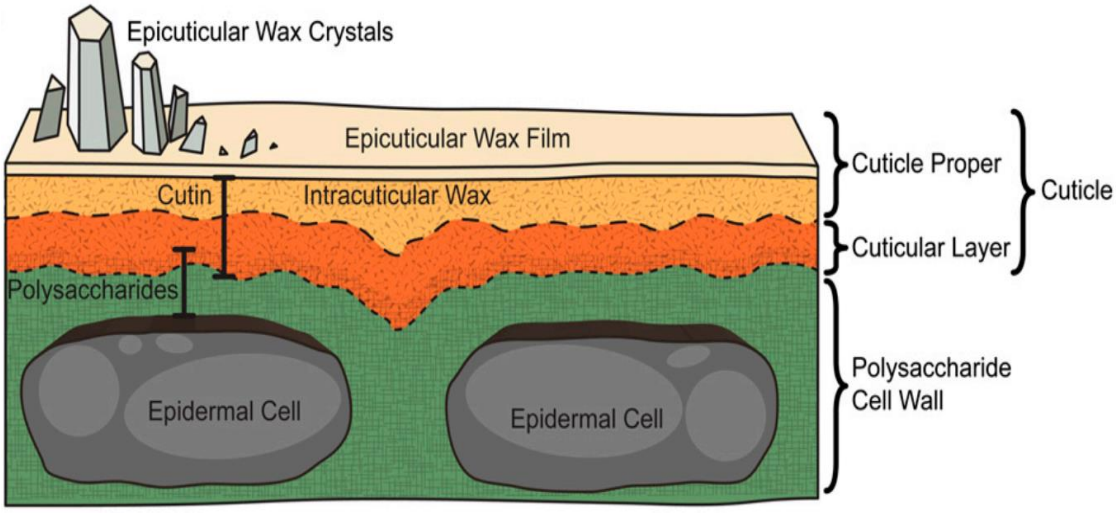

Figure 1-3. Schematic diagram plant epicuticular waxed structures and distribution. Figure from (Yeats & Rose, 2013)

The morphology of epicuticular waxes is microstructural variable. The 3D structures of waxes are filaments, platelets, crystals and tubules (**Figure 1-4**), which have been verifed by different techniques, like scanning electron microscopy (SEM) and X-ray powder diffraction (XRD) and so on (Wilhelm Barthlott et al., 1998; Jetter, Kunst, & Samuels, 2008; Rashotte & Feldmann, 1998). The various surface waxes structures usually result from the crystal self-assembly processes, chemical composition and environmental factors (Jetter, Schäffer, & Riederer, 2000; Koch & Barthlott, 2006; Koch, Neinhuis, Ensikat, & Barthlott, 2004).

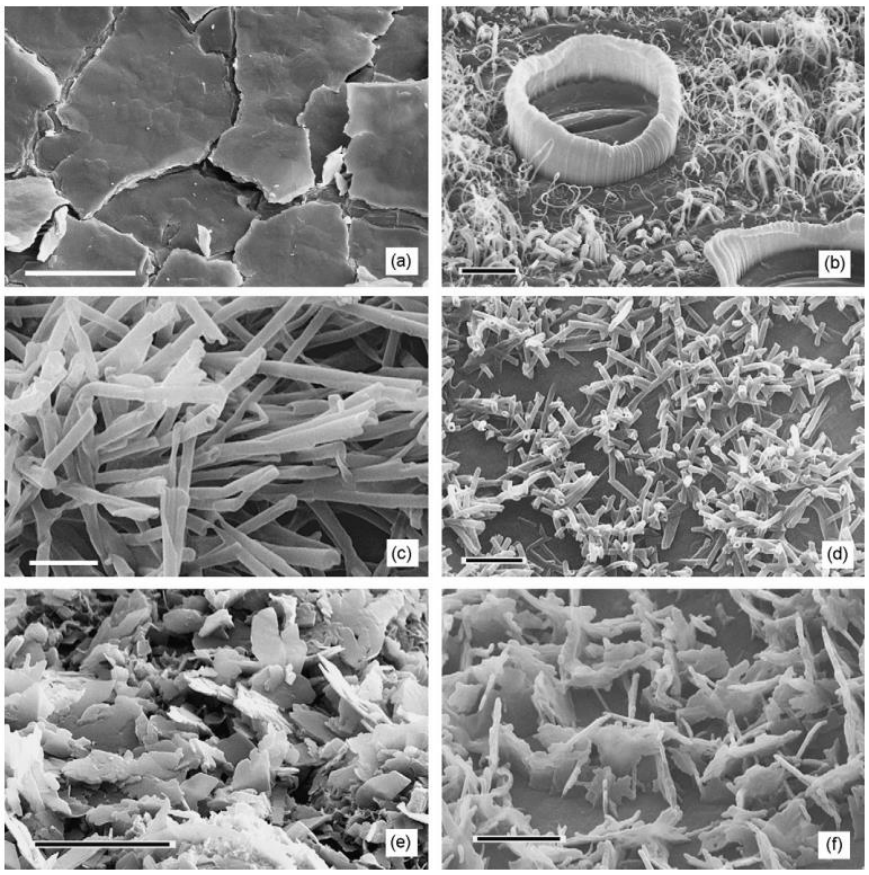

Figure 1-4. Different morphology of epicuticular waxes: **a** the wax crust on *Crassula ovata* **b** wax chineys on *Heliconia collinsiana* **c and d** wax tubes on an *Eucalyptus gunnii* and *Thalictrum flavum glaucum*,separately **e and f** wax platelets on *Aloe porphyrostachys* and *Euphorbia characias* respectively. Figures from (Koch & Ensikat, 2008).

1.6 Wax chemical components

Epicuticular waxes are lipophilic complex mixtures. Because of the hydrophobic property known as Lotus effect (W. Barthlott & Neinhuis, 1997), the components of the wax layer can be extracted with organic solvents like chloroform supplemented with local heating (Schonherr & Riederer, 1989). Further the wax compounds are analyzed by GC/MS (Zeisler-Diehl, Barthlott, & Schreiber, 2018). There are more than 30 plants being investigated with regard to wax components (Sharma, Kothari, Rathore, & Gour, 2018). And the waxes are mainly composed of a series of very-long chain compounds and their derivatives. Among them, the

carbon chain lengths of ketones and secondary alcohols are in majority of an odd-number ,while for primary alcohols, esters and fatty acids, they are mostly even-numbered (Von Wettstein-Knowles, 2018). In addition, there are traces of secondary metabolites like triterpenoids, terpenoids, sterols, and aromatic compounds (Razeq, Kosma, Rowland, & Molina, 2014; E. Wollenweber, Kraut, & Mues, 1998). Although these substances are rare in most species, they appear main wax components in others species, such as flavonoids in ferns and angiosperms (Post-Beittenmiller, 1996; Eckhard Wollenweber, 1978; Eckhard Wollenweber & H. Dietz, 1981).

1.7 The function of surface waxes in the defense against abiotic and biotic stress

The plant surface waxes are protective barriers between the plant and the external environment because of the chemical properties. Several papers have verified that the wax layer can prevent non-stomatal water loss during drought stress (Premachandra, Saneoka, Fujita, & Ogata, 1992; Williams, Rosenqvist, & Buchhave, 2000). Waxes effectively reflect, scatter and absorb harmful light such as high-energy short-wave UV lights (Clark & Lister, 1975; Holmes & Keiller, 2002; S. Wang, Duan, Eneji, & Li, 2007). And the waxes are also efficient barriers to block harmful substances such as organic pesticides (Culberson, Martin, & Juniper, 1971; Sharma et al., 2018).

Moreover, the outside waxes promote water droplet formation because of the superhydrophobic property and self-cleaning ability, which deceases the occurrence of particles and residues on the leaf surface and restricts the attachment and invasion of pathogens (Burton & Bhushan, 2006; Culberson et al., 1971; Jeffree, 2007) . At the same time, the fungal colonization process is also influenced by the wax layer (Leveau, 2018; Marcell & Beattie, 2002). The thickness and compositions of waxes play a role in herbivorous insects for host selection and spawning (Eigenbrode & Espelie, 1995; Moharramipour, Tsumuki, Sato, Murata, & Kanehisa, 1997; Ni, Quisenberry, Siegfried, & Lee, 1998).

1.8 The regulation of plant development by the epicuticular waxes

In addition, the wax development regulates plant growth like leaf expension and flower formation (X. Chen, Goodwin, Boroff, Liu, & Jenks, 2003; Jenks, Rashotte, Tuttle, & Feldmann, 1996; Rhee, Hlousek-Radojcic, Ponsamuel, Liu, & Post-Beittenmiller, 1998). Then the surface wax of pollen is involved in the signal recognition between the pollen and the stigma and regulation of fertility (Millar et al., 1999).

1.9 Wax biosynthesis mechanism in *Arabidopsis*

The wax biosynthesis pathway has been investigated basically clearly in *Arabidopsis* recently through GC/MS, nuclear magnetic resonance, and

isotope tracing techniques (Jenks, Tuttle, Eigenbrode, & Feldmann, 1995; L. Kunst & Samuels, 2003; Lewandowska et al., 2020; McNevin, Woodward, Hannoufa, Feldmann, & Lemieux, 1993). The process of wax synthesis completely occurs in different organelles of epidermal cells, and it is a series of enzymatic reactions coordinated by multienzyme complexes (Davies, 1980; H. U. Kim, 2020; Samuels, Kunst, & Jetter, 2008). The wax snythesis process can be divided into three parts (**Fig. 1-5**).

The first step is the de novo fatty acids synthesis with chain lengths of C16-C18 in the plastid, then they are transported into the endoplasmic reticulum (ER) to process, modify and extend the fatty acid chains, resulting in C26-C34 very long chain fatty acids (VLCFAs). Finally through the alkane and alcohols formation pathway, VLCFAs are metabolically modified to form the main components of surface waxes (Ljerka Kunst & Samuels, 2009; Lee & Suh, 2015; Suh et al., 2005).

1.9.1 De novo fatty acids synthesis

Acetyl CoA, as the precursors in plastid, synthesize malonyl-CoA through the acetyl-CoA carboxylase (ACC) multi-enzyme complex. Malonyl-CoAs are continuously catalyzed and polymerized by the fatty acid synthase system (FAS) till finally C16-C18 fatty acids generation (H. U. Kim, 2020; Mazliak, 1973).

1.9.2 VLCFAs formation in the ER

The extension of the chain lengths is accomplished by the action of the fatty acid elongase complex (FAE), which includes β-ketoacyl-CoA synthase (KCS) (Fiebig et al., 2000; Franke et al., 2009; L Kunst, Taylor, & Underhill, 1992; Todd, Post-Beittenmiller, & Jaworski, 1999), reductase (KCR) (Beaudoin et al., 2009), β-hydroxyacyl-CoA dehydratase (HCD) (Bach et al., 2008; Racovita, Peng, Awakawa, Abe, & Jetter, 2015), and trans-2, 3-enoyl-CoA reductase (ECR) (H. Zheng, Rowland, & Kunst, 2005).The enzyme complex (FAE) uses malonyl-CoAs as substrates to repeat a four steps cycle, further synthesizes C26- C34 VLCFAs (Bernard & Joubès, 2013; Li-Beisson et al., 2013).

1.9.3 The alkane formation pathway of VLCFAs derivation

The VLCFAs derivatives as aldehydes, alkanes, secondary alcohols and ketones are generated in the alkane formation pathway. The substances mostly account for 80%~ 90% of the wax compositions, alkanes relatively highest (Schneider-Belhaddad & Kolattukudy, 2000). CER1, WAX2/CER3 and CYTB5 regulate aldehydes synthesis (Bernard et al., 2012; X. Chen et al., 2003; McNevin et al., 1993). And odd-numbered chain length of alkanes, alcohols and ketones produce by MNH1 removing the carbonyl groups (Greer et al., 2007).

1.9.4 The alcohol formation pathway of VLCFAs derivation

The alcohol formation pathway synthesizes primary alcohols and esters. FAR3/CER4 encodes fatty acyl-coenzyme reductase (FAR) to affect the production of primary alcohols (Hooker, Lam, Zheng, & Kunst, 2007; McNevin et al., 1993). Esters are mainly reguated by WSD1 (F. Li et al., 2008; Metz, Pollard, Anderson, Hayes, & Lassner, 2000; Patwari et al., 2019).

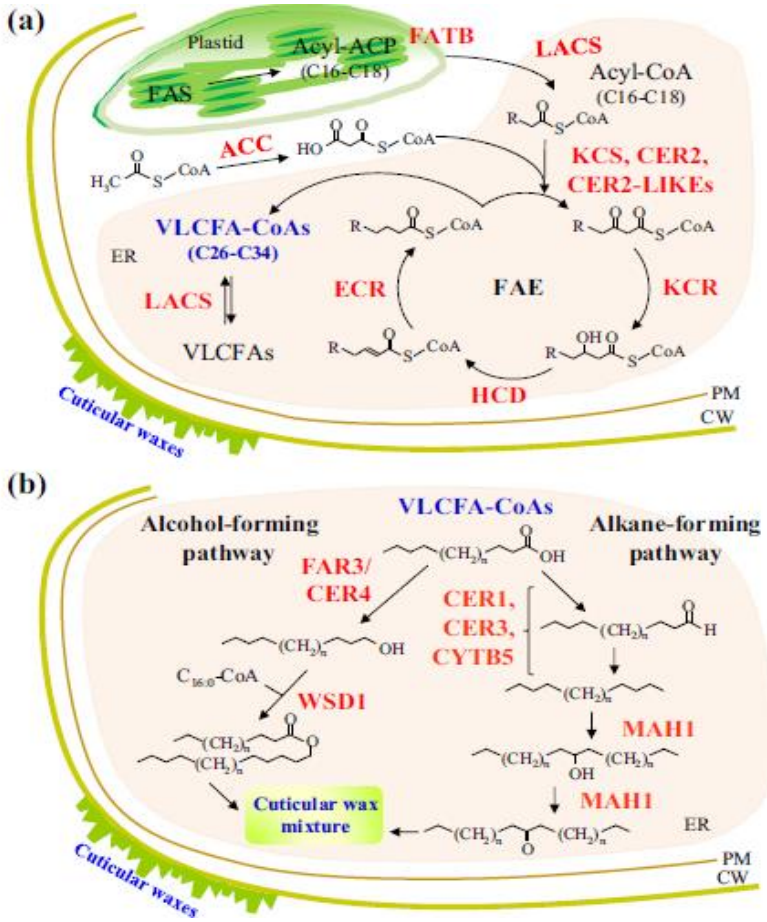

Figure 1-5. Cuticular wax biosynthesis in *Arabidopsis* **a** VLCFA formation **b** VLCFA metabolism. Figures from (Lee & Suh, 2015)

1.10 Wax transport

The waxes are ultimately located outside, however the sites of wax synthesis are in the plastid and ER of epidermal cells. Hence, there are transportation processes of cuticular waxes from synthesis sites to function place (L. Kunst & Samuels, 2003; Ljerka Kunst & Samuels, 2009).

1.10.1 Wax precursors go into the ER

C16-C18 fatty acids are released from the precursors , the C16-C18 acyl-ACPs (**Fig. 1-5**), by thioesterases (FATB) (Bonaventure, Salas, Pollard, & Ohlrogge, 2003; N. Li, Xu, Li-Beisson, & Philippar, 2016; Salas & Ohlrogge, 2002). And they are immediately esterified by LACS (long-chain-acyl-CoA synthetases) to prevent them from being reversed into the plastid, further transfer into ER (Fulda, Shockey, Werber, Wolter, & Heinz, 2002; Shockey, Fulda, & Browse, 2002; Weng, Molina, Shockey, & Browse, 2010).

1.10.2 Transport from the ER to the PM

There are two transport mechanisms to explain the route from the ER to the cell membrane. One is that the ER is directly fused into plasma membrane (Grabski, De Feijter, & Schindler, 1993; Staehelin & Chapman, 1987). The other is to transport wax components through the Golgi vesicles networks (McFarlane et al., 2014; Millar, Wrischer, & Kunst, 1998).

1.10.3 Wax components through the PM into the apoplast

The ABC transporters provide energy by hydrolyzing ATP to help the wax components to pass through the bilayer of PM, when these macromoleculars reach the PM (D. A. Bird, 2008; N. Chen et al., 2018; Lacey Samuels, Mcfarlane, Shin, & Bird, 2010; Pighin et al., 2004). And there are CER5/ABCG12 and WBC11/ABCG11 being distinguished that their location on the plasma membrane could encode the semitransporter of the ABC transporter (D. Bird et al., 2007; Panikashvili et al., 2007) (**Figure 1-6**).

1.10.4 Wax components export from the epidermal cell

The final barrier for wax components is through the hydrophilic plant cell wall. There are some lipid transporter proteins (LTPs) on the plasma membrane that carry macromolecular waxes through the cell wall to the leaf surface, where epicuticular waxes continuously accumulate (DeBono, 2011; Edstam, Blomqvist, Eklöf, Wennergren, & Edqvist, 2013). Ealier studies have shown that both LTPG1 and LTPG2 had substrate specificity, and the absence of both caused a decrease in surface wax content (H. Kim et al., 2012; Lee et al., 2009).

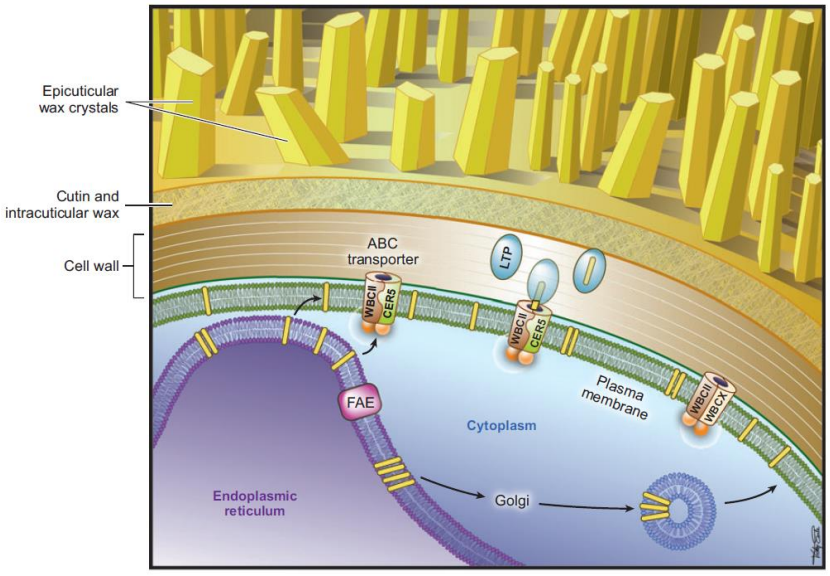

Figure 1-6. A model of wax export from synthesis site to the epidermis. Figure from (Jetter et al., 2008)

1.11 MYB30 and MYB 106 function in *Arabidopsis*

MYB30 and MYB 106, as the positive transcription factors, play a role in transcriptional regulation of *Arabidopsis* wax biosynthesis. MYB30 directly activates genes such as KCS, KCR1, ECR and CER2 in the fatty acyl chains elongation and also influence other genes expression like CER3 and WIN1 (S. R. F. Vailleau et al., 2008).And MYB106 was the postive regulator of WIN1, which could regulate not only the KCS1 and CER2 in the fatty acyl chains elongation, but also the CER1 in the alkane formation pathway (Kannangara et al., 2007; Oshima et al., 2013). Furthermore, MYB30 responds brassinosteroid, abscisic acid and ROS signal activation to enhance *Arabidopsis* defense (L. Li et al., 2009; Mabuchi et al., 2018; Y. Zheng, Schumaker, & Guo, 2012). MYB30 could also regulate root cell elongation and flower development (Liu et al., 2014;

Mabuchi et al., 2018) For MYB106, a role in the regulation of the trichome development in *Arabidopsis* has been described (Jakoby et al., 2008).

1.12 Scope of the study

Powdery Mildew is still one of the worldwide and deleterious disease of grapes and most of European cultivars are extremely susceptible to Powdery Mildew (Brewer & Milgroom, 2010). Fungicides are broadly applied for prevention and treatment of Powdery Mildew (D. M. Gadoury et al., 1994). Viticulture consequently is a fungicide-consuming agricultural system. However, long-term and extensive use of fungicides not only increases production costs and environmental risks, but also is potentially a risk for the development of the fungicide resistance. Therefore, it is urgent to investigate the Powdery Mildew infection mechanism and cultivate new varieties. Because Powdery Mildew produces appressoria to invade grape epidermal cells for propagation, the epicuticular waxes covering the surface of epidermal cells may play a role in preventing the invasion and penetration. The surface waxes of grapevine are still poorly understood. Several questions are thus put forward:

1. What are surface waxes morphology and distribution in the grapevine accession?

2. How do grapevine surface waxes develop and accumulate?

3. What kind of relationship between the surface wax and the resistance to Powdery Mildew?

4. What are the key genes to be involved in the grapevine wax biosynthesis pathway?

5. How do the genes regulate the grapevine wax biosynthesis?

To answer these questions, we have firstly screened 115 ancestor wild grapevine collections to examine the grapevine wax structures under Cryo-SEM, and investigate the mechanism of wax formation and accumulation in the accession. Further the resistance to Powdery Mildew were studied. Moreover, the relationship between the surface wax and the resistance to Powdery Mildew has been analyzed. And the process of Powdery Mildew invasion has been discussed preliminarily.

Furthermore, one pair of wild grapes, Ke114 and Ke35, were selected as the materials to uncover the grapevine wax biosynthesis mechanism, according to the SNP polygenic tree. The master regulators of wax biosynthesis, MYB106 and MYB30, were chosen to investigate the expression pattern in the pair and further to reveal the gene function in grapevine wax biosynthesis mechanism. Chitosan was used as an elicitor to check if it could regulate the promoter activity of MYB106 and MYB30, further to regulate the grapevine wax accumulation in the study.

2. Materials and methods

2.1 Plant material

This study was conducted using the germplasm collection established in the Botanical Garden of the Karlsruhe Institute of Technology, and comprised 102 genotypes, mainly from the last viable German population for *Vitis vinifera ssp. sylvestris* at Ketsch peninsula in an alluvial forest at the banks of the Rhine river between Karlsruhe and Mannheim along with a few residual individuals from other sites of the Upper Rhine valley. In addition, 8 *V. vinifera ssp. vinifera* varieties were included into the study that are either common in German and French vineyards, along with 5 traditional landraces from Central Europe, Tunisia, and Tenerife (Canary Archipelago). The majority of these genotypes have been fully sequenced (Liang et al., 2019), and their phylogenetic relationships assessed based on maximum-likelihood clustering based on genome-wide single-nucleotide polymorphisms, which allows to group the *sylvestris* population into five clades (**Suppl. Fig. S2**). Identity, accession codes, and origin of the individual accessions used in this study are compiled in **Suppl. Table 1.**

2.2 Cryo-Scanning electron microscopy analysis (cryo-SEM)

Small leaf samples of about 5 x 5 mm were excised from freshly harvested leaves and immediately fixed on a plane cryo transfer shuttle with

conductive mounting medium (1:1 mix of Tissue-Tek® O.C.T™ compound and colloidal graphite, Agar Scientific Ltd., Stansted, United Kingdom). Subsequently, they were shock frozen by plunging them into nitrogen slush (ca. -210 °C) and instantly transferred to the cryo chamber (PP2000 T, Quorum Technologies Ltd., Laughton, United Kingdom), which had been pre-cooled to -135 °C. Inside the cryo chamber, the sample was sublimated at -90 °C for 15 mins (K. McDonald, 2007). To minimize charging problems, the samples were sputtered with platinum in an Argon atmosphere (30 s coating at a current of 5-10 mA) and finally transferred to the cryo-stage in the SEM chamber (T = -135 °C). Imaging was carried out with a Quanta 250 FEG field emission scanning electron microscope (FEI, Brno, Czech Republic) under high vacuum (~$3*10^{-7}$ mbar) with an Everhart-Thornley detector, a working distance of 5 mm, and an accelerating voltage of 10 kV (Beckett & Read, 1986; K. L. McDonald, 2009; Wille et al., 2017).

2.3 Quantification of wax structures

The wax structures on the upper surface of grapevine leaves were measured by quantitative image analysis from the digital images obtained by scanning electron microscopy using the freeware ImageJ (https://imagej.nih.gov/ij/). Images were converted into binary images and inverted, such that the wax structures appeared black on a white

background **(Suppl. Fig. S1B)**. These structures were then automatically selected by the Analyze Particle tool based on their size and circularity. To exclude background noise, the minimal level for detection was set to 1 square pixels, to exclude unspecific particles, such as dust on the leaf surface, the maximal level for detection was set to 1000 square pixels. A circularity filter of 0-0.2 was then used to select elongated structures (wax wings and ribs), a circularity filter of 0.2-1 selected rounder structures, such as wax crystals. For each circularity setting, the total area of the selected structures was recorded and set into relation of the total ROI area to estimate the wax coverage. All experiments were measured in 3 biological replications.

2.4 Inoculation with *Erysiphe necator*

For infection with *Erysiphe necator* (the causative agent of Powdery Mildew of Grapevine) a field isolate from a vineyard in Neustadt an der Weinstraße (Palatinate, Germany) was used that has been maintained on the susceptible variety *V. vinifera ssp. vinifera* cv. 'Müller-Thurgau' in the greenhouse of the Dienstleistungszentrum Rheinland-Pfalz (Neustadt an der Weinstraße). The pathogen culture was maintained by placing the recipient plants between heavily infected donor plants.

The fresh, fully expanded leaves from infested plants were collected at the stage of sporulation as source for *E. necator* conidia for controlled

inoculation. Leaf discs were excised from the (fully elongated) sixth leaf for the susceptible *V. vinifera ssp. vinifera* cv. 'Müller-Thurgau', and two representative *V. vinifera ssp. sylvestris* genotypes, Ke35 (belonging to clade C of the Ketsch population) and Ke114 (belonging to clade D of the Ketsch population), and maintained on wet filter paper in plastic Petri dishes (16cm diameter, 10mm height) with the adaxial side up. To simulate natural infection, where the conidia drop from upper to lower leaves, a paper cylinder of 60 cm height was placed on top of the leaf discs, and the infested donor plant was shaken above the cylinder. To prevent the inoculated leaf discs from desiccation, the petri dish was closed and wrapped by Nescofilm. Then the specimen was incubated at 22-24°C in 16 h light/8 h dark. These leaf discs were sampled at 2, 6, 10, 14, 18 and 22 h post inoculation (hpi). Three biological replicates with three individual discs from three different leaves were performed.

2.5 Microscopic analysis and staging of *E. necator* development

The leaf discs were transferred directly abaxial side down on a slide with around 2-3 drops of 0.1% w/v Fluorescent Brightener 28 (Sigma-Aldrich, Deisenhofen, Germany) in 50 mM Tris HCl (pH 9) complemented with 0.1 % v/v Tween 20, and incubated 10-20 mins at room temperature. Excess dye was rinsed off with buffer, and then the specimen was viewed by fluorescence microscopy (Apotome, Zeiss, Jena) after adding sufficient

buffer from side of the cover slip to allow the leaf disc to assume a flat shape. The conidia of per leaf disc were examined using excitation at 450-490 nm, a beam splitter at 515 nm, and a long-pass emission filter >520 nm. Conidia were classified (Rumbolz, Kassemeyer, V Steinmetz, et al., 2000; Welter, Tisch, Kortekamp, Töpfer, & Zyprian, 2017) as illustrated in **Fig. 3-6** into different stages (stage 0, ungerminated spores; stage 1, spores with initiated germ tubes; stage 2, spores which had developed an appressorium; stage 3, spores that had generated a first hypha; stage 4, spores, where a secondary hypha had appeared and stage ap*, spores with aberrant or absent appressorium).

2.6 Grapevine cell culture

Vitis vinifera cv. 'Pinot Noir' and *Vitis vinifera ssp. sylvestris* genotype 'Ke15' as the grapevine cell culture materials were examined in the study. The suspension cells originating from the callus tissue induced by the leaf mesophyll (Seibicke, 2002), were cultured weekly by 8 or 10 mL of mother stock cells into 100 mL Erlenmeyer flask including 30 mL of fresh liquid MS medium, which contained 4.3 $g \cdot L^{-1}$ Murashige and Skoog salts (Duchefa, Haarlem, The Netherlands), 1 $mg \cdot L^{-1}$ thiamine, 100 $mg \cdot L^{-1}$ inositol, 200 $mg \cdot L^{-1}$ KH2PO4, 0.2 $mg \cdot L^{-1}$ 2, 4-dichlorophenoxyacetic acid (2, 4-D) and 30 $g \cdot L^{-1}$sucrose, at pH 5.8. Then they were incubated on a horizontal shaker (KS250 basic, IKA Labortechnik, Staufen, Germany) at

150 rpm in the dark, 27°C.

2.7 *Arabidopsis* mutants and growth conditions

The *Arabidopsis* mutants were purchased from the TAIR website (https://www.Arabidopsis.org/). For the *Arabidopsis myb106* mutant, we used the T-DNA–tagged line SALK_025449 (Alonso et al., 2003; Oshima et al., 2013). And for the *Arabidopsis myb30* mutant, the GABI-KAT T-DNA line 022F04 was chosen for the complementation experiment (Kleinboelting, Huep, Kloetgen, Viehoever, & Weisshaar, 2012; Rosso et al., 2003; S. R. F. Vailleau et al., 2008). Furthermore, the wild type Columbia (Col) was provided by the Botanical Garden of the KIT.

All the *Arabidopsis* seeds were sterilized with 1 mL 4% sodium hypochlorite in an Eppendorf tube, shaking at room temperature for 5 mins. Then they were centrifuged for 30 seconds at 6000 rpm, the supernatant was discarded. Afterwards, they were washed with 1mL ddH_2O for three times and 1 mL ddH_2O was added for overnight stratification at 4 °C in the dark.

The seeds were submerged in 50 mL of 0.1% Agarose-ddH_2O in a 50 mL screw cap tube and discretely sown on solid agar media supplemented with 4.9 $g \cdot L^{-1}$ Murashige and Skoog salts (Duchefa, Haarlem, The Netherlands), 10 $g \cdot L^{-1}$ sucrose at pH 5.7 with or without kanamycin antibiotic, and incubated at 22°C in 16h light /8h dark for two weeks. Then seedlings were transferred into greenhouse for further experiments.

2.8 RNA extraction

The young leaves of *Vitis vinifera ssp. sylvestris* genotypes ‘Ke114’ and ‘Ke35’ were sampled and quickly frozen. Then they were ground by the Tissuelyser (Qiagen, Germany) with a frequency of 18~ 20 Hz for around 1 min. The Spectrum™ Plant Total RNA Kit (Sigma-Aldrich) was used to extract total RNA of the genotypes ‘Ke114’ and ‘Ke35’ according to the manufacturer’s instruction. The total RNA was treated with RNase-Free DNase (Qiagen, Germany) to remove traces of genomic DNA. The purity and quality were checked by the NanoDrop spectrophotometer (Radnor, USA) and electrophoresis.

2.9 cDNA synthesis

RNA was reversely transcribed into cDNA following the two steps methods of reverse transcription by using M-MuLV cDNA synthesis kit (New England Biolabs; Frankfurt am Main, Germany). Firstly, the mixtures with 1 μg of extracted RNA, 2 μL of oligo-dT (40 μM) and 1 μL of dNTP (10mM) were incubated at 70 °C for 5 mins. Then there were added 2 μL 10×RT buffer, 0.5 μL M-MuLV reverse transcriptase (200 U/μL) and 0.5 μL RNase inhibitor (10U/μL) and incubated at 42 °C for 1 hour. By increasing the temperature into 90 °C for 10 mins to finish the cDNA synthesis.

2.10 Quantitative real-time PCR

The mRNA expression levels of selected genes were analyzed by CFX96 Touch™ Real-Time PCR Cycler (Bio-Rad, USA), as previously described (Duan et al., 2015; Guan et al., 2020). The related transcriptional levels were normalized by the averaged Ct values of internal standards, elongation factor 1α and ubiquitin (Svyatyna et al., 2014). The final data statistics were analyzed by the $2^{-\triangle\triangle Ct}$ method (Livak & Schmittgen, 2001).

2.11 Cloning the protein-coding regions of MYB30 and MYB106 in Ke114 and Ke35

The templates for cloning MYB30 (accession number NM001281017) and MYB106 (accession number XM010665048) were cDNAs from the leaves of *Vitis vinifera* ssp. *sylvestris* genotypes 'Ke114' and 'Ke35'. They were amplified by PCR using Phusion High-Fidelity DNA polymerase (NEB, Frankfurt, Germany) and the appropriate primers **(Suppl. table 3)**. Then they were cloned into the pGEM®-T Easy Vector (Promega) and transformed into *E. coli* DH5α for sequence verification (Eurofins Genomics, Germany). The phylogenetic tree was subsequently constructed via the MEGA 7.0 software (https://www.megasoftware.net/) (Kumar, Stecher, & Tamura, 2016), using the neighbor joining method (Felsenstein, 1985; Saitou & Nei, 1987).

2.12 Construction of plasmids and establishment of transgenic MYB30 and MYB106 lines

To obtained the constructs p35S:MYB30-GFP, p35S:MYB106-GFP and p35S:MYB106-RFP, gateway recombination cloning technology was used in the study (Karimi, Inzé, & Depicker, 2002; Nakagawa, Ishiguro, & Kimura, 2009). Firstly, the PCR fragments were cloned into pDONR ™/Zeo vector (Invitrogen Corporation, Paisley, UK) by BP cloning. Then the plasmids were separately transferred into the pH7FWG2.0 and pH7RWG2.0 destination binary vectors by LR cloning. After sequencing verification, these plant expression vectors, containing GFP or RFP reporter genes, were introduced into GV3101 strains of *Agrobacterium tumefaciens* by heat shock transformation method.

The above constructs were transformed into *Arabidopsis* mutants by the floral dip method, as described previously (Clough & Bent, 1998; Logemann, Birkenbihl, Ülker, & Somssich, 2006; X. Zhang, Henriques, Lin, Niu, & Chua, 2006). The overnight growth *Agrobacterium* cultures were centrifuged at 4500 rpm for 15 mins, further resuspended in 800 mL infiltration medium, including 2 g Murashige and Skoog salts (Duchefa, Haarlem, The Netherlands), 40 g Sucrose, 3.4 µL Benzylaminopurine (BAP) (Sigma-Aldrich), 400 µL Silwet L-77(Sigma-Aldrich), and 800 µL Acetosyringone (Sigma-Aldrich), at pH 5.7.

After mixing well, the inflorescences and rosettes of *Arabidopsis* were

inverted and dipped into the cell suspension for 20 seconds with a circular motion. The plants were laid down horizontally on the prepared black box with a plastic cover overnight. Afterwards, the plants were put upright back to the greenhouse and grew normally until collection of the seeds.

2.13 Epidermal wax content analysis

Cuticular wax was extracted from around 6-week-old *Arabidopsis* stems by immersing tissues in chloroform at room temperature for 1 min. Afterwards, the addition docosane was added as an internal standard and the samples were dried under stable streams of N_2 gas. Then the extracted monomers were dissolved into 100 µL of BSTFA-TMCS [*N*,*O*-bis(trimethylsilyl)trifluoroacetamide):trimethylchlorosilane (99 : 1; Sigma-Aldrich)] for 30 mins at around 80-100 °C. The surplus BSTFA-TMCS was subsequently evaporated under N_2 gas. Samples were dissolved in 200 µL hexane before being analyzed by GC/MS (gas chromatography–mass spectrometer).

During gas chromatography, helium was used as the carrier gas (Column flow: 1.5 mL/min and average velocity: 31.97 cm/sec). Injector and detector temperatures were separately set at 300 °C and 310 °C. During the run, temperature was initially set at 160°C for 1 min and increased to 200 °C by 50 °C/min, with a final hold for 1 min. Afterwards, temperature increased again to 310 °C at 4 °C /min, then held for 10 mins. By using an

HP-5 column (30 m x 0.320 mm, 025 μm) and an Agilent 5975 mass spectrometric detector, the qualitative analysis were implemented (Bourdenx et al., 2011; Oshima et al., 2013; S. R. F. Vailleau et al., 2008; W. Wang et al., 2014).

2.14 Protein interaction between MYB30 and MYB106

The BiFC (bimolecular fluorescence complementation) constructs were also generated by the gateway recombination cloning technology (Karimi et al., 2002; Nakagawa et al., 2009) as mentioned. However the destination vectors were pMAV-GW-YC, pMAV-GW-YN, pMAV-YC-GW and pMAV-YN-GW, being derived from the pMAV4 vector (Kircher et al., 1999). All the vectors were provided by Dr. Thomas Kretsch (Stolpe et al., 2005). Further the plasmid of p35S:FABD2-RFP, which localized to actin, was used as the negative control (Klotz & Nick, 2012).

A gold particle bombardment system was performed for transient transformation assay (Maisch, Fierová, Fischer, & Nick, 2009). The split YFP and the RFP negative control constructs (1μg of each plasmids) coated with gold particles (1.5-3.0 μM; Sigma-Aldrich, Germany) were loaded onto microcarriers (Bio-Rad Hercules, CA USA). Then they were shot into three-day-old *Vitis vinifera* cv. ‘Pinot Noir’ cells by three times at pressure 1.5 bar under vacuum (-0.8 bar). Then the cells were incubated in dark overnight prior to fluorescence analysis by using Apotome fluorescence

microscope (Zeiss, Germany). The YFP fluorophores were excited at 524 nm wavelength and emission was detected at 536 nm, and RFP fluorophores were excited at 545 nm, and emission was detected at 572 nm. The pictures were processed by ZEN software (Zeiss, Germany).

2.15 Analysis and cloning the promoter of MYB30 and MYB106

The promoter regions of MYB30 and MYB106 genes were amplified from *Vitis vinifera ssp. sylvestris* genotypes 'Ke114' and 'Ke35' genomic DNAs, which were extracted by a CTAB method with some modifications (Doyle & Doyle, 1987). The ground leaves were mixed with 900 µL 1.5% CTAB (75 mM Tris, 1.05 M NaCl, 15 mM EDTA and 15 $g \cdot L^{-1}$ Cetyltrimethylammonium bromide at pH 8.0),then incubated at 65 °C for 1h. Afterwards, 630 µL Chloroform: isoamyl alcohol solution (24:1) was added and vortexed for 15 mins, then centrifugation for 10 mins at 15,000 rpm. The supernatants were transferred into 2/3 (v/v) ice-cold isopropanol and incubated at -20 °C for 20 mins. The samples were centrifuged for 15 mins at 15,000 rpm, 4 °C. After removing the supernatant, the pallet containing DNA was washed with 1 mL 70% ethanol and centrifuged for 15 mins at 15,000 rpm, 4 °C, with another once 15 mins centrifugation for drying. The genome DNA was ready for the follow experiments after dissolving into nuclease free water.

Then the PCR products were ligated with the pGEM®-T Easy Vector (Promega), and transformed into *E. coli* DH5α. The plasmids were isolated

and analyzed for verification of the sequence (Eurofins Genomics, Germany). The promoter fragments were aligned by the SnapGene software (https://www.snapgene.com/). For the promoter of MYB30, 2834 bp upstream of the start codon in both two genotypes were used. In the MYB106 promoter there were two alleles, which included 3012 bp (named pMYB106-1) and 3015bp (named pMYB106-2) in the two accessions, respectively. Further the putative regulatory elements were investigated using the PlantCARE database (Lescot et al., 2002) (http://bioinformatics.psb.ugent.be/webtools/plantcare/html/).

2.16 Promoter activity assay

For the dual-luciferase assay, the destination vector of pLUC was used to make the constructs MYB30pro: LUC, MYB106-1pro: LUC and MYB106-2pro: LUC by the gateway cloning technology, as mentioned above. The MYB14/pART7 plasmid as effector of STS29pro: LUC was transformed with the reporter as the positive control, which were kindly provided by Prof. Dr. Jochen Bogs (DLR Neustadt). The vectors were bombarded into three-day-old cells of *Vitis vinifera* cv. 'Pinot Noir' and *Vitis vinifera* ssp. *sylvestris* genotype 'Ke15', then they were incubated in two days. Further as the internal standard, 100 ng of a modified Renilla luciferase vector (pRLUC, Promega) was co-bombarded to normalize and calibrate the promoter activities (Czemmel et al., 2009; Duan et al., 2016; Jiao, Xu, Duan, Wang, & Nick, 2016; Oshima et al., 2013).

Twenty-four hours after the bombardment, the transiently transformed cells were treated with chitosan as an elicitor and related solvent (acetic acid) as the control, further incubated another 24 h (El-kenawy, 2017; Portu, López, Baroja, Santamaría, & Garde-Cerdán, 2016). Then they were ground around 1-2 min in 200 μL of 2 × passive lysis buffers (PLB, Promega, Madison, WI) on ice. 20 μL supernatant was separately added 50 μL Beetle juice and 50 μL Renilla Glow Juice (PJK, Kleinbittersdorf, Germany), after centrifugation of 1 min at 10,000 rpm. Firefly luminescence and Renilla luminescence were recorded by Lumat LB9507 luminometer (Berthold Technologies, Bad Wildbad Germany). All experiments were measured in technical triplicates and 4 biological replications.

3. Results

3.1 Different types of surface wax structures depend on genotype and on cell differentiation in *Vitis*.

In order to understand the surface wax morphology in *Vitis.*, 115 grapevine accessions were investigated by cryo-scanning electron microscopy (**Suppl. Table S1**). Surface waxes at adaxial and abaxial sides of fully expanded leaves could be distinguished into three types. The first one was the long wing-like structure (**Fig. 3-1A**). The second type was small wax crystal (**Fig. 3-1B**), The last one was mixed occurrence of long wax wing-like structure and small wax crystal (**Fig. 3-1C**). In addition, cell differentiation had an influence on the distribution of different surface waxes structures. The long wing-like structures were found along the epidermal cells covering leaf veins, but were absent from intercostal regions in the adaxial side (**Fig. 3-1D**). Furthermore, the surface waxes differed between the abaxial side (**Fig. 3-1E**) and the adaxial side (**Fig. 3-1F**). Thus, the different wax structures depended on genotype and on cell differentiation in the grapevine collection.

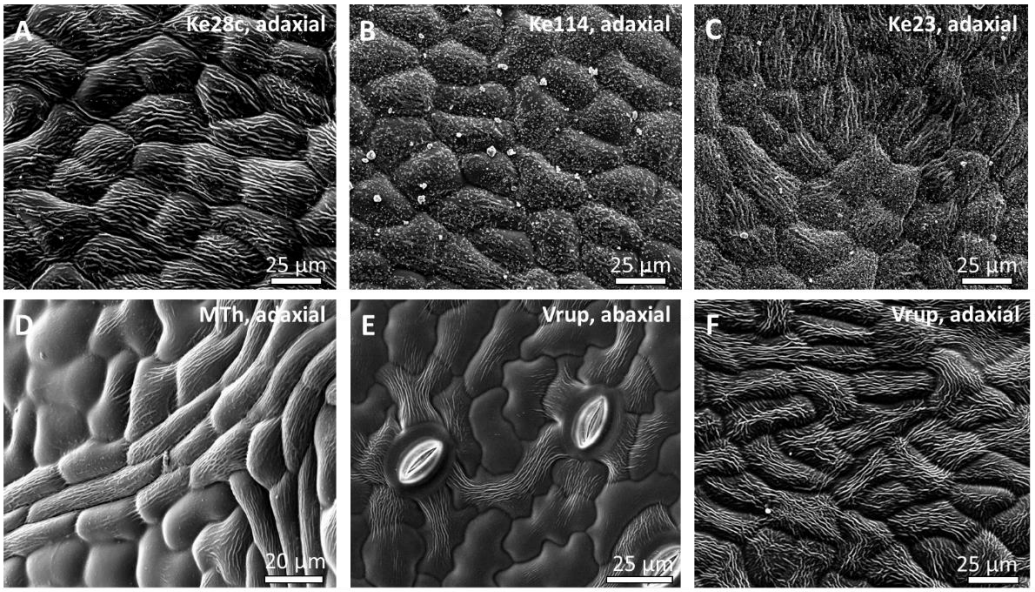

Figure 3-1. Surface-wax structures depend on genotype and on cell differentiation in *Vitis*. Representative images obtained by cryo-scanning electron microscopy from fully expanded leaves. **A-C** Different structures of surface waxes from intercostal regions at the adaxial side to illustrate different structures of surface waxes, such as **A** long wax wings in *V. sylvestris* Ke28c, **B** small wax crystals in *V. sylvestris* Ke114, **C** mixed occurrence of long wax wings and small wax crystals in *V. sylvestris* Ke23. **D-F** Cell type differences of surface waxes. **D** Long wax wings are found along the epidermal cells covering leaf veins, but are absent from intercostal regions in the adaxial side in *V. vinifera* cv. 'Müller-Thurgau'. E, F Surface waxes differ between the abaxial (**E**) and the adaxial (**F**) side in *V. rupestris*.

3.2 The time course of surface wax formation depends on leaf development

Further the surface wax formation has been explored from the shoot axis to the base in different accessions. As the representative samples, the surface wax generated from the second leaf position from the apex in *V. sylvestris* Ke35 (**Figs. 3-2B, E**) and Ke114 (**Figs. 3-2G, J**). However, the wax abundance of the second leaf has already shown differences between the two genotypes. Further there were more waxes in the young leaves of *V. sylvestris* Ke114 and surface waxes were gradually stable and slow accumulation in the subsequent leaf stages (**Figs. 3-2G, J**). However, for

V. sylvestris Ke35, the wax abundance was not protruding in the early leaf stages and as the leaf development, wax accumulation gradually increased (**Figs. 3-2B, E**). Then we could say that the surface waxes accumulated with the leaf expansion and development (**Fig. 3-2**).

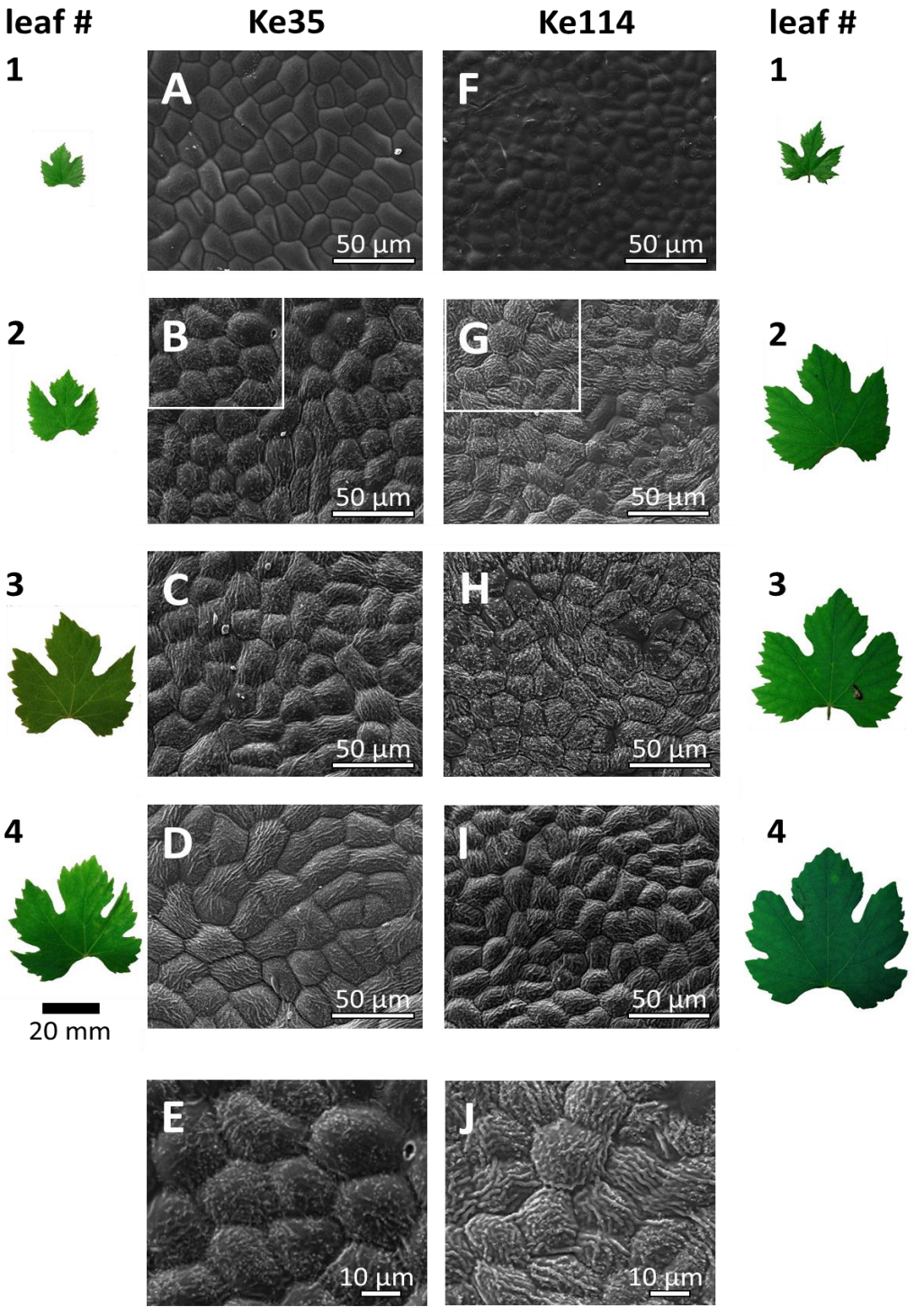

Figure 3-2. Surface-wax formation depends on leaf development. Representative images obtained by cryo-scanning electron microscopy from the adaxial surface of leaves at different position from the apex in *V. sylvestris* Ke35 (**A-E**) versus Ke114 (**F-J**). Representative specimens of the leaves are shown in parallel to visualize the progress of leaf expansion. Close-ups from leaf #2 (white squares in **B, G**) are shown in **E** and **J** to show the different abundance of wax wings between the two genotypes.

3.3 The surface wax pattern in the different clades

In order to better understand the surface wax development, sixty representative genotypes were separated into five sylvestris clades, defined as A to E, according to the phylogenetic tree of the entire European wild grapevine population (**Suppl. Fig. S2**). Nine representative grapevine genotypes from five clades were picked up and quantified wax abundance by quantitative image analysis to investigate the time course. The screening indicated that there was considerable variation. The surface wax content increased gradually over time, although the accumulation varied in the different genotypes. And the wax abundance was basically stable in the fully expanded leaves. Further compared with the cultivar *V. vinifera* cv. 'Müller-Thurgau', all *sylvestris* genotypes accumulated wax earlier and higher abundance (**Fig. 3-3**). Moreover, the wax development pattern could be quite different even within one clade. For instance, Ke35 started to form waxes from second leaf (**Fig. 3-3B**), while Ke28a, belonging to the same clade, did not produce any significant wax structures till fifth leaf (**Fig. 3-3A**). Further Ke74 genotype started to generate wax in the early leaf stages in the clade A, while Hoe17 started to form wax a little bit late, but accumulated wax very swiftly. And Hoe29 needed a long time to

accumulate waxes (**Fig. 3-3C**).

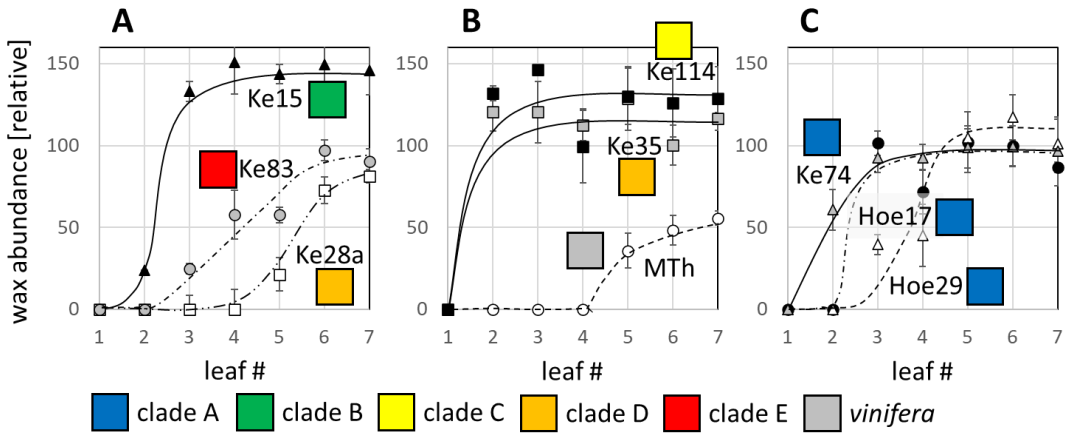

Figure 3-3. Time course of surface-wax formation in representative genotypes from different clades of the *sylvestris* population (as defined in **Suppl. Fig. S2**) along with the *vinifera* variety Müller-Thurgau. Adaxial wax was determined from cryo-SEM images based on quantitative image analysis in subsequent leaves starting from newly formed leaves (#1). Full expansion was achieved from #5. Data represent mean values and SE from 3 individual leaves per data point.

3.4 The correlations for the different clades in surface wax accumulation

Moreover, the surface wax contents of fully expanded leaves were analyzed in the different clades separately. The wax abundance was considerable variation for the genotypes within each clade (**Fig. 3-4A**). For instance, in clade A, genotype Ke110, accumulated waxes more than 6 times than Hoe17. In addition, to test for significant differences, we pooled all 115 genotypes of this study (**Suppl. Table 1**) and ranked them according to the measured wax levels (**Fig. 3-8D**). while the surface wax accumulation of the clade A, C, D, E were not statistically different, clade B had a significantly lower median of rank, which meant, it was definitely

higher in wax accumulation than the others (**Fig. 3-4B**).

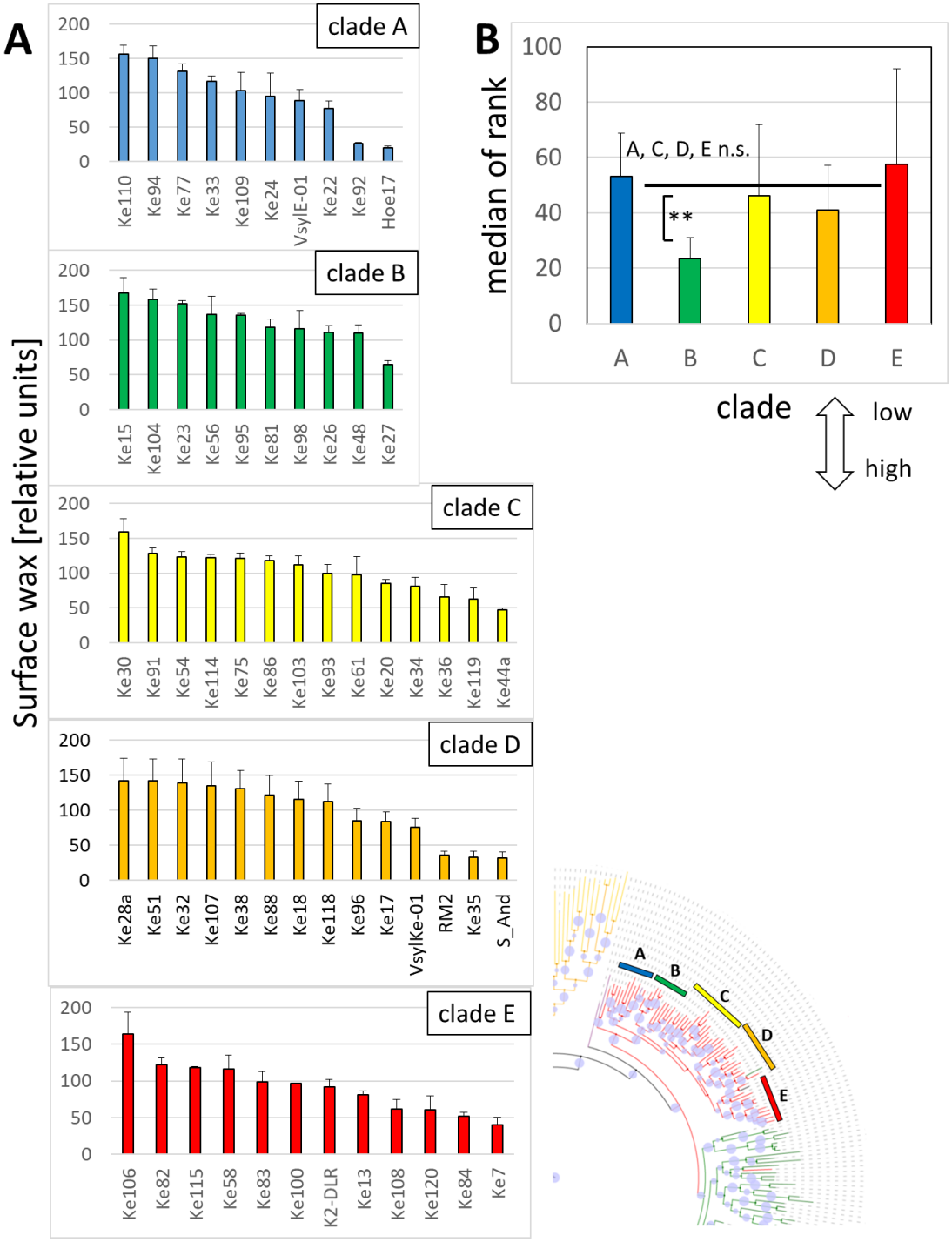

Fig. 3-4. Genetic variability of surface-wax formation within the different clades of the *sylvestris* population (as defined in **Suppl. Fig. S2**). The different genotypes were cultivated side by side, summer 2017 in the Botanical Garden of the KIT. Data represent mean values and SE from 3 individual leaves per genotype collected from fully expanded leaves (#6). **A** Wax abundance for the individual genotypes of clades A-E. **B** clade differences in wax accumulation. All genotypes were pooled and ranked with respect to their wax accumulation. Data represent median and quartiles for each clade. Note that the median for clade B is significantly ($P < 1\%$) lower as compared to the

other clades based on a non-parametrical Kruskal-Wallis test meaning that clade B overall accumulates more wax than the other clades.

3.5 The link between surface wax content and Powdery Mildew susceptibility

During the process of Powdery Mildew infection, spores penetrate and invade into the host cells by specialized infectious structure called appressorium. The successful invasion depended on the interaction with the leaf surface (Armijo et al., 2016; David M. Gadoury, Cadle-Davidson, Wilcox, Dry, See, et al., 2012; Qiu et al., 2015; Rumbolz, Kassemeyer, Steinmetz, et al., 2000). Therefore, we have assumed that the surface wax abundance may have a relationship with the infection process of Powdery Mildew. To verify the hypothesis, Powdery Mildew susceptibility of the representative grapevine genotypes were studied by Dr. Christine Tisch (Tisch, 2017). Then we ranked a set of 83 genotypes according to Powdery Mildew susceptibility **(Suppl. Fig. S4)**. Low numbers represented a high degree of resistance, high numbers a high degree of susceptibility. Then we plotted the ranks obtained for symptom of Powdery Mildew susceptibility over those obtained for wax abundance (**Fig. 3-5A**). Up to rank 70 for wax abundance, susceptibility was unchanged and relatively low. However, above this threshold, an increase in the rank for wax abundance was accompanied by a concomitant increase of susceptibility, which meant that as long as a certain wax abundance was maintained, the Powdery Mildew susceptibility was constantly low, but when wax abundance was below the

threshold, this strongly increased the Powdery Mildew infection (**Fig. 3-5A**).

Afterwards, the Powdery Mildew susceptibility was dissected in the different clades. The five clades were not significantly different, except clade E, which was significantly more susceptible (**Fig. 3-5B**). The clade B, which in average had more wax (**Fig. 3-4B**) than the other clades, was not more resistant because of this. It was consistent with **Fig. 3-5A** that susceptibility went up only when the wax layer was below a certain threshold.

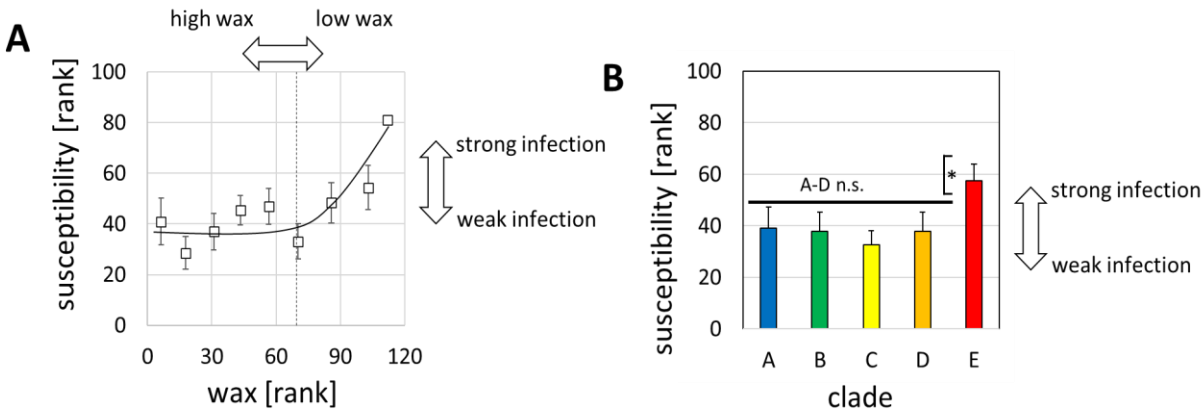

Figure 3-5. Relationship between susceptibility to Powdery Mildew and abundance of surface waxes in the *sylvestris* population. **A** Susceptibility over wax abundance using a ranking system (susceptibility was scored by a bonitation system, therefore, a non-parametrical approach was used to probe for correlations). For each genotype, the rank in susceptibility (increasing numbers mean increasing susceptibility) and wax abundance (increasing numbers mean decreasing wax abundance) were determined and plotted. Data represent median and quartile values from pools of ten genotypes following in the ranking list for wax abundance. **B** Susceptibility of the different clades of the *sylvestris* population (as defined in **Suppl. Fig. S2**). Data represent median and quartiles for susceptibility of all genotypes belonging to the respective clade. * significance at $P<0.05$ based on a non-parametrical Kruskal-Wallice test.

3.6 The stages of Powdery Mildew spores' development on fully expanded leaves

To better understand the process of Powdery Mildew infection, the spore's

development system was analyzed (Delp, 1954; Leinhos, Randall E. Gold, Düggelin, & Guggenheim, 1997; Rumbolz, Kassemeyer, V Steinmetz, et al., 2000). The spores' growth system was separated into five stages on fully expanded leaves of the Müller-Thurgau over time. The stage 0 represented the non-germinated spores (**Fig. 3-6A**). Then the spores began to germinate on the leaf surface, with the germ tube growing out gradually at one side of the spores, which was stage 1 (**Fig. 3-6B**). Shortly thereafter, it became thick at the distal end and formed a specialized infectious structure called appressorium, which was characterized the stage 2 (**Fig. 3-6C**). After the appressorium formation, the primary hyphae usually emerged from the spores at the site different from the appressorium (**Fig. 3-6E**). The secondary hyphae outgrew from the appressorium over time indicated as stage 4 (**Fig. 3-6F**). While the formation of an appressorium was not observed in some spores, instead, an aberrant stage ap* was found, where appressorium was perturbed (**Fig. 3-6D**).

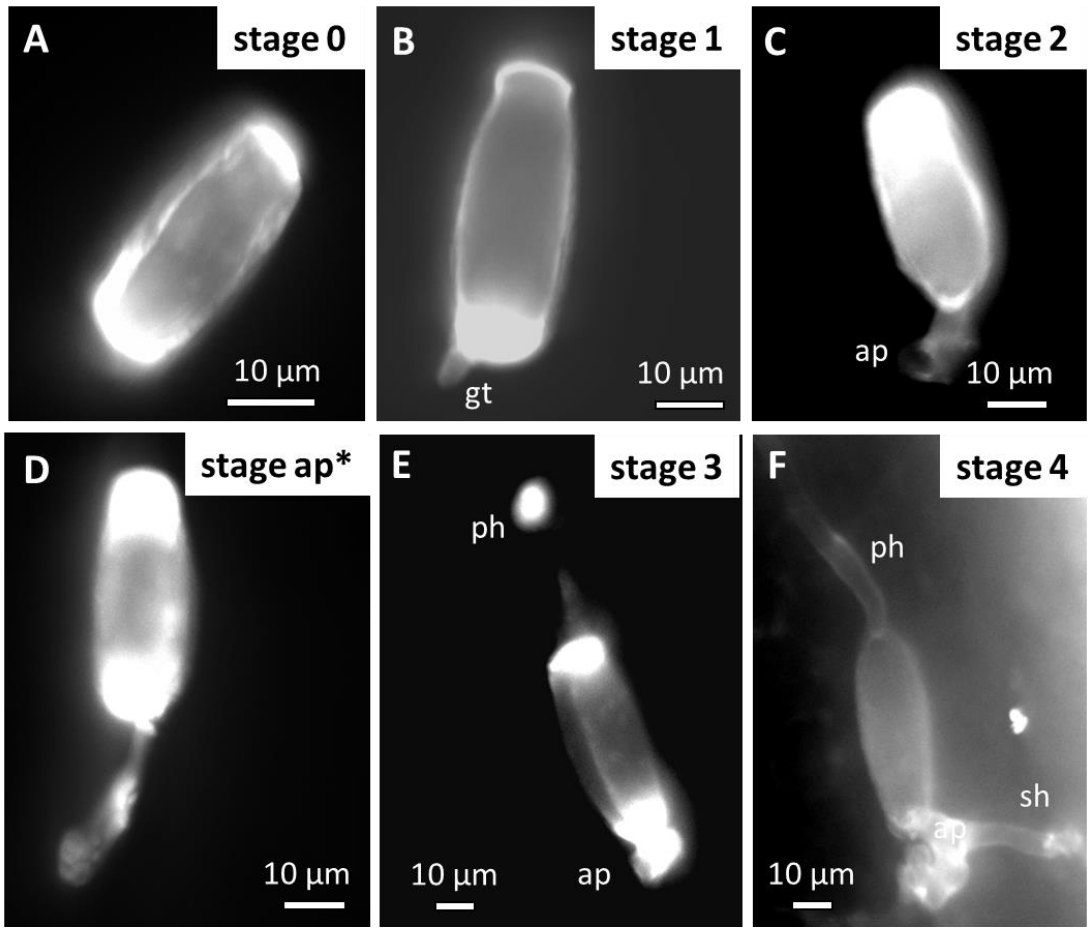

Figure 3-6. Stageing of Powdery Mildew development on fully expanded leaves of *V. sylvestris* assessed by fluorescence microscopy after staining with Fluorescent Brightener 28. **A** Stage 0 (ungerminated spores). **B** Stage 1 characterized by the emergence of a germ tube (gt). **C** Stage 2 characterized by the formation of an appressorium (ap). while the formation of an appressorium was not observed, instead, an aberrant stage ap* **D** was found, where appressorium was perturbed **E** Stage 3 characterized by the outgrowth of a primary hyphae (ph) from the spore at sites different from the appressorium. **F** Stage 4 characterized by the outgrowth of a secondary hyphae (sh) from the appressorium.

3.7 Abundant surface wax can interfere with appressorium formation

As mentioned before, the wax abundance, in a certain threshold, would influence the Powdery Mildew susceptibility of the plant (**Fig. 3-5**). Further how the wax abundance changing the infection process as a question should be solved. Three represented genotypes were chosen to investigate, Müller-Thurgau as control, Ke114 as high wax representative,

Ke35 as low wax representative (**Fig. 3-3B**). The Powdery Mildew spores grew gradually from the germ tube generation (**Fig. 3-6B**) to appressorium formation (**Fig. 3-6C**), further to the hyphae appearance (**Fig. 3-6E**) in all the accessions over time (**Fig. 3-7**). The development of spores in Müller-Thurgau (**Fig. 3-7A**) was much faster than in the other two genotypes with regard to spore germination or spore invasion (**Figs. 3-7B and C**). Hence Müller-Thurgau was also far more sensitive to Powdery Mildew than the other two genotypes. In addition, the spores in stage 2 grew much slower and less in Ke114 (**Fig. 3-7B**) than in Ke35 (**Fig. 3-7C**) over time. While the number of spores in the aberrant stage ap***(Fig. 3-6D),** which represented the spores which hardly generated any appressoria, was much higher in Ke114 than in Ke35 from 10 h to the end. Since the wax abundance of Ke114 was higher than the one of Ke35 (**Fig. 3-3B),** and the appressorium was harder to form, the higher surface wax abundance, in a certain threshold, could prevent the spores further generating the appressorium, instead, the aberrant stage ap* (only hyphae growth) appearance, thus influence the Powdery Mildew susceptibility

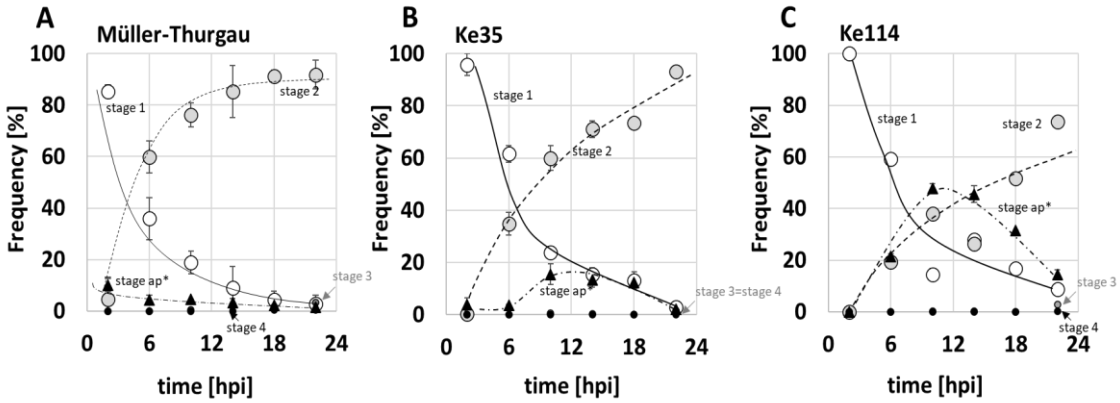

Figure 3-7. Development of Powdery Mildew on leaves of the *V. vinifera* variety Müller-Thurgau (**A**) as compared to the *V. sylvestris* genotypes Ke35 (**B**), and Ke114 (**C**). Frequencies of the different stages as defined in Fig.3-6 have been plotted over time in hours post infection (hpi). Data represent mean and standard errors from three biological replicates conducted in fully expanded leaves (#6). Stage ap* represents the aberrant stage found on *sylvestris* leaves, where appressorium development is affected.

3.8 The genotypes of Ke114 and Ke35 are close relationship, though the phenotypes are extremely different

In order to understand the relationship in the 115 *V. sylvestris* accessions, they were separated into three clades **(Fig. 3-8)**, high wax abundance clade **(Fig. 3-8A)**, medium wax accumulation group **(Fig. 3-8B)** and low wax accumulation subset **(Fig. 3-8C)** according to the surface wax content.

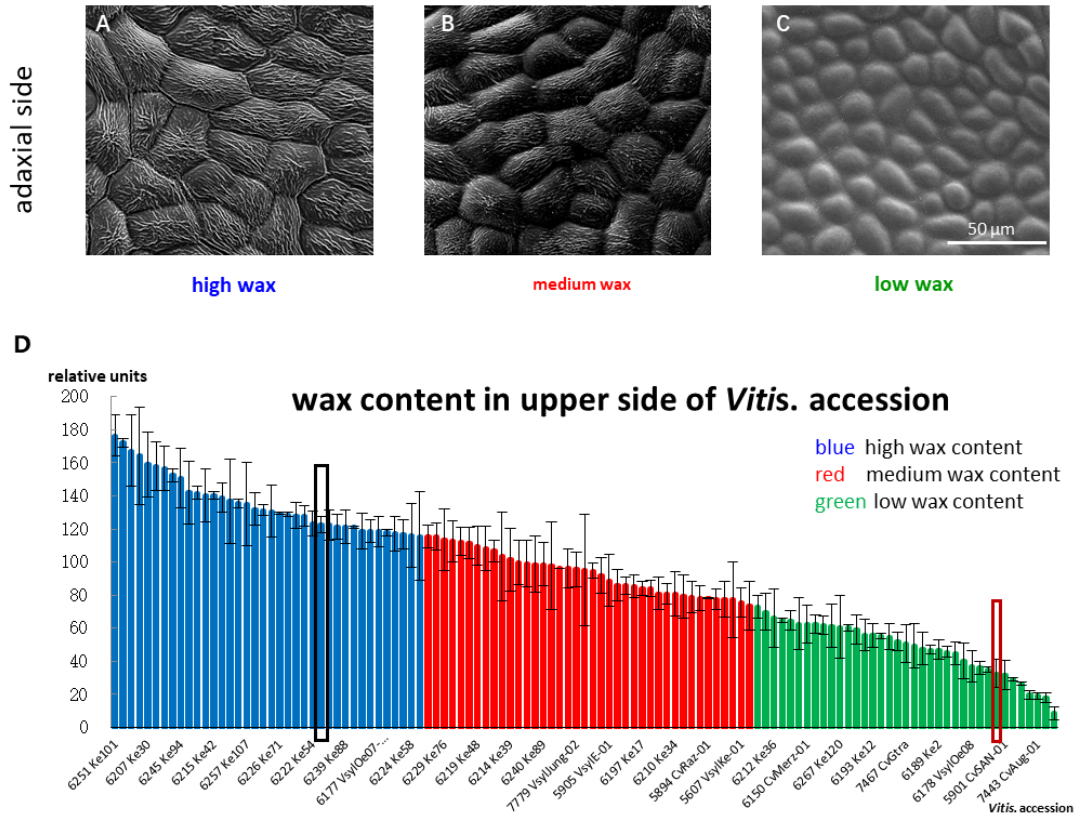

Figure 3-8. Separation the *Vitis.* accessions according to the surface-wax content. **(A-C)** Representative pictures of different surface wax abundance obtained by cryo-SEM. **A** high wax abundance clade in blue color, **B** medium wax accumulation in red color, **C** low wax accumulation subset in green **D** Separation of 115 genotypes into three clusters. Ke114 indicated in black square, Ke35 indicated in red square.

Then the accession was matched into the SNPs polygenic tree **(Fig. 3-9)** which was created by whole genome sequencing (Khattab et al., 2020). The genotypes of Ke114 and Ke35 were genetically close to each other, although the phenotype of wax accumulation was extremely different. Thus, the pair of the genotype Ke114 and Ke35 was selected as the material for all the following experiments.

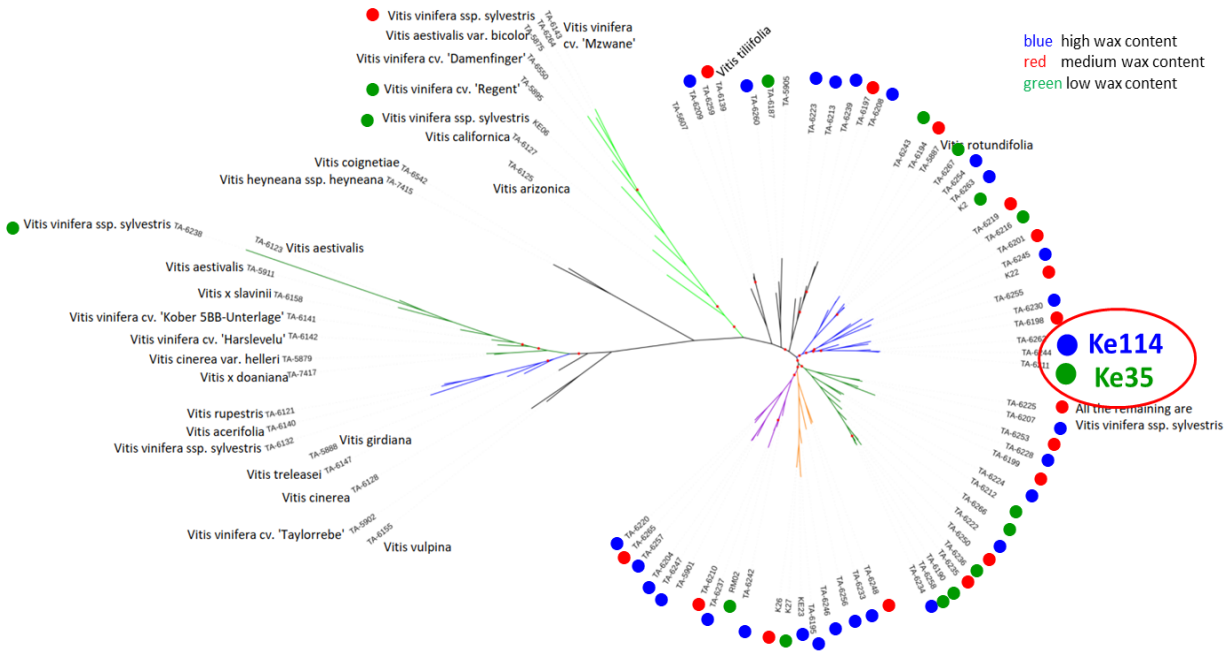

Figure 3-9. Match all different phenotypes of wax content into polygenic tree constructed from genome-wide SNPs for 89 accessions of cultivated *Vitis vinifera* and wild species from Europe, Asia and America (Khattab et al., 2020). Blue circles indicate high wax abundance clade, while red circles mean medium wax accumulation phenotypes, and the green circles are low wax accumulation subset. The highlight position in the tree is the group of Ke114 and Ke35 analysis in the study.

3.9 Cloning and sequence analysis of MYB106 and MYB30 in the *V. sylvestris* group of Ke114 and Ke35

To get further insight into the wax biosynthesis regulation mechanism in Ke114 and Ke35, the transcription factors MYB106 and MYB30 were chosen as targets for further research. This approach was chosen as according to the literature that AtMYB106 (Oshima et al., 2013) and AtMYB30 (S. R. F. Vailleau et al., 2008) are transcription factors, which regulate many genes of *Arabidopsis* wax biosynthesis pathway (Lee & Suh, 2015). A phylogenetic tree was constructed by the Neighbor joining method. Separately for each transcription factor based on homology search

by BLAST in the UniProtKB database using the sequences of *A. thaliana* MYB106 (AT3G01140) and MYB30 (AT3G28910) **(Fig. 3-10)**. From the tree, MYB106 and MYB30 were relatively conserved both in *Arabidopsis thaliana* and *V. vinifera* cv. 'Pinot Noir'. The predicted MYB30 (accession number NM001281017) and MYB106 (accession number XM010665048) were characterized in *Vitis vinifera.* And they were both localized on the 17th chromosome **(Fig. 3-10)**.

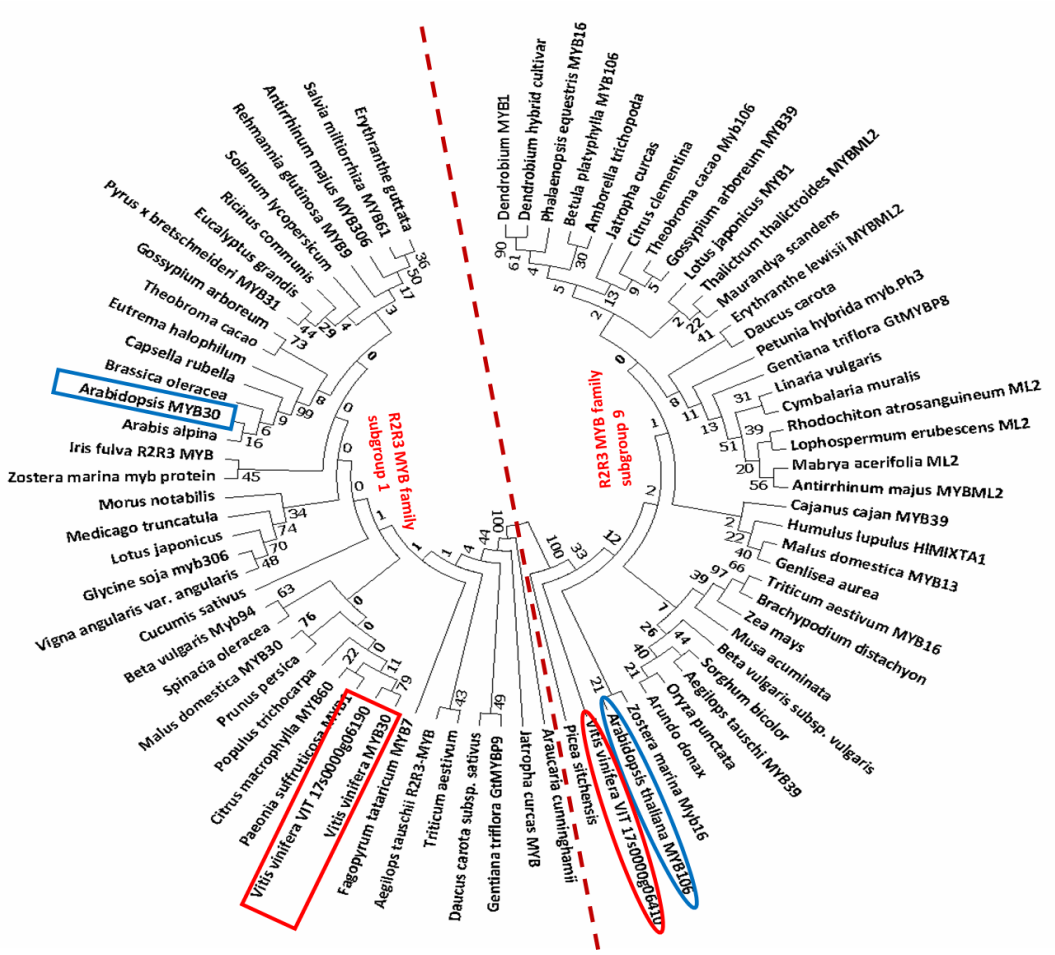

Figure 3-10. Phylogenetic relationship of MYB106 homologs (R2R3 MYB family subgroup 9) in 39 species and MYB30 homologs (R2R3 MYB family subgroup1) in 39 species. The NJ phylogenetic tree was constructed using MEGA7 and 1000 replicates. Values near the branches represent the percentage of replicate trees in which the associated taxa clustered together. The position of predicted MYB106 and predicted MYB 30 sequence from *V. vinifera* cv. 'Pinot Noir' indicated in red circle and red square, respectively. and the MYB106 and MYB 30 sequence from *Arabidopsis thaliana* indicated in blue circle and blue square, separately (Kumar et al., 2016).

Afterwards, the coding sequences of MYB106 and MYB30 in Ke114 and Ke35 were identified, respectively. For MYB106, there were two alleles, named D-MYB106 and S-MYB106 **(Fig. 3-11A and Suppl. Fig. S5)**, both in the Ke114 and Ke35.There were four SNPs in the two types of MYB106. And among them, three SNPs changed amino acids. In the first site, threonine changing into proline (T10P), was near the SANT domain, which had DNA binding function. The mutation in the second site resulted in a change of serine into alanine(S27A), was within the SANT domain. In the last site, phenylalanine was changed into Leucine (F331L). For MYB30, same with MYB106, it was heterozygous both in the Ke114 and Ke35, and two alleles of MYB30 were named D-MYB30 and S-MYB30 **(Fig. 3-11B and Suppl. Fig. S5).** The SNPs in Ke114 and Ke35 caused two different amino acids in the respective position of MYB30. In the P42T site, proline was changed into threonine in the SANT domain. In the other site, valine was changed into alanine(V304A).

The predicted 3D protein structure of the various types of MYB106 and MYB30 are shown in **Fig. 3-11C and D**. The sites of T10P and S27A in MYB106 **(Fig. 3-11C)**, in addition, P42T site in the MYB30 **(Fig. 3-11D)** were in or nearly the DNA binding sequence according to the 3D protein structure model of the template 3zqc.3. Taken together, because of molecular backbone of proline and nucleophilic property of serine, the T10P, S27A and P42T substitution sites maybe play a role in regulation

DNA binding function of MYB106 and MYB30.

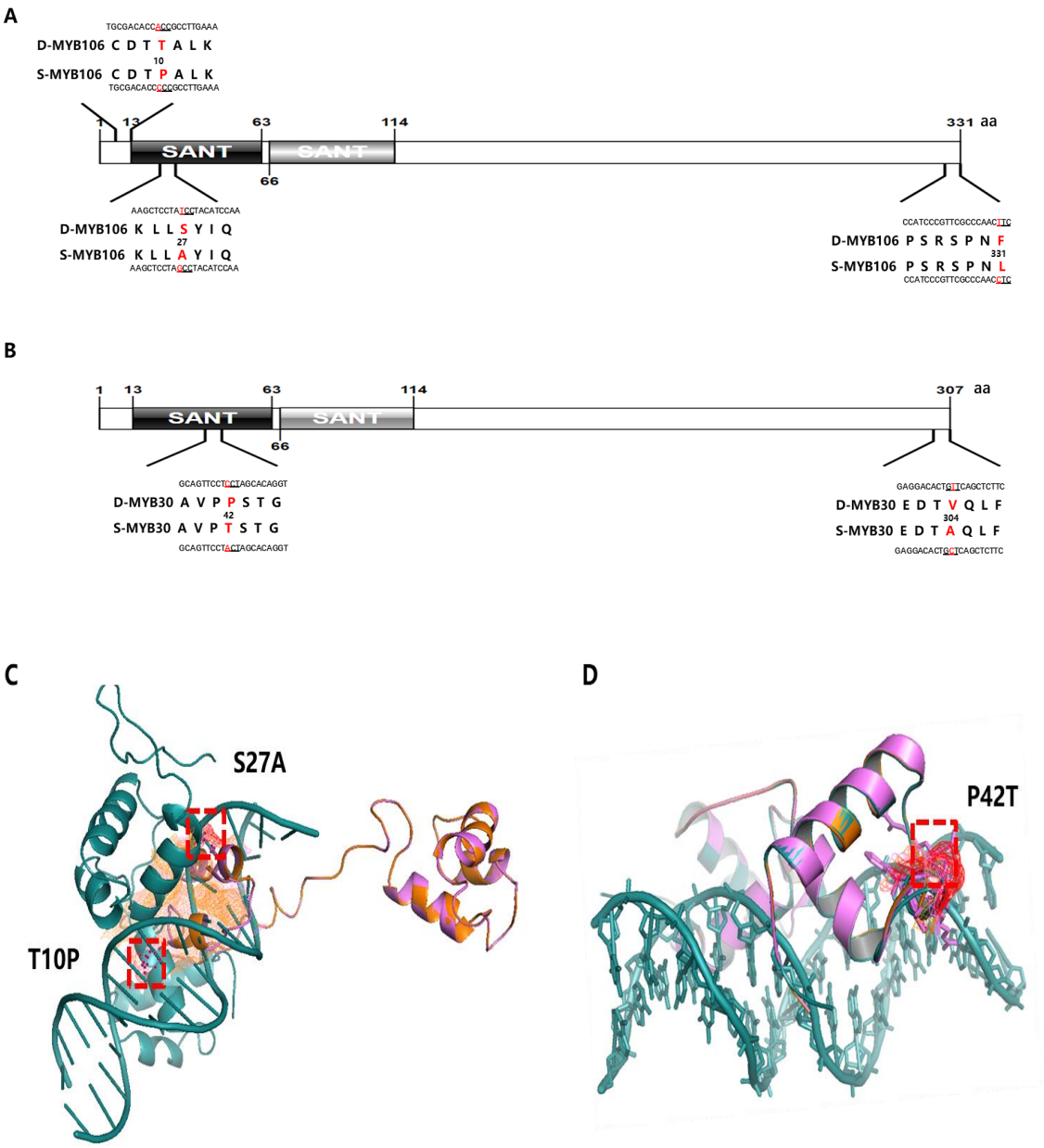

Figure 3-11. Protein sequence analysis of MYB106 **(A and C)** and MYB30 **(B and D)** in the *V. sylvestris* genotypes Ke35 and Ke114. **A** Predicted domains in the two alleles of MYB106 in the group of genotypes Ke35 and Ke114. The mutant sites in the two alleles of MYB106 were identified. The SNP sites indicated in red between the D-MYB106 and S-MYB106. Details shown in the Appendix. **B** Predicted domains in the two alleles of MYB30 in the group of genotypes Ke35 and Ke114.The variation sites in the two alleles of MYB30 were identified. The SNP sites indicated in red between the D-MYB30 and S-MYB30. SANT, DNA binding domain. **C** Mapping of the T20P and S27A sites (red squares) in the three-dimensional structure of two alleles of MYB106 and template 3zqc.3 (SWTL ID). D-MYB106(orange), S-MYB106(violet), 3zqc.3(deep teal). **D** Mapping of the P42T site (red square) in the three-dimensional structure of two alleles of MYB30 and template 3zqc.3(SWTL ID). D-MYB30(orange), S-MYB30(violet), 3zqc.3(deep teal).

3.10 Two alleles of MYB106 complement the *Arabidopsis myb106* mutant, not only the wax content, but also the over-branched trichome phenotype

Moreover, to better understand the function of the two types of MYB106, the full-length coding regions of D-MYB106 and S-MYB106 fused the Cauliflower mosaic virus 35S promoter were transformed in the *Arabidopsis myb106* mutant, respectively. The confirmation of the transgenes and the background were genomic DNA level **(Suppl. Figs. S6A, C and D)** and RNA level **(Suppl. Fig. S7A)**. For genomic DNA level confirmation, if there was a band by using the primer of LBb1.3and RP, and there was not any band by using the primer of FP and RP, it meant that the line was T-DNA insertion *myb106* mutant, otherwise it was the wild type **(Suppl. Fig. S6A)**. And if there was a band by using the primer of SP and 7F, it was the transgenic MYB106 lines **(Suppl. Figs. S6C and D)**. And for RNA level verification, the At MYB106 expression level has been checked in the transgenic lines and it was obviously lower than in the wild type **(Suppl. Fig. S7A)**. Representative transgenic lines were chosen for the subsequent detailed studies. Two types of MYB106 transgenic lines partially complemented the phenotype of defect wax content in *myb106* mutant background **(Figs. 3-12B and F)**, not only in the stem, but also in the rosette leaves **(Figs. 3-12C, G and D, H)**. And the wax accumulation in the D-MYB106 and S-MYB106 transgenic lines **(Figs. 3-12C, G and**

D, H) were similar to the *Arabidopsis* wild type **(Figs. 3-12A and E)**.

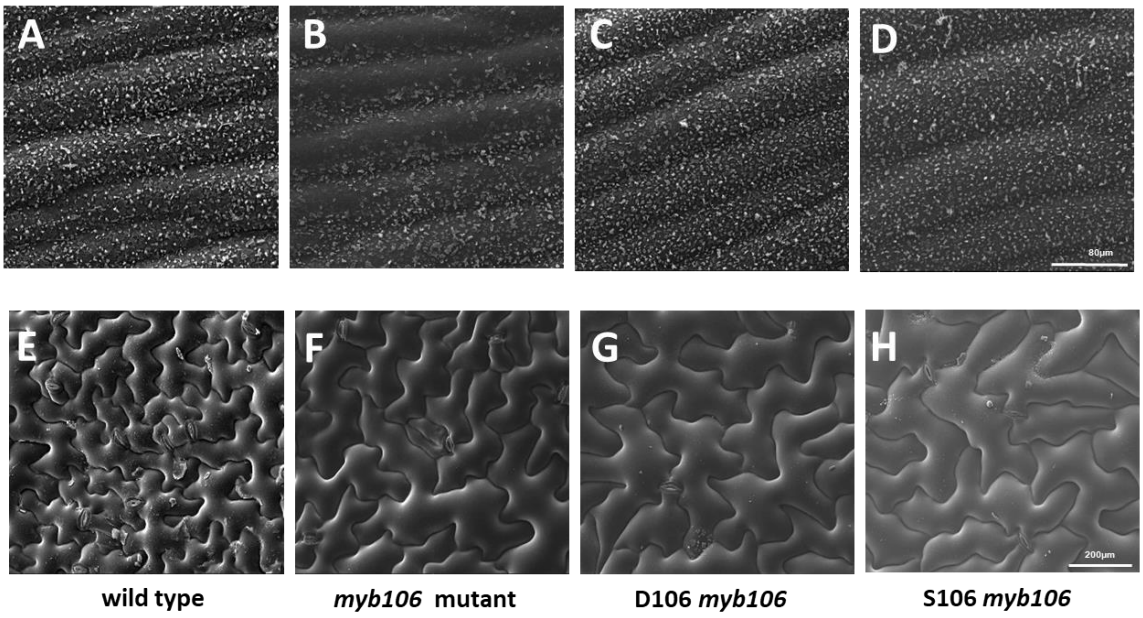

Figure 3-12. Phenotypic analysis of wax structure in p35S:D-MYB106 and p35S:S-MYB106 transgenic *Arabidopsis myb106* mutant lines. **(A-D)** Wax structure in the stem under cryo-SEM. **A** wild type **B** *myb106 Arabidopsis* mutant **C** p35S:D-MYB106 transgenic *Arabidopsis myb106* mutant line **D** p35S:S-MYB106 transgenic *Arabidopsis myb106* mutant line. Scale bars: 80 μm. **(E-H)** Wax structure in the rosette leaves under cryo-SEM. **E** wide type **F** *myb106 Arabidopsis* mutant **G** p35S:D-MYB106 transgenic *Arabidopsis myb106* mutant line **H** p35S:S-MYB106 transgenic *Arabidopsis myb106* mutant line. Scale bars: 200 μm.

The wax compositions were further investigated in different *Arabidopsis* lines to analyze the function of two alleles of MYB106. Compared with the wild type, there were significant differences in *myb106* mutant with regard to wax production and constituents (around 48% decrease), especially for the alkanes (around 45% decrease), which were the main components (**Fig. 3-13A**). The modifications were majorly caused by C29 alkanes and C33 alkanes (around 77% and 76% decrease in *myb106* mutant) (**Fig. 3-13B**). The decrease of C29 ketones and C30 primary-alcohols (74% and 80%, separately) further influenced the wax accumulation in the

myb106 mutant (**Fig. 3-13B**). And D106 and S106 overexpression in the *myb106* background partial rescued the wax biosynthesis (around 1.64-fold and 1.47-fold, respectively) (**Fig. 3-13A**). Among the wax components in D106 *myb106* and S106 *myb106* lines, mainly C29 alkanes, C33 alkanes, C29 ketones and C30 primary-alcohols were increased (**Fig. 3-13B**).

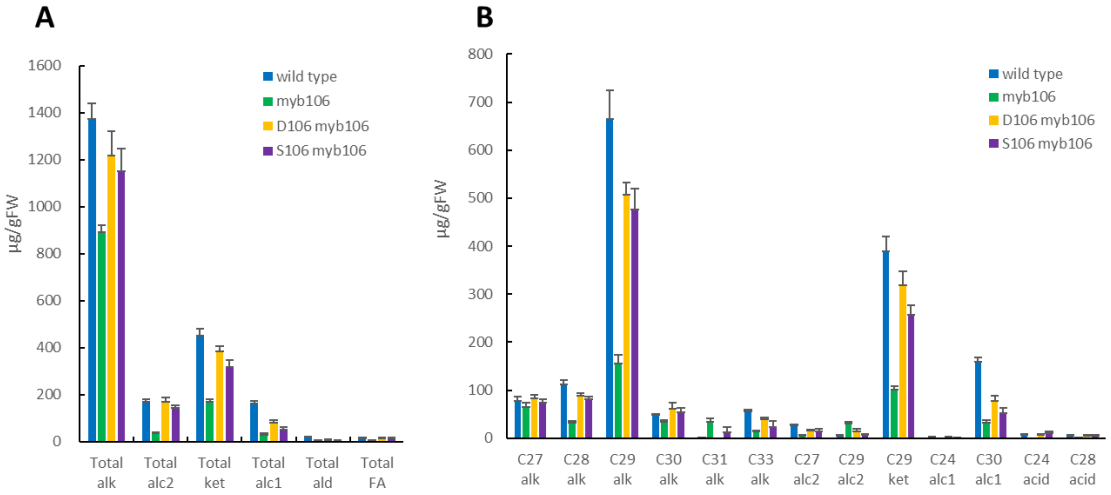

Figure 3-13. Cuticular wax total amounts **A** and major components **B** of inflorescence stems from wild type, *myb106*, D106 and S106 transgenic *Arabidopsis* plants. **A** Mean value (µg/g FW) of total wax load and coverage of individual component classes were measured. **B** Each epicuticular wax constituent is designated by carbon chain length. The data represent means ± SD of 3 replicates.

In addition, there were mostly three branched trichomes **(Fig. 3-14B)** in the WT lines. However, for *myb106* mutants, four and five branched trichomes were in the majority, further three and four branched trichomes predominated in the transgenic lines **(Fig. 3-14A)**. Furthermore, the number of over-branched trichomes in complemental transgenic lines sharply declined, especially the five branched **(Fig. 3-14D)** and six branched trichomes **(Fig. 3-14E)**, compared with the *myb106* mutants.

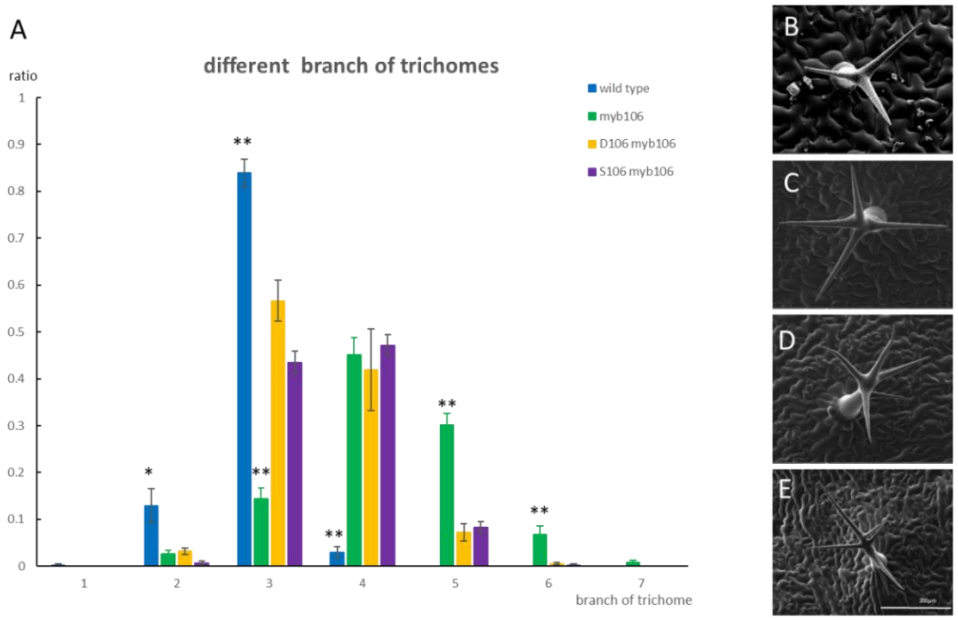

Figure 3-14. Phenotypic analysis of leaf surface trichomes in p35S:D-MYB106 and p35S:S-MYB106 transgenic *Arabidopsis myb106* mutant lines. **A** Distribution of different branch trichome **(B-E)** Representative images of different branch trichome under cryo-SEM. **B** three-branched trichome **C** four branched trichome **D** five branched trichome **E** six branched trichome. * indicate significant differences, $P < 0.05$. **indicate extreme significant difference, $P < 0.01$.

3.11 Two alleles of MYB30 complement the defective wax accumulation phenotype of *Arabidopsis myb30* mutant

To further verify the function of two alleles of MYB30 in regulating the wax formation in the different protein versions, overexpression of D-MYB30 and S-MYB30 constructs were transformed into *Arabidopsis myb30* mutant. Genomic PCR **(Suppl. Figs. S6B, E and F)** and qPCR **(Suppl. Fig. S7B)** were used for verification. For genomic DNA level detection, if there was a band by using the primer of o8474and RS07, and there was not any band by using the primer of FP and RP, it meant that the line was T-DNA insertion *myb30* mutant, otherwise it was the wild type **(Suppl. Fig. S6B)**. And if there was a band by using the primer of PF1 and

7F, it was the transgenic MYB30 lines **(Suppl. Figs. S6E and F)**. And for RNA level verification, the At MYB30 expression level has been examined in the transgenic lines and it was obviously lower than in the wild type **(Suppl. Fig. S7B)**. For the examination of surface wax accumulation, the stem and the rosette leaves of the transgenic lines, *myb30* mutants and wild types were examined by cryo-SEM **(Fig. 3-15)**. From the figure, similar with MYB106 function, the alleles of D-MYB30 **(Figs. 3-15C and G)** and S-MYB30 **(Figs. 3-15D and H)** transgenic lines partially complemented the phenotype of defect wax content in *myb30* mutant background **(Figs. 3-15B and F)**, not only in the stem, but also in the rosette leaves **(Figs. 3-15C, G and D, H)**.

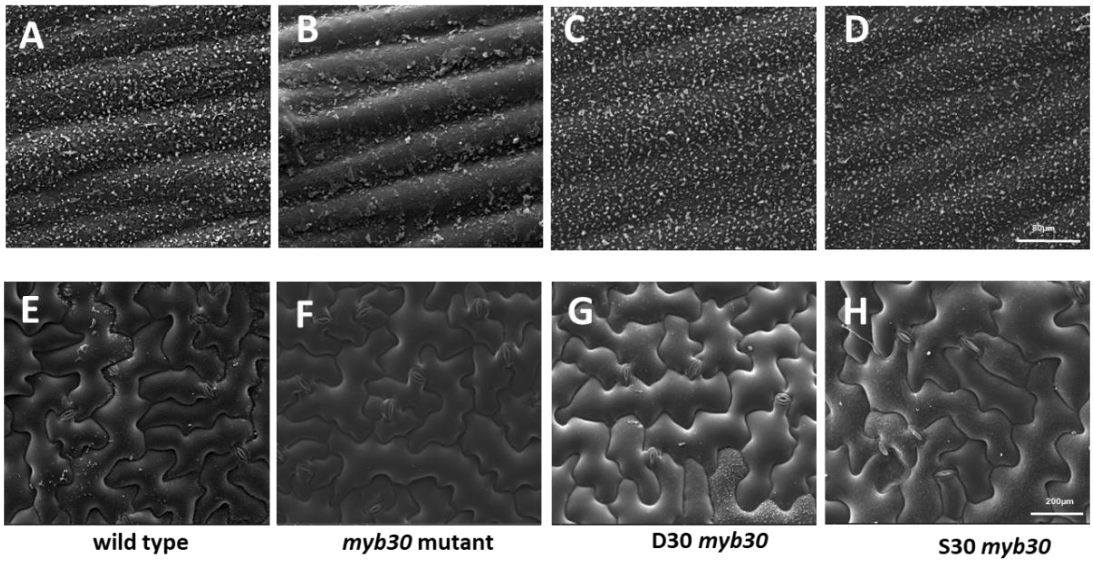

Figure 3-15. Phenotypic analysis of wax structure in p35S:D-MYB30 and p35S:S-MYB30 transgenic *Arabidopsis myb3*0 mutant lines. **(A-D)** Wax structure in the stem under cryo-SEM. **A** wild type **B** *myb30 Arabidopsis* mutant **C** p35S:D-MYB30 transgenic *Arabidopsis myb30* mutant line **D** p35S:S-MYB30 transgenic *Arabidopsis myb3*0 mutant line. Scale bars: 80 µm. **(E-H)** Wax structure in the rosette leaves under cryo-SEM. **E** wide type **F** *myb30 Arabidopsis* mutant **G** p35S:D-MYB30 transgenic *Arabidopsis myb30* mutant line **H** p35S:S-MYB30 transgenic *Arabidopsis myb30* mutant line. Scale bars: 200 µm.

To determine which components influenced total wax composition, the surface wax was extracted and analyzed by GC-MS. In the *myb30* mutant, the wax constituents obviously declined around 44%, as shown in **Fig. 3-16A**. And the alkanes which accounted for 73.7% of total wax contents in the mutant strongly decreased, such as C29 alkanes and C33 alkanes (70% and 73.5% decrease), compared with in the wild type (**Fig. 3-16B**). The total wax accumulations of D30 and S30 overexpression in the *myb30* background were rescued to 89% and 97% of the level found in the wild type (**Fig. 3-16A**). The amount of C29 alkanes in D30 and S30 transgenic lines increased 1.5- and 1.8-folds respectively to complement the *myb30* mutant phenotype (**Fig. 3-16B**).

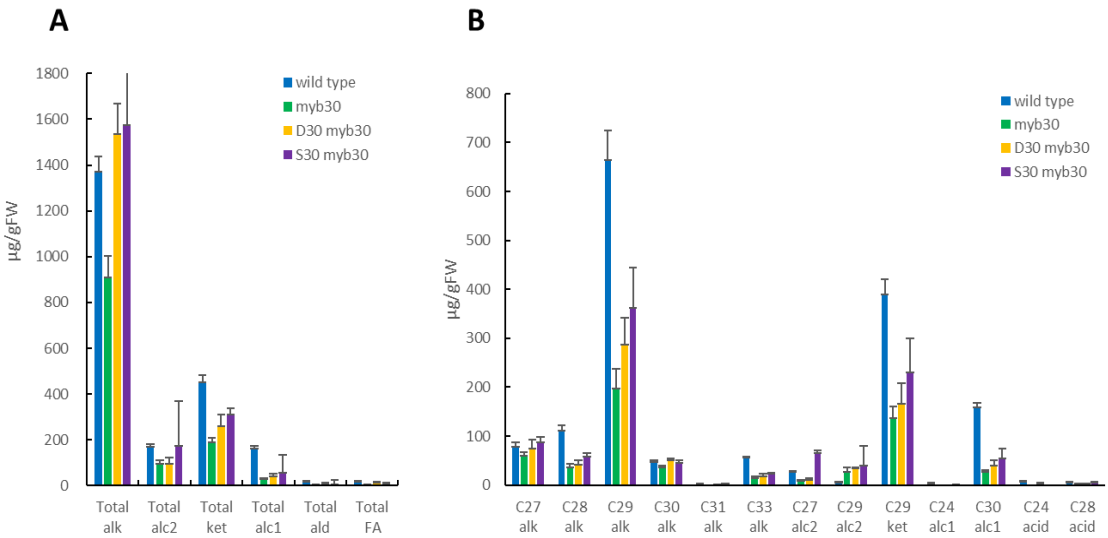

Figure 3-16. Cuticular wax total loads **A** and major components **B** of inflorescence stems from wild type, *myb30*, D30 and S30 transgenic *Arabidopsis* plants. **A** Mean value (µg/g FW) of total wax contents and coverage of individual constituent classes are measured. **B** Each epicuticular wax constituent is designated by carbon chain length. The data represent means ± SD of 3 replicates.

3.12 Expression pattern of two alleles of MYB106 and two alleles of MYB30 in Ke114 and Ke35

Then the MYB106 and MYB30 gene expression pattern were analyzed in the Ke114 and Ke35 **(Fig. 3-17)**. The expression levels of MYB106 and MYB30 were evaluated in the leaves from the first leaf to the fourth leaf. Compared with Ke35, the MYB106 expression in Ke114 was much higher from the first leaf to the fourth leaf, especially the first leaf and second leaf **(Fig. 3-17A)**. However, there was not much difference of the MYB30 expression in Ke114 and Ke35 **(Fig. 3-17B)**.

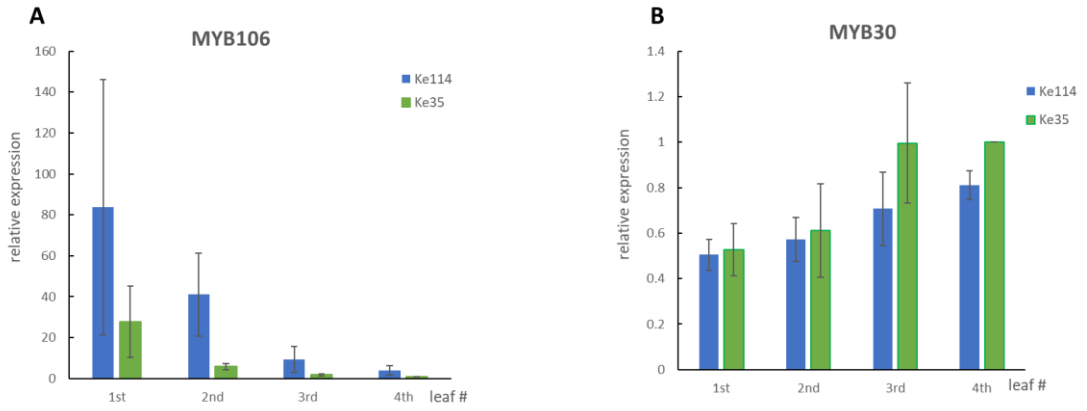

Figure 3-17. Expression pattern of MYB106 and MYB30 in the group of the *V. sylvestris* genotypes Ke35 and Ke114. **A** MYB106 relative expression pattern **B** MYB30 relative expression pattern

3.13 Subcellular co-localization of two alleles of MYB106 and two alleles of MYB30

In order to determine subcellular localization of two alleles of MYB106 and two alleles of MYB30, D-MYB106 and S-MYB106 fused RFP with D-MYB30 and S-MYB30 fused GFP were transiently transformed

together into *V. vinifera* cv. 'Pinot Noir' cells **(Fig. 3-18)**. The 'Pinot Noir' cells were examined as the negative control **(Fig. 3-18A)**, the free RFP and free GFP co-transformation as the positive control **(Fig. 3-18B)**. The fusion proteins with RFP and GFP showed fluorescent signals in the nucleus **(Figs. 3-18C, F)**, respectively, which means the two alleles of MYB106 and MYB30 both localized in the nucleus.

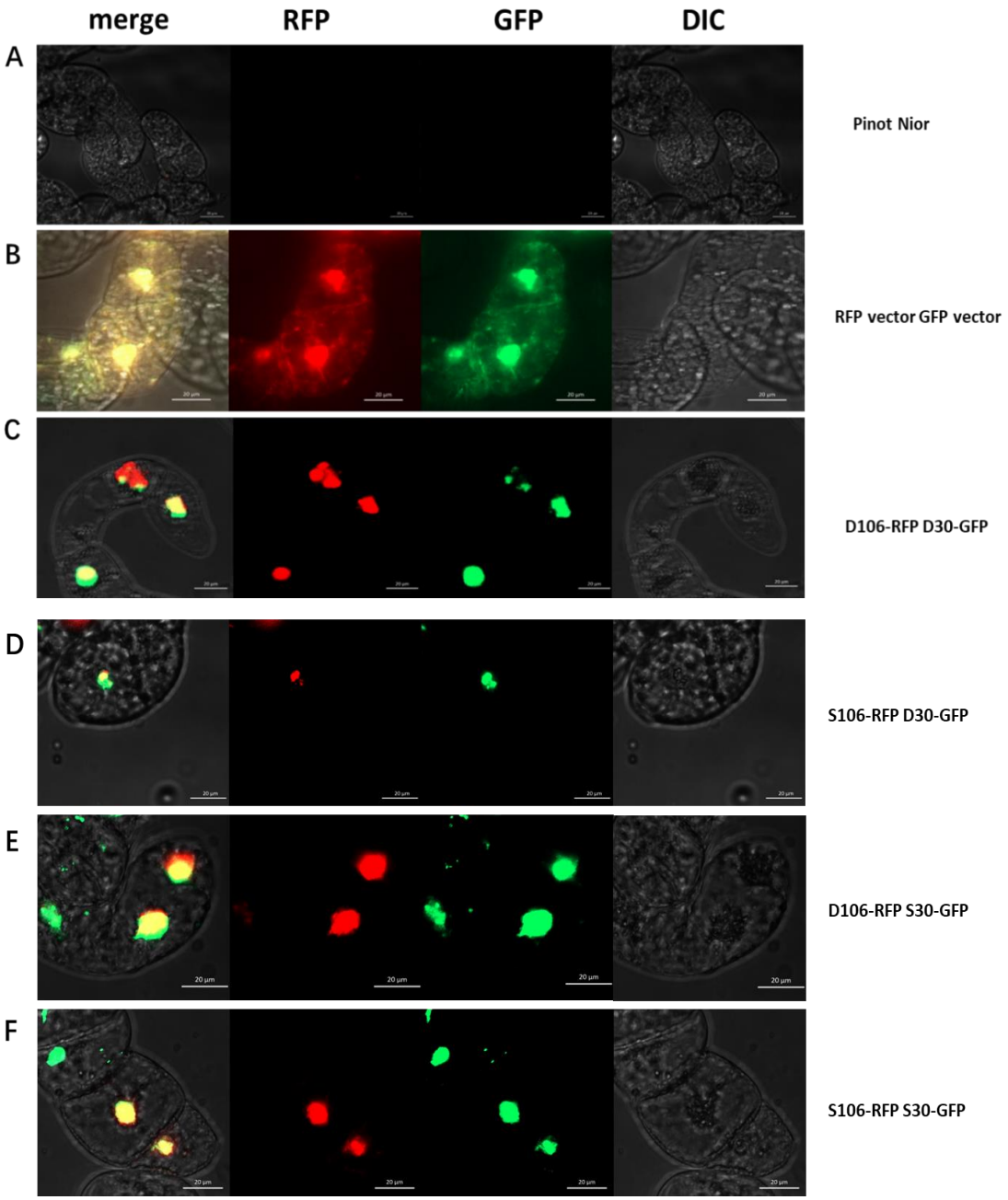

Figure 3-18. Subcellular co-localization of two alleles of MYB106-RFP (D106 and S106) and two alleles of MYB30-GFP (D30 and S30) from *the sylvestris* genotypes Ke35 and Ke114 transient transformation in the 'Pinot Noir' cells. **A** Empty 'Pinot Noir' cell as negative control **B** Free RFP and GFP co-transformation, as positive control **C** D106-RFP and D30-GFP subcellular co-localization **D** S106-RFP and D30-GFP subcellular co-localization **E** D106-RFP and S30-GFP subcellular co-localization **F** S106-RFP S30-GFP subcellular co-localization. Scale bars: 20 μm.

3.14 MYB106 interacts with MYB30 to regulate the wax formation in the genotypes Ke114 and Ke35

MYB106 and MYB30 both partially complemented the phenotype of defect wax content in *myb106* mutant **(Figs. 12 and 15)**. In addition, the property of the MYB transcription factors is frequently forming polymers to be functional (Dubos et al., 2010; Latchman, 1997; Riechmann et al., 2000). We hypothesize that MYB106 interacts with MYB30 to regulate the wax formation. To verify the hypothesis, bimolecular fluorescence complementation (BiFC) assays were conducted in *V. vinifera* cv. 'Pinot Noir' cells **(Fig. 3-19)**. Further the YFP fluorescence was examined in these combinations. It was discovered both in the D30YC D106YN combination **(Fig. 3-19A)**, as well as the YCD106 YND30 combination **(Fig. 3-19B)**, similar with the other type of MYB106 and MYB30 combinations. However, the YFP fluorescence was not detected in all negative controls **(Suppl. Fig. S8)**. These results suggested that two alleles of MYB106 interact with two alleles of MYB30, both in C-terminal interaction and in N-terminal interaction.

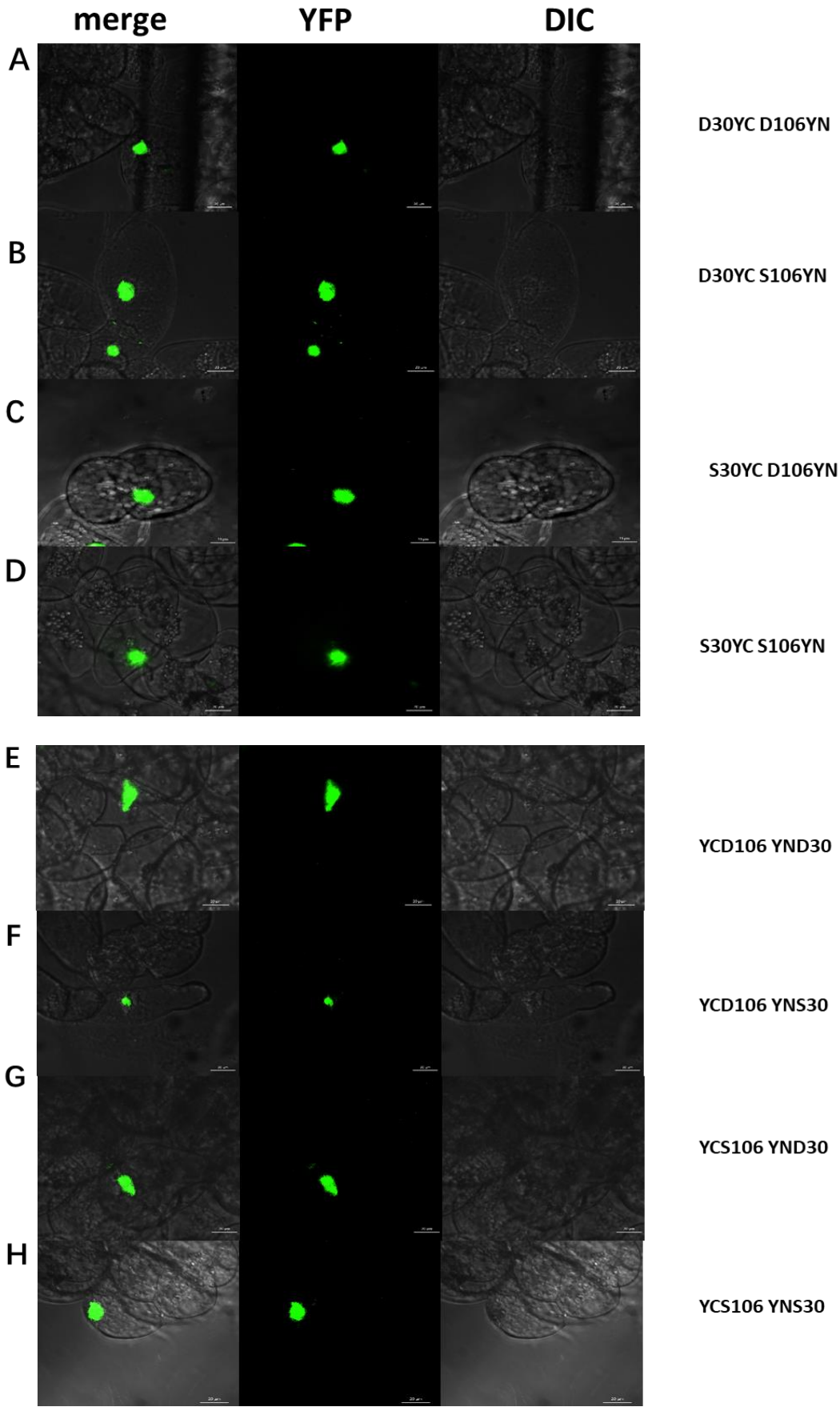
merge
YFP
DIC
A
B
C
D
E
F
G
H
D30YC D106YN
D30YC S106YN
S30YC D106YN
S30YC S106YN
YCD106 YND30
YCD106 YNS30
YCS106 YND30
YCS106 YNS30

Figure 3-19. Protein interaction between two alleles of MYB30 and two alleles of MYB106 in the 'Pinot Noir' cells by BiFC experiment. The C or N terminus of yellow fluorescent protein designated as YC or YN, respectively. Different combinations of the fused constructs were used. **A** D30YC D106YN **B** D30YC S106YN **C** S30YC D106YN **D** S30YC S106YN **E** YCD106 YND30 **F** YCD106 YNS30 **G** YCS106 YND30 **H** YCS106 YNS30.

3.15 Plant hormones, light and low temperature may regulate MYB106 and MYB30 expression in the cis-acting regulatory elements analysis

To further reveal the MYB106 and MYB30 regulation mechanism in the pair, the promoter sequences of the two genes were cloned. The predicted cis-acting regulatory elements were analyzed using the PlantCARE database (Lescot et al., 2002). For promoter of MYB106, there were two alleles in the pair, named pMYB106-1 and PMYB106-2, although the predicted cis-acting regulatory elements were identical in the two alleles **(Figs. 20A and B)**. The two alleles of MYB106 were putatively regulated by many factors, including plant hormones like abscisic acid, indicated by the presence of ABA responsive elements (ABRE), auxin, indicated by the presence of auxin-responsive elements (TGA-element), gibberellic acid, indicated by the presence of gibberellin-responsive element (P-box and TATC-box), and salicylic acid, indicated by the presence of TCA-elements. There were also evidences for their regulation by environmental factor such as low temperature (LTR elements), or light (G-Box, GT1-motif, GATA-motif, LAMP element and TCT-motif). Furthermore, there were MYB binding sites to regulate the two alleles of MYB106 expression. In case of promoter of MYB30, there were additional motifs, like the MBS

motif of drought-inducibility, as well as CGTCA-motif and TGACG-motif of MeJA-responsiveness **(Fig. 3-20C)**.

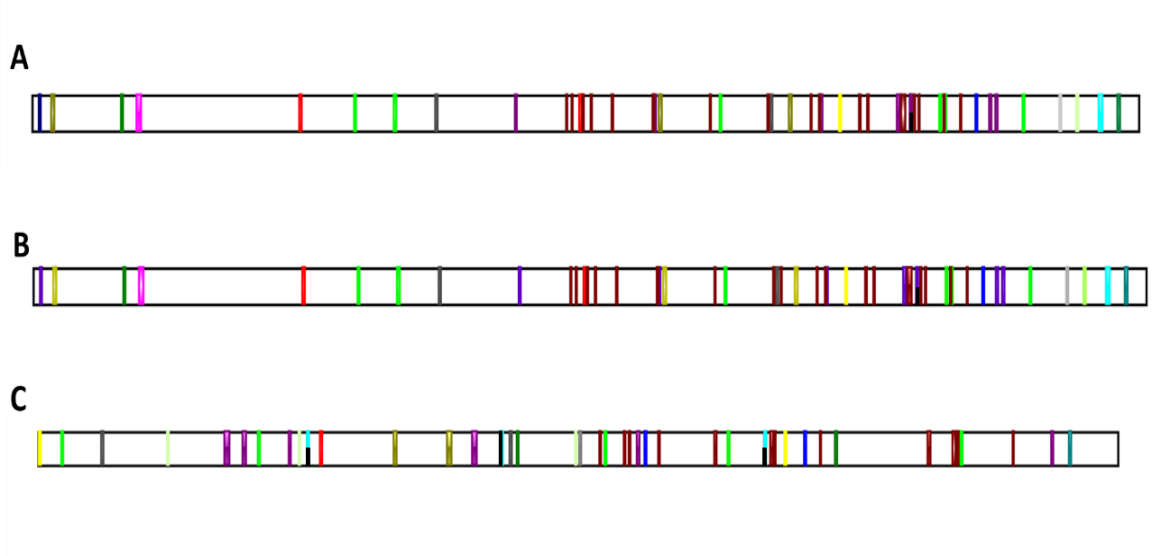

Figure 3-20. Structures of two alleles MYB106 (pMYB106-1 and PMYB106-2) and MYB30 promoter sequence with the predicted cis-acting regulatory elements. **(A and B)** pMYB106-1 and PMYB106-2 promoter structures, separately. Blue color indicates A-box motif, cis-acting regulatory element; cyan color is AACA motif, endosperm-specific negative expression; black color is ABRE motif, the abscisic acid responsiveness element; green color is Box 4 motif and ATC motif , part of a conserved DNA module involved in light responsiveness; light gray color is CAT-box , cis-acting regulatory element related to meristem expression; firebrick color is CAAT-box, promoter and enhancer regions; violet color is G Box, GT1-motif, GATA-motif, LAMP element and TCT-motif, part of a light responsive element; magentas color is HD-Zip 1, element involved in differentiation of the palisade mesophyll cells; yellow color is LTR, low-temperature responsiveness; smudge color is MYB binding site; red color is MRE motif, MYB binding site involved in light responsiveness; grey color is P-box motif, gibberellin-responsive element; chartreuse color is TATC-box, gibberellin-responsiveness; limon color is TCA-element, salicylic acid responsiveness; blue color is TGA-element, auxin-responsive element; deep teal color is TATA-box , core promoter element around-30 of transcription start. **C** MYB30 promoter structure. The motifs are basically same, except cyan color is G-box, cis-acting regulatory element involved in light responsiveness; blue color is MBS motif, MYB binding site involved in drought-inducibility; magentas color is CCAAT-box, MYBHv1 binding site; chartreuse color is CGTCA-motif and TGACG-motif, in the MeJA-responsiveness. Details are in the Appendix.(Lescot et al., 2002)

3.16 Chitosan regulates the promoter of MYB106 and MYB30 activity

The higher epicuticular wax abundance, in a certain threshold, could play a role in the Powdery Mildew susceptibility by preventing the spores further from generating the appressorium **(Figs. 3-5 and 7)**. Therefore, the activation of the promoters of MYB106 and MYB30 in response to fungal chitosan as elicitor was tested in the 'Pinot Noir' and 'Ke15' cells by the dual-luciferase reporter assay. The activity of reporter of pSTS with or without the effector MYB14 was as the positive control **(Fig. 3-21A)**. The activity of promoter MYB30 was measured in response to chitosan and it could be upregulated with 20μg/mL chitosan treatment **(Fig. 3-21B)**. In case of the two alleles of the MYB106 promoter, they were also regulated in response to chitosan, but the responsiveness was different **(Figs. 3-21C and D)**. pMYB106-1 was slightly regulated with low concentration chitosan **(Fig. 3-21C)**, yet pMYB106-2 was strongly induced in response to 20μg/mL chitosan treatment **(Fig. 3-21D)**. These data indicated the promoter of MYB106 and MYB30 could be regulated by chitosan as the elicitor.

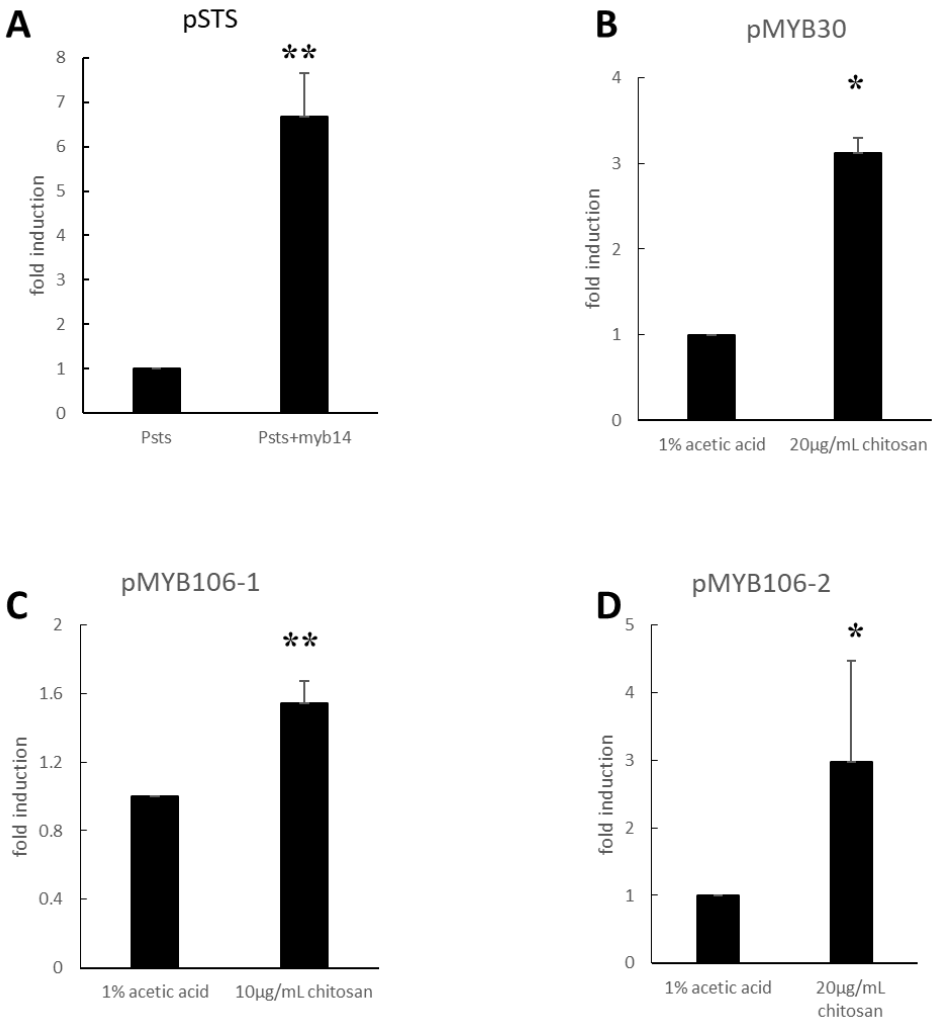

Figure 3-21. Promoter activity assay of two alleles of MYB106 and MYB30 after the different concentration of chitosan treatment. **A** The fold induction of STS promoter activity with MYB14 as the positive control. **B** The MYB30 promoter activity after 1% acetic acid and 20μg/mL chitosan treatments. **C** pMYB106-1 promoter activity after 1% acetic acid and 10μg/mL chitosan treatments. **D** pMYB106-2 promoter activity after 1% acetic acid, 20μg/mL chitosan treatments. * indicates the differences that are statistically significant on the $P < 0.05$ level. ** indicates the differences that are statistically extreme significant on the $P < 0.01$ level, 4 independent experimental series.

4. Discussion

In the study, we have investigated the surface wax morphology, distribution, formation and wax accumulation in different grapevine accessions. Furthermore, the relationship between epicuticular wax and resistance to Powdery Mildew and regulation mechanism have been analyzed. One phylogenetically closely related pair from the wild *Vitis.* collection has been compared with regard to wax content. Then we have studied MYB106 and MYB30 function, expression pattern and regulation mechanism of surface wax biosynthesis in wild grapevine genotypes. Chitosan, an elicitor of plant defense, was used to check if it could regulate the promoter activity of MYB106 and MYB30, further to regulate the grapevine wax accumulation.

4.1 Genetic variation of surface wax morphology and development in *V. sylvestris*

There are distinct wax morphologies, mostly like filaments, platelets, crystals and tubules in *Arabidopsis* and other plants being verified (**Fig. 1-4**) (Wilhelm Barthlott et al., 1998; Jetter et al., 2008; Rashotte & Feldmann, 1998). However, the knowledge about surface wax morphology in grapevines is limited. 115 varieties in the wild ancestor grapevine accession, along with a couple of commercial and traditional varieties

(**Suppl. Table S1**) have been screened to investigate the surface wax morphology and development. Here we have studied adaxial and abaxial sides of fully expanded leaves under cryo-SEM and found that the wax morphology in grapevine was different from other plants. There were basically three types of the epicuticular wax structures, long wing-like structures, small wax crystals and appearance of both long wax wings and small wax crystals (**Figs. 3-1 A, C**).

Moreover, the wax distribution has shown significantly distinct. The abundance of surface waxes at the upper side was generally higher than at the lower side. The distribution of long wing-like wax structures was much higher on the epidermal cells covering leaf veins, but less in intercostal regions at the adaxial side **(Fig. 3-1D)**. At the abaxial side, wax usually accumulated on the surface of the accessory cells of the stomatal complex **(Fig. 3-1E)**.

The developmental time course of wax formation and accumulation showed diversities in the representatives from all clades of the European wild grapevine population. Some of the varieties formed wax earlier, faster and more, while others accumulated higher amounts of wax, though slower. And others developed wax earlier and faster, but at a low final wax content **(Figs. 3-2 and 3)**. In general, the process of wax accumulation was basically stable in the full expansion leaves of diverse genotypes.

There was a considerable variety for the wax abundance of fully expanded

leaves within individual clades, which were separated by molecular phylogeny based on the entire genomes. But wax accumulation of the clade A, C, D, E were statistically not obviously different, clade B had a significantly lower median which meant wax accumulation was significantly higher in this clade as compared to the others **(Fig. 3-4).** It was reasonable to conclude that, the wax has shown genetic variation in morphology, distribution, formation and accumulation of the *V. sylvestris.*

4.2 Low wax content genotypes are more susceptible to Powdery Mildew

There have been several studies to investigate the relationship between wax components, wax crystallization pattern and susceptibility to pathogens (Lewandowska et al., 2020). The spore germination and differentiation of *Blumeria graminis* on Maize adaxial leaf were significantly declined after treatment with C22 fatty acid, C22 alcohol and C44-alkyl ester (Hansjakob, Riederer, & Hildebrandt, 2011). And the reduction of cuticular monomers in the *atmin7* mutant, an ARF-GEF (ADP ribosylation factor guanine nucleotide exchange factor protein) caused the increase of susceptibility to the *Pto* (*Pseudomonas syringae* pathovar tomato) pathogen (Zhao et al., 2020). However, there is limited knowledge about the relationship between wax accumulation and Powdery Mildew in grapevines. Therefore, we have investigated the relationship between the wax abundance and the resistance

to Powdery Mildew in the different accessions available to us. The susceptibility to Powdery Mildew was constantly low with the wax increased accumulation above a certain threshold. During the Powdery Mildew infection when wax abundance was below a certain threshold, this strongly increased the Powdery Mildew infection **(Fig.3-5A)**. Moreover, the susceptibility to Powdery Mildew has been analyzed between 5 clades of *V. sylvestris*. It was generally similar between the clades, except clade D which was more susceptible. Clade B had higher wax abundance **(Fig. 3-4B)**, although the resistance to Powdery Mildew was similar with the other three. This was consistent with the observation that susceptibility went up only when the wax layer was below a certain threshold **(Fig. 3-5A)**. These results taken together indicate that low wax content genotypes were more susceptible to Powdery Mildew.

4.3 Abundant surface waxes regulate appressorium formation of Powdery Mildew spores

The spore germination and differentiation were regulated in maize leaves with different wax components treatments like C22 fatty acid, C22 alcohol or C44 wax ester. Wax morphology in maize leaves further was involved in the regulation the plant resistance to pathogens by fungal colonization process (Hansjakob et al., 2011; Reisberg, Hildebrandt, Riederer, & Hentschel, 2013). Thus, we have examined the spores' development in

‘Müller-Thurgau’ and two *V. sylvestris* genotypes Ke114 and Ke35. The developmental process of spores in two genotypes with relatively high abundance of wax were much slower, compared with ‘Müller-Thurgau’. The stage ap* with perturbed appressorium development appeared both in Ke114 and Ke35. There was a constantly higher proportion of stage ap* in Ke114 (where wax content was maximal), compared with Ke35 (where wax accumulation was lower).

And over time, the proportion of stage ap* gradually decreased both in Ke114 and Ke35, which meant that some spores in stage ap* also generated normal appressorium after some delays (**Fig. 3-7**). In addition, the infection severity and infection frequency of Powdery Mildew were highest in ‘Müller-Thurgau’, followed by Ke35, Ke114 was the least **(Suppl. Fig. S4)** (Tisch, 2017). Here was the conclusion that abundant surface waxes disturbed appressorium formation of Powdery Mildew spores to decline the rate and number of spores’ differentiation into normal appressorium, further to regulate plant defense in Müller-Thurgau’ and two genotypes Ke114 and Ke35.

4.4 MYB106 and MYB30 are associated with wax biosynthesis pathway in grapevines

MYB106 and MYB30 have been verified to take part in wax biosynthesis pathway (Oshima et al., 2013; S. R. F. Vailleau et al., 2008). And

MdMYB30 homolog also has been shown to be able to regulate the wax biosynthesis in apple (X. Wang et al., 2020; Y.-L. Zhang et al., 2019). Here, VvMYB106 was a MIXTA-like MYB family homolog in grapevine and VvMYB30 was a R2R3MYB family homolog in grapevine **(Fig. 3-10)**.

The transcriptional abundance of MYB106 was much higher in the leaves of the genotype of Ke114 which belonged to the high wax accumulation group, especially the second leaf, compared with the genotype Ke35 which was in the low wax content cluster **(Fig. 3-8 and 17)**. These results indicated that MYB106 and MYB30 may regulate the wax biosynthesis in grapevines.

Further in the complementation experiment of *Arabidopsis* mutants, ectopic expression of MYB106 and MYB30 all promoted the wax accumulation and very-long-chain compositions increase, especially the C29 alkanes, C33 alkanes and C29 ketones which were the main wax compounds, compared with *Arabidopsis* mutant, respectively **(Figs. 3-12, 13,15,16)**. Hence our results revealed that MYB106 and MYB30 are likely involved in the grapevine wax accumulation.

In addition, the MYB transcription factors usually form polymers to be functional (Dubos et al., 2010; Latchman, 1997; Riechmann et al., 2000). And MYB106 and MYB30 were relatively close to each other in the phylogenetic tree **(Fig. 3-10)**. Therefore, the BiFC assay was used to investigated the physical interaction between MYB106 and MYB30 **(Fig.**

3-19). All the results showed that they could interact with each other, which uncovered that MYB106 interacted with MYB30 to regulate the wax biosynthesis pathway in grapevine.

4.5 The genes' functions of two alleles of MYB106 and two alleles of MYB30 have less differences, separately

There were two alleles of MYB106 and MYB30 in Ke114 and Ke35 **(Figs. 3-11 and Suppl. Fig. S5)**. There were two SNPs, T10P and S27A, between D-MYB106 and S-MYB106 to be predicted near or in the DNA binding domain **(Fig. 3-11 A and C)**. Similar to MYB106, there was one P42T site between D-MYB30 and S-MYB30 predicted in the DNA binding domain **(Fig. 3-11 B and C)**. We hypothesized that there was the possibility of differences in the regulation of DNA binding in the two alleles MYB106 and two alleles of MYB30, because of alteration in the molecular backbone in the encoded proteins due to the properties of proline and nucleophilic serine. However, there was not any difference in nuclear localization of two alleles of MYB106 and two alleles of MYB30, respectively **(Fig. 3-18)**. And all of them could partially complement the glossy phenotypes of *myb106 Arabidopsis* mutant and *myb30 Arabidopsis* mutant, respectively (Oshima et al., 2013; S. R. F. Vailleau et al., 2008). The wax content and compositions of D-MYB106 and S-MYB106 (with proline and alanine in the SNP sites) transgenic lines were in general similar, even though the wax

components of C29 alkanes, C33 alkanes, C29 ketones and C30 primary-alcohols were a little bit lower in S-MYB106 transgenic lines **(Figs. 3-12,13).** For the two alleles of MYB30, the differences of wax accumulation and components in the D-MYB30 and S-MYB30 complemented *Arabidopsis* lines were consistent with the two alleles of MYB106 transgenic lines **(Figs. 3-15,16).**

In rescuing the phenotype of over-branched trichomes, for *myb106* mutant, four and five branched trichomes were in the majority, even there was quite a bit of six branched trichomes. However, both D-MYB106 and S-MYB106 transgenic lines had generally less five and six branched trichomes, compared with *myb106* mutant. And the number of over-branched trichome reduction was actually similar with each other **(Fig. 3-14)**.

In addition, two alleles of MYB106 and two alleles of MYB30 could interact with each other to regulate the wax biosynthesis in Ke114 and Ke35 **(Fig.3-19)**. These results suggested that for MYB106 and MYB30, there were not any obvious differences in two alleles with regard to their ability in wax formation or phenotypic alterations.

4.6 MYB106 is more relatively conserved, compared with MYB30

From the phylogenetic tree, the similarity of MYB106 in *Arabidopsis thaliana* and MYB106 in *V. vinifera* cv. ‘Pinot Noir’ was relatively higher,

compared with the similarity of MYB30 in *Arabidopsis thaliana* and MYB30 in *V. vinifera* cv. 'Pinot Noir' **(Fig. 3-10)**.

In the previous studies, modulation of MYB106 expression directly influenced WIN1, further regulated the genes expression in the fatty acyl chains elongation and in the alkane forming pathway (Kannangara et al., 2007; Oshima et al., 2013). And MYB30 overexpression could also induce gene expression in the fatty acyl chain elongation and in the alkane forming pathway (S. R. F. Vailleau et al., 2008).

In the *Arabidopsis* mutant complementation experiments, the wax components of C29 alkanes, C33 alkanes, C29 ketones and VLCFAs increased around 3-fold in MYB106 transgenic *Arabidopsis* lines, compared with *myb106* mutant, although these compositions increased only 1.5-fold in MYB30 transgenic *Arabidopsis* lines, compared with *myb30* mutant **(Fig. 3-13,16)**.

Furthermore, MYB106 reduced the number of over-branched trichomes in *Arabidopsis* **(Fig. 3-14).** Therefore, MYB106 of grapevine was functionally more conserved to its *Arabidopsis* homolog, compared with MYB30.

4.7 MYB106 and MYB30 are involved in defense regulation

For MYB30 in *Arabidopsis* and apple, it has been shown that the gene expression level has significantly increased under pathogen attack, and the

responsiveness to flg22 and *B. dothidea* infection was improved in the DmMYB30ox lines. After inoculation with Pst DC3000 (Pseudomonas syringae), MYB30 overexpression resulted in enhanced HR phenotype in *Arabidopsis* (F. Vailleau et al., 2002; S. R. F. Vailleau et al., 2008; Y.-L. Zhang et al., 2019). In this study, wax abundance below a certain threshold (rank 70 in the separation by wax content) has been studied that it was positively correlated with the resistance to Powdery Mildew **(Fig. 3-5)**. Fungal chitosan as elicitor was used to investigate the promoter activities of MYB106 and MYB30 **(Fig. 3-21B)**. The dual-luciferase assay indicated that MYB106 and MYB30 could response to the fungal chitosan stressor, which meant that MYB106 and MYB30 could regulate the plant defense under the fungus attack.

4.8 Conclusion

We have examined the surface wax property and the link between surface wax and the resistance to Powdery Mildew in European wild grapevine accession, further explored MYB106 and MYB30 wax biosynthesis mechanism in *Vitis*. in our study. Based on our results, we can conclude that there are basically three types of the epicuticular wax structures, long wing-like structures, small wax crystals and appearance of both long wax wings and small wax crystals in the wild grapevine accessions. We also conclude that:

1. Surface wax morphology, distribution, formation and accumulation are genetically variable in *V. sylvestris*.

2. Low wax abundance is positively correlated with the susceptibility to Powdery Mildew.

3. Abundant surface wax can interfere with appressorium formation, and influence the penetration of Powdery Mildew spores.

4. MYB106 physically interacts with MYB30 indicating that they might regulate grapevine wax biosynthesis pathway together.

5. D-MYB106 and S-MYB106 function have only small differences in the regulation of wax biosynthesis and in rescuing the over-branched phenotype of respective *Arabidopsis* mutants, similar to D-MYB30 and S-MYB30.

6. MYB106 is more functionally conserved to its *Arabidopsis* orthologue, compared with MYB30.

7. MYB106 and MYB30 are regulated by the fungal chitosan stressor indicating a possible role in defense gene regulation.

4.9 Outlook

Wax crystallization pattern, wax components and their proportions played roles in regulating pathogen infection (Gniwotta et al., 2005; Reisberg et al., 2013; Tsuba, Katagiri, Takeuchi, Takada, & Yamaoka, 2002; X. Wang et al., 2020; Zhao et al., 2020).

Therefore, the wax components in the different accession need to be further analyzed and to figure out if there are also other factors regulate the plant resistance to Powdery Mildew.

And we could also investigate that if there are some differences in wax content, wax components and proportions under different abiotic stress, such as drought stress, UV light stress. Then the key regulators should also be analyzed. Furthermore, we could understand the wax biosynthesis and regulation pathway in the *Vitis*.

For well understood what kinds of genes in the wax biosynthesis take part into the resistance to Powdery Mildew regulation, the transcriptional expression level of related genes needs to be examined after Powdery Mildew inoculation. Then we could find out the link between them and deduce the regulation mechanism.

To further understand the regulation mechanism in the transgenic MYB106 and MYB30 lines, the related wax biosynthesis genes need to be investigated and further to verified the function and regulation network.

Appendix

Supplementary Table 1. Identity and origin of the grapevine accessions used in this study

Taxon	Voucher ID	Source	Origin
Vitis vinifera ssp. vinifera			
Commercial cultivars			
cv. Müller-Thurgau	5585	WBI Freiburg	Economically important German variety
cv. Cabernet Sauvignon	7471	JKI Siebeldingen	Economically important French variety
cv. Pinot Noir	7474	JKI Siebeldingen	Economically important traditional French variety, background of genome project
cv. Riesling	6144	WBI Freiburg	Traditional German variety
cv. Gewürztraminer	7464	Antes Nursery	Traditional Alsacian variety
cv. Chardonnay	7472	JKI Siebeldingen	Traditional French variety
Hybrid varieties			
cv. Merzling	6150	WBI Freiburg	German variety, pedigrée of North American and Chinese species
cv. Regent	5895	JKI Siebeldingen	German variety, pedigrée of North American species
Traditional landraces			
cv. Razegui	5894	Borj Cedria	Tunisian landrace
cv. Augster Weiß	7443	JKI Siebeldingen	Central European medieval landrace, male sterile
cv. El Tanque	5898	Tenerife, Canarian Islands	Canarian landrace
cv. Guimar	5899	Tenerife, Canarian Islands	Canarian landrace
cv. San Andres	5889	Tenerife, Canarian Islands	Canarian landrace
Vitis vinifera ssp. sylvestris			
Isolated, Upper Rhine			

VSylE	5905	WBI Freiburg	Alsace, near Colmar
Co5	6186	DLR Neustadt	Alsace, near Colmar
Klaus	6173	Dr. Schubert	Reiß Island, near Mannheim
Blau	6183	Dr. Schubert	Reiß Island, near Mannheim
Rosa	6185	Dr. Schubert	Reiß Island, near Mannheim
Hö17	6187	Own collection	Hördt, Rhine bank
Hö29	6188	Own collection	Hördt, Rhine bank
Ketsch population, Rhine			
Ke 2	6189	Own collection	Ketsch peninsula, Rhine bank
Ke 7	6190	Own collection	Ketsch peninsula, Rhine bank
Ke 10	6191	Own collection	Ketsch peninsula, Rhine bank
Ke 11	6192	Own collection	Ketsch peninsula, Rhine bank
Ke 12	6193	Own collection	Ketsch peninsula, Rhine bank
Ke 13	6194	Own collection	Ketsch peninsula, Rhine bank
Ke 15	6195	Own collection	Ketsch peninsula, Rhine bank
Ke 16	6196	Own collection	Ketsch peninsula, Rhine bank
Ke 17	6197	Own collection	Ketsch peninsula, Rhine bank
Ke 18	6198	Own collection	Ketsch peninsula, Rhine bank
Ke 20	6199	Own collection	Ketsch peninsula, Rhine bank
Ke 22	6200	Own collection	Ketsch peninsula, Rhine bank
Ke 24	6201	Own collection	Ketsch peninsula, Rhine bank
Ke 26	6202	Own collection	Ketsch peninsula, Rhine bank
Ke 27	6203	Own collection	Ketsch peninsula, Rhine bank
Ke 27 neu	8618	Own collection	Ketsch peninsula, Rhine bank
Ke 28a	6204	Own collection	Ketsch peninsula, Rhine bank
Ke 28b	6205	Own collection	Ketsch peninsula, Rhine bank
Ke 28c	6206	Own collection	Ketsch peninsula, Rhine bank
Ke 30	6207	Own collection	Ketsch peninsula, Rhine bank
Ke 32	6208	Own collection	Ketsch peninsula, Rhine bank
Ke 33	6209	Own collection	Ketsch peninsula, Rhine bank
Ke 34	6210	Own collection	Ketsch peninsula, Rhine bank
Ke 35	6211	Own collection	Ketsch peninsula, Rhine bank
Ke 36	6212	Own collection	Ketsch peninsula, Rhine bank
Ke 38	6213	Own collection	Ketsch peninsula, Rhine bank
Ke 39	6214	Own collection	Ketsch peninsula, Rhine bank
Ke 42	6215	Own collection	Ketsch peninsula, Rhine bank
Ke 44a	6216	Own collection	Ketsch peninsula, Rhine bank
Ke 47	6218	Own collection	Ketsch peninsula, Rhine bank
Ke 48	6219	Own collection	Ketsch peninsula, Rhine bank
Ke 51	6220	Own collection	Ketsch peninsula, Rhine bank
Ke 53	6221	Own collection	Ketsch peninsula, Rhine bank
Ke 54	6222	Own collection	Ketsch peninsula, Rhine bank

Ke 56	6223	Own collection	Ketsch peninsula, Rhine bank
Ke 58	6224	Own collection	Ketsch peninsula, Rhine bank
Ke 61	6225	Own collection	Ketsch peninsula, Rhine bank
Ke 71	6226	Own collection	Ketsch peninsula, Rhine bank
Ke 74	6227	Own collection	Ketsch peninsula, Rhine bank
Ke 75	6228	Own collection	Ketsch peninsula, Rhine bank
Ke 76	6229	Own collection	Ketsch peninsula, Rhine bank
Ke 77	6230	Own collection	Ketsch peninsula, Rhine bank
Ke 78	6231	Own collection	Ketsch peninsula, Rhine bank
Ke 81	6233	Own collection	Ketsch peninsula, Rhine bank
Ke 82	6234	Own collection	Ketsch peninsula, Rhine bank
Ke 83	6235	Own collection	Ketsch peninsula, Rhine bank
Ke 84	6236	Own collection	Ketsch peninsula, Rhine bank
Ke 86	6237	Own collection	Ketsch peninsula, Rhine bank
Ke 87	6238	Own collection	Ketsch peninsula, Rhine bank
Ke 88	6239	Own collection	Ketsch peninsula, Rhine bank
Ke 89	6240	Own collection	Ketsch peninsula, Rhine bank
Ke 90	6241	Own collection	Ketsch peninsula, Rhine bank
Ke 91	6242	Own collection	Ketsch peninsula, Rhine bank
Ke 92	6243	Own collection	Ketsch peninsula, Rhine bank
Ke 93	6244	Own collection	Ketsch peninsula, Rhine bank
Ke 94	6245	Own collection	Ketsch peninsula, Rhine bank
Ke 95	6246	Own collection	Ketsch peninsula, Rhine bank
Ke 96	6247	Own collection	Ketsch peninsula, Rhine bank
Ke 98	6248	Own collection	Ketsch peninsula, Rhine bank
Ke 99	6249	Own collection	Ketsch peninsula, Rhine bank
Ke 100	6250	Own collection	Ketsch peninsula, Rhine bank
Ke 101	6251	Own collection	Ketsch peninsula, Rhine bank
Ke 1016	6252	Own collection	Ketsch peninsula, Rhine bank
Ke 103	6253	Own collection	Ketsch peninsula, Rhine bank
Ke 104	6254	Own collection	Ketsch peninsula, Rhine bank
Ke 106	6256	Own collection	Ketsch peninsula, Rhine bank
Ke 107	6257	Own collection	Ketsch peninsula, Rhine bank
Ke 108	6258	Own collection	Ketsch peninsula, Rhine bank
Ke 109	6259	Own collection	Ketsch peninsula, Rhine bank
Ke 110	6260	Own collection	Ketsch peninsula, Rhine bank
Ke 112	6261	Own collection	Ketsch peninsula, Rhine bank
Ke 114	6262	Own collection	Ketsch peninsula, Rhine bank
Ke 115	6263	Own collection	Ketsch peninsula, Rhine bank
Ke 116	6264	Own collection	Ketsch peninsula, Rhine bank
Ke 118	6265	Own collection	Ketsch peninsula, Rhine bank
Ke 119	6266	Own collection	Ketsch peninsula, Rhine bank
Ke 120	6267	Own collection	Ketsch peninsula, Rhine bank
K2 DLR	6268	DLR Neustadt	Ketsch peninsula, Rhine bank

RM 2	6269	DLR Neustadt	Ketsch peninsula, Rhine bank
VSylJung-1	7778	Dr. Jung	Ketsch peninsula, Rhine bank
VSylJung-2	7779	Dr. Jung	Ketsch peninsula, Rhine bank
Ke 23-ITA	8323	JKI Siebeldingen	Ketsch peninsula, Rhine bank
KE 006-GSH	8324	Geisenheim	Ketsch peninsula, Rhine bank
VvsBgFfm	8581	BG Frankfurt	Ketsch peninsula, Rhine bank
Isolated, Danube			
Ö3	6174	Naturgarten	Lobau, Danube bank, Austria
Ö5	6175	Naturgarten	Lobau, Danube bank, Austria
Ö6	6176	Naturgarten	Lobau, Danube bank, Austria
Ö7	6177	Naturgarten	Lobau, Danube bank, Austria
Ö8	6178	Naturgarten	Lobau, Danube bank, Austria
Ö9	6179	Naturgarten	Lobau, Danube bank, Austria
Ö10	6180	Naturgarten	Lobau, Danube bank, Austria
Ö11	6181	Naturgarten	Lobau, Danube bank, Austria
Ö12	6182	Naturgarten	Lobau, Danube bank, Austria
VsylRO-01	6556	Prof. Dr. Dister	Romania, Danube bank

Supplementary table 2. The list of oligonucleotide primers information for qPCR analysis

Gene name	Accession number	Primer sequence
EF1α	EC959059	Sense:5'-TGTCATGTTGTGTCGTGTCCT-3' Antisense:5'- CCAAAATATCCGGAGTAAAAGA-3'
Ubiquitin	XR002030722	Sense:5'-GAGGGTCGTCAGGATTTGGA-3' Antisense:5'- GCCCTGCACTTACCATCTTTAAG-3'
VvMYB106	XM010665048	Sense:5'-CGCGTCGTCTTGACGTACTA -3' Antisense:5'-CGTTGAGGTTGGTGATGGGA-3'
VvMYB30	NM001281017	Sense:5'-ACCAGACCTGTCCAAGCATC-3' Antisense:5'-TGTAGTTGCCCCTTCACTGG-3'
SAND	AT2G28390	Sense:5'- AACTCTATGCAGCATTTGATCCACT -3' Antisense:5'- TGATTGCATATCTTTATCGCCATC-3'
AtMYB106	AT3G01140	Sense:5'- CAAACCAAGGAAACGGAGACCAA-3' Antisense:5'- CTGCTATCCGTAGGGATTCCTA-3
AtMYB30	AT3G28910	Sense:5'- GCAGCAAGAGTTGTAGACTTAGATGGA -3' Antisense:5'- GCAGAAGAAGACGATGGTGAAGATGA-3

Supplementary table 3. The list of primers information for the constructs of MYB106 and MYB30 and their promoters

Primer name	Primer sequence	Destination vector
MYB106-S	GGGGACAAGTTTGTACAAAAAAGCAGGCTTCAT	PH7FWG2.0
	GGGAGGATCTCCCTGC	PH7RWG2.0
MYB106-A	GGGGACCACTTTGTACAAGAAAGCTGGGTCGAA	pMAV-GW-YN
	GTTGGGCGAACG	pMAV-YC-GW
MYB30-S	GGGGACAAGTTTGTACAAAAAAGCAGGCTTCAT	
	GGGGAGGCCACCTTG	PH7FWG2.0
MYB30-A	GGGGACCACTTTGTACAAGAAAGCTGGGTCGAA	pMAV-GW-YC
	GAGCTGAACAGTGTCCT	pMAV-YN-GW
pMYB106-S	GGGGACAAGTTTGTACAAAAAAGCAGGCTTCGC	
	TGATCTACCCATGTTGTGTCC	
pMYB106-A	GGGGACCACTTTGTACAAGAAAGCTGGGTCTTT	pLUC
	GAGGGAGTGCCCAGTGA	
pMYB30-S	GGGGACAAGTTTGTACAAAAAAGCAGGCTTCTT	
	TTCGGTATTTTTACTCGATTGTG	
pMYB30-A	GGGGACCACTTTGTACAAGAAAGCTGGGTCGGC	pLUC
	TTTTCGCTCTCTCTCTCTG	

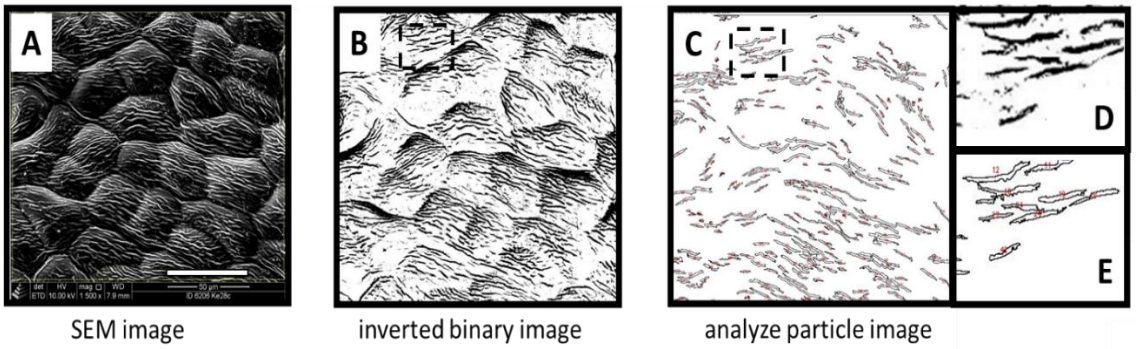

Supplementary Figure S1. Quantification of surface wax from cryo-SEM images. **A** Original cryo-SEM image of a grapevine leaf surface with wax structures. Scale bars: 50 µm. **B** Inverted binary image used for automatic detection. Inset refers to the zoom-in in **D**, **C** Automatic detection of surface wax structures using the Analyze Particle tool, the inset refers to the zoom-in in **E**. **D** and **E** show a zoom in of the inverted binary image and the automatically recognized wax structures used for quantification.

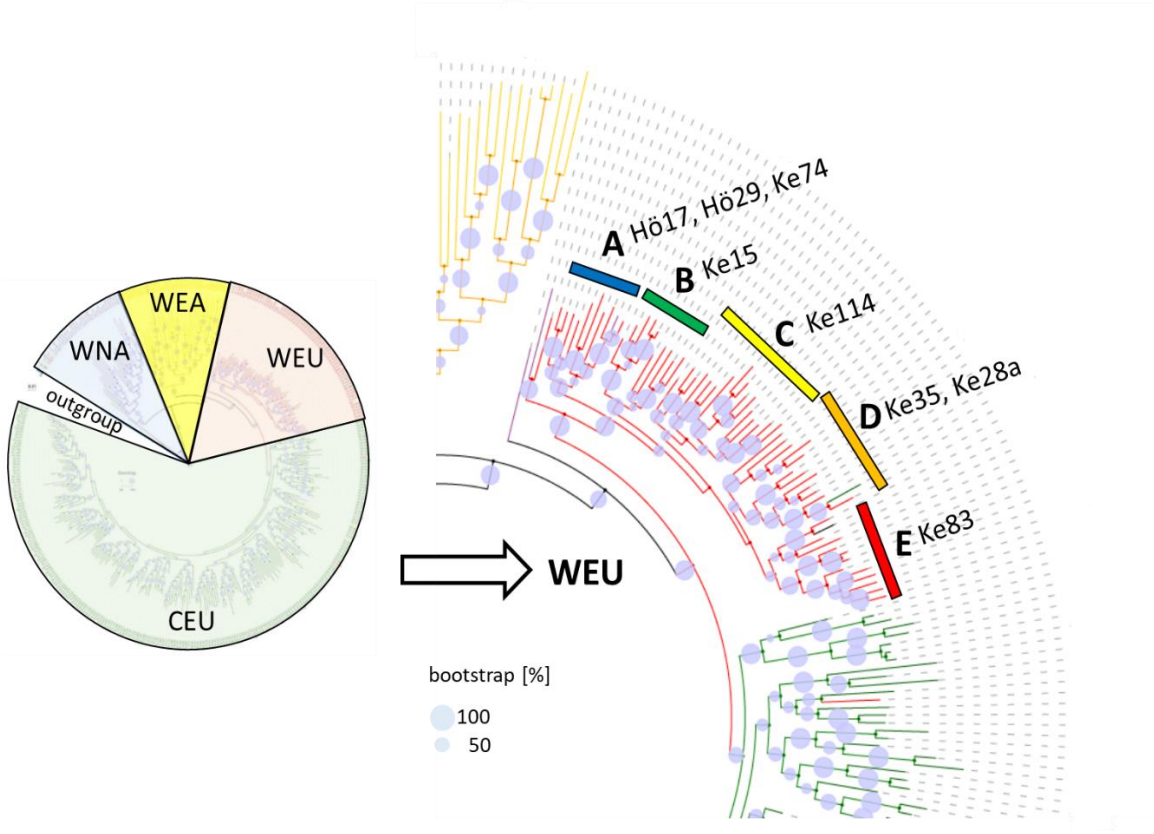

Supplementary Figure S2. Phylogenetic relationship of the *sylvestris* accessions inferred from whole-genome sequencing by Maximum Likelihood (from Liang et al. 2019) and position of the five clades and the representative genotypes shown in **Figure**.

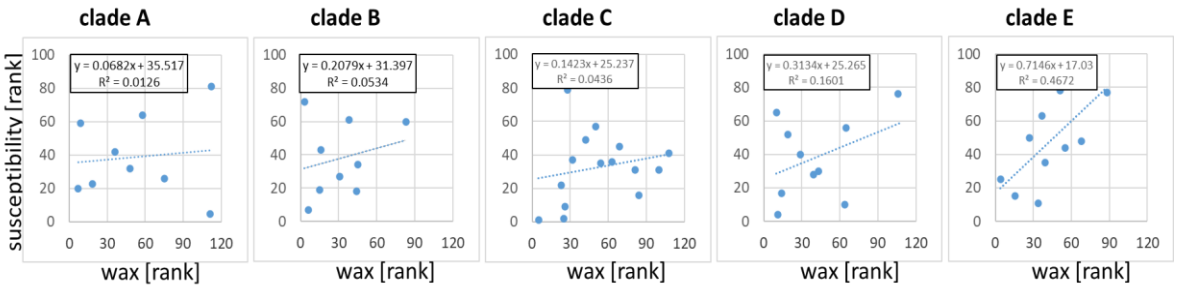

Supplementary Figure S3. Relationship between susceptibility to Powdery Mildew and abundance of surface waxes in the *sylvestris* population broken down for the different clades individually using a ranking system. For each genotype, the rank in susceptibility (increasing numbers mean increasing susceptibility) and wax abundance (increasing numbers mean decreasing wax abundance) were determined and plotted.

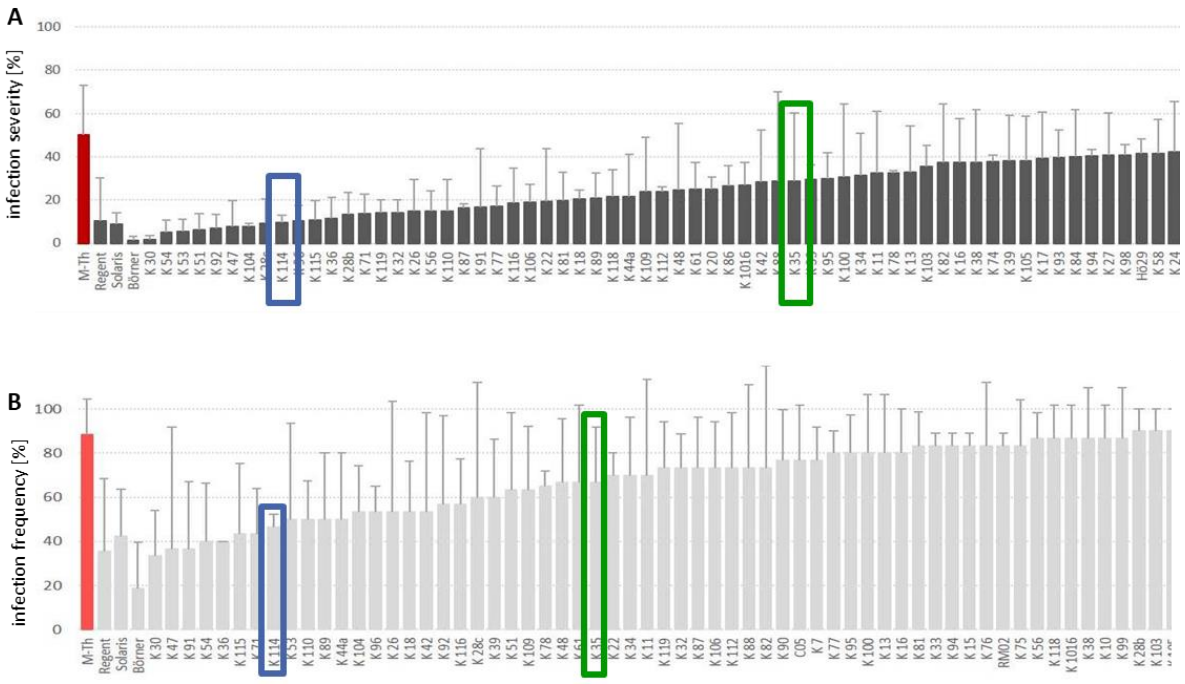

Supplementary Figure S4. Powdery Mildew **A** infection severity [%] and **B** infection frequency [%] red is 'Müller-Thurgau' blue is Ke114 green is Ke35. Figure from (Tisch, 2017).

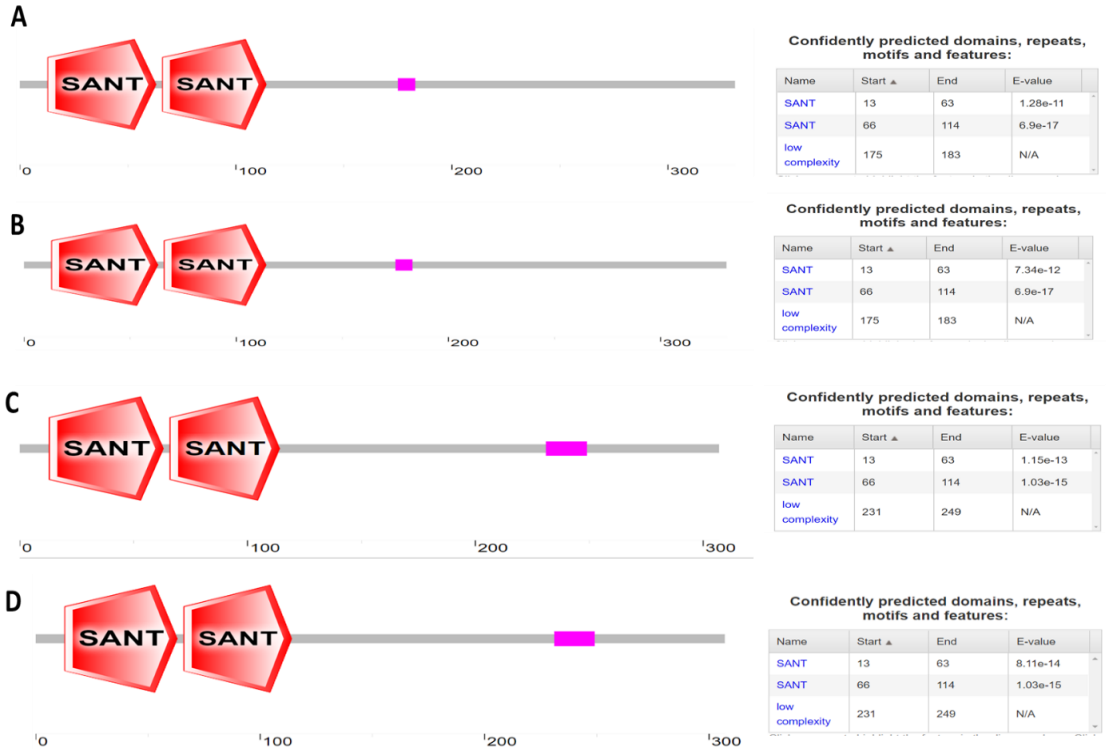

Supplementary Figure S5. Predicted domains analysis in two alleles of MYB106 and two alleles of MYB30 by SMART. **A** D-MYB106 **B** S-MYB106 **C** D-MYB30 **D** S-MYB30.

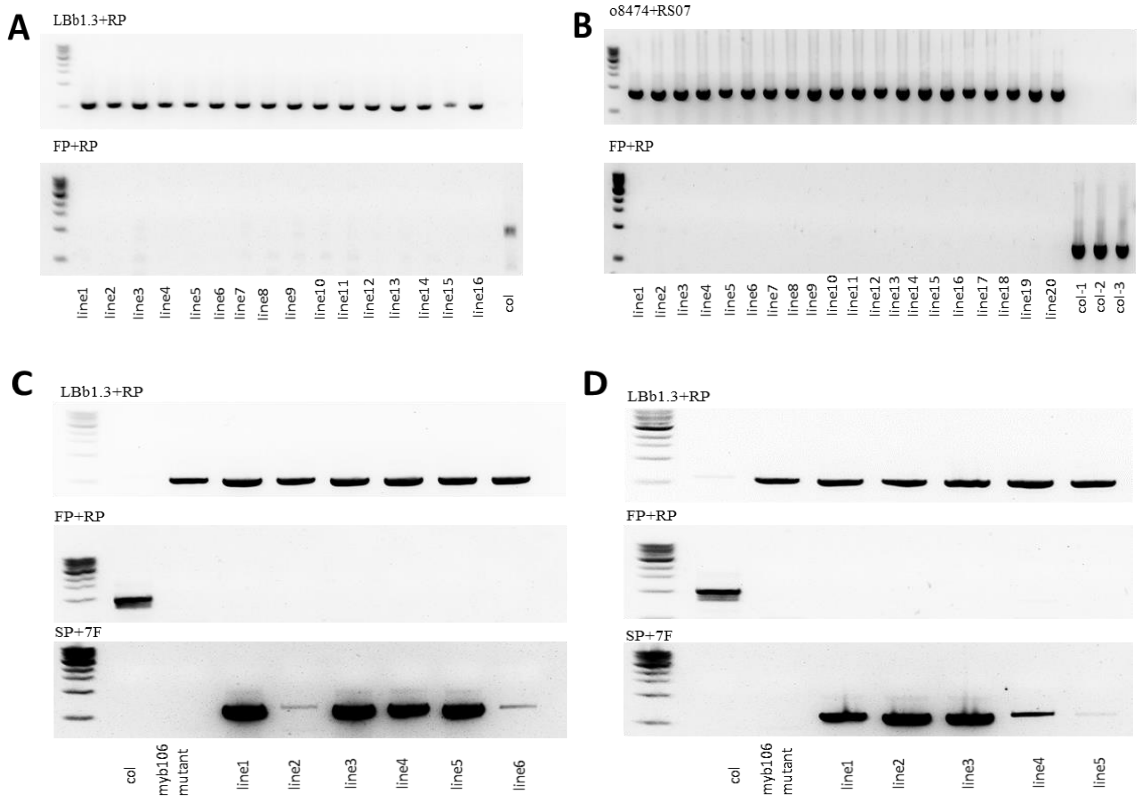

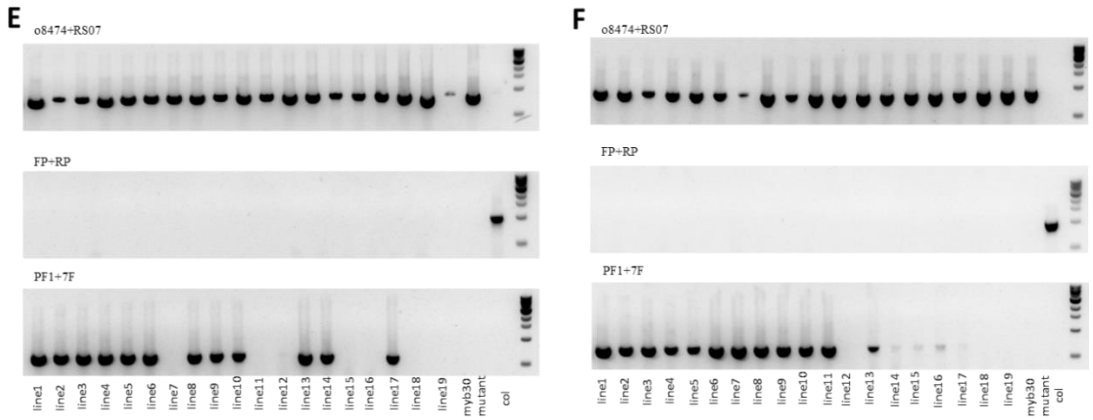

Supplementary Figure S6. Confirmation the homolog of T-DNA insertion *Arabidopsis myb106*, *myb30* mutants and transgenic MYB106 lines, transgenic MYB30 lines. **A** *myb106* mutants detection with primers: LBb1.3 5'-ATTTTGCCGATTTCGGAAC-3', FP 5'-TTCAATTGCTTGCACTCAGC-3', and RP 5'-CCAAGGTAAGGGACACATCG-3' **B** *myb30* mutants detection with primers: o8474 5'-ATAATAACGCTGCGGACATCTACATTTT-3', RS07 5'- CACTTCTCAAACAAAGACCATTGA-3', FP 5'-TTCATTCATCATCTCTCCTCTCTACC -3', and RP 5'- AGTTTTGAGTCTTCGGCGAGT -3' **(C and D)** transgenic MYB106 lines with primers: LBb1.3 5'-ATTTTGCCGATTTCGGAAC-3', FP 5'-TTCAATTGCTTGCACTCAGC-3', RP 5'- CCAAGGTAAGGGACACATCG-3', SP 5'-CGCGTCGTCTTGACGTACTA -3' and 7F 5'-CTGCACGCCGTAGGTCAG-3' **C** transgenic D-MYB106 lines **D** transgenic S-MYB106 lines **(E and F)** transgenic MYB30 lines with primers: o8474 5'-ATAATAACGCTGCGGACATCTACATTTT-3', RS07 5'- CACTTCTCAAACAAAGACCATTGA-3', FP 5'-TTCATTCATCATCTCTCCTCTCTACC -3', RP 5'- AGTTTTGAGTCTTCGGCGAGT -3', PF1 5'-ACCAGACCTGTCCAAGCATC -3' and 7F 5'-CTGCACGCCGTAGGTCAG-3' **E** transgenic D-MYB30 lines **F** transgenic S-MYB30 lines.

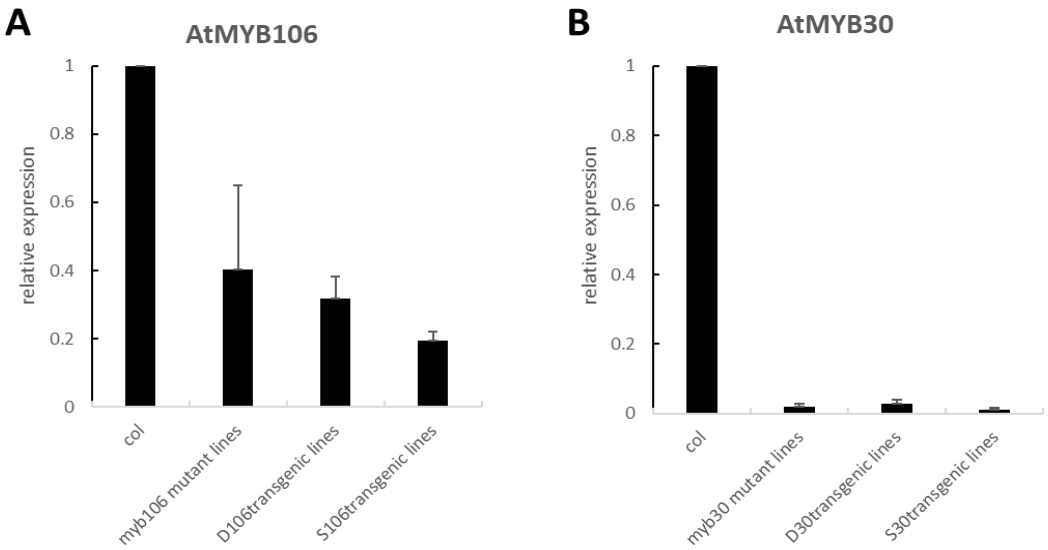

Supplementary Figure S7. Detection AtMYB106 and AtMYB30 expression in the transgenic *Arabidopsis* lines and *Arabidopsis* mutant background. **A** AtMYB106 relative expression **B** AtMYB30 relative expression.

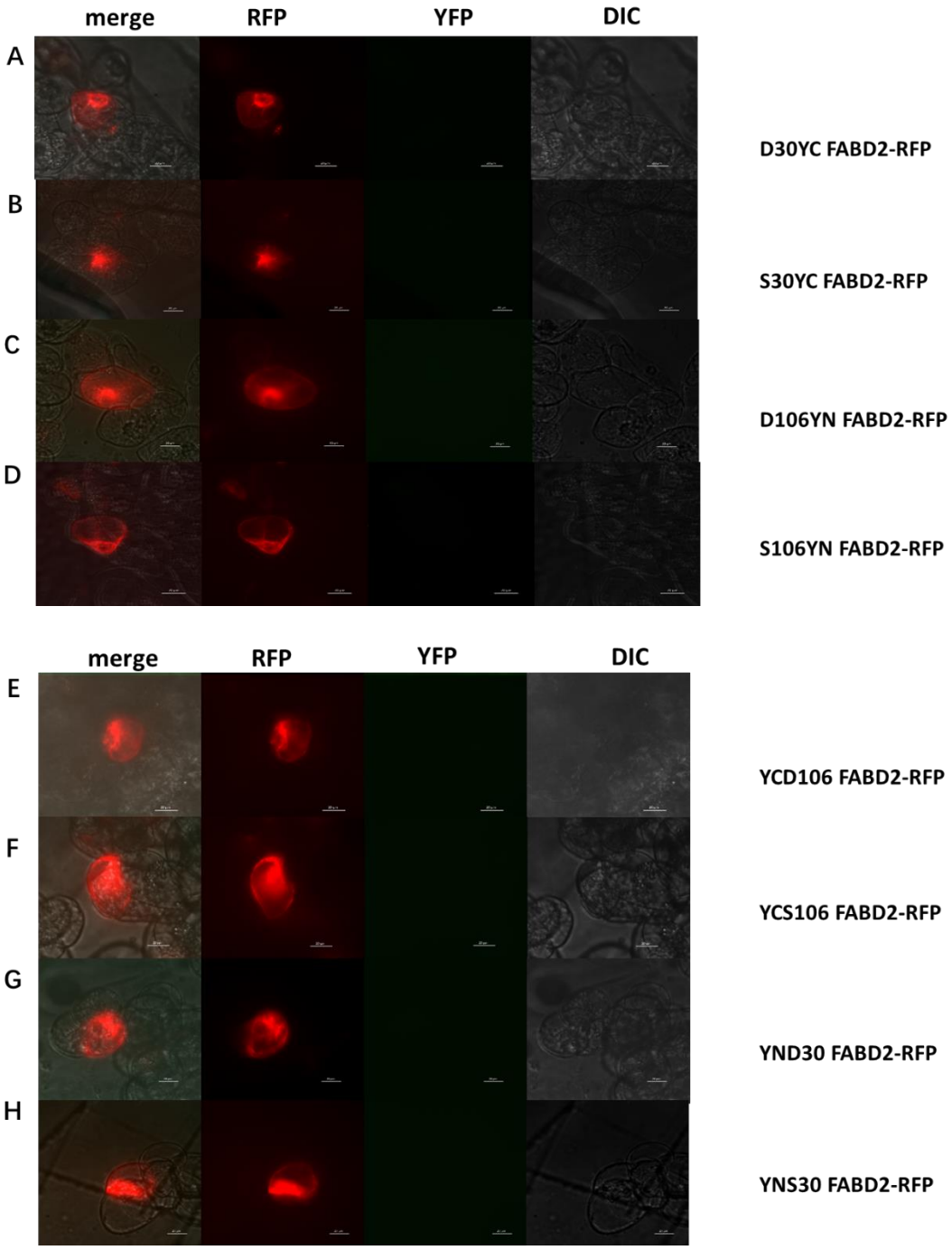

Supplementary Figure S8. Negative controls of protein interaction between two alleles of MYB30 and two alleles of MYB106 in the *V. vinifera* cv. 'Pinot Noir' cells by BiFC. **A** D30YC FABD2-RFP **B** S30YC FABD2-RFP **C** D106YN FABD2-RFP **D** S106YN FABD2-RFP **E** YCD106 FABD2-RFP **F** YCS106 FABD2-RFP **G** YND30 FABD2-RFP **H** YNS30 FABD2-RFP.

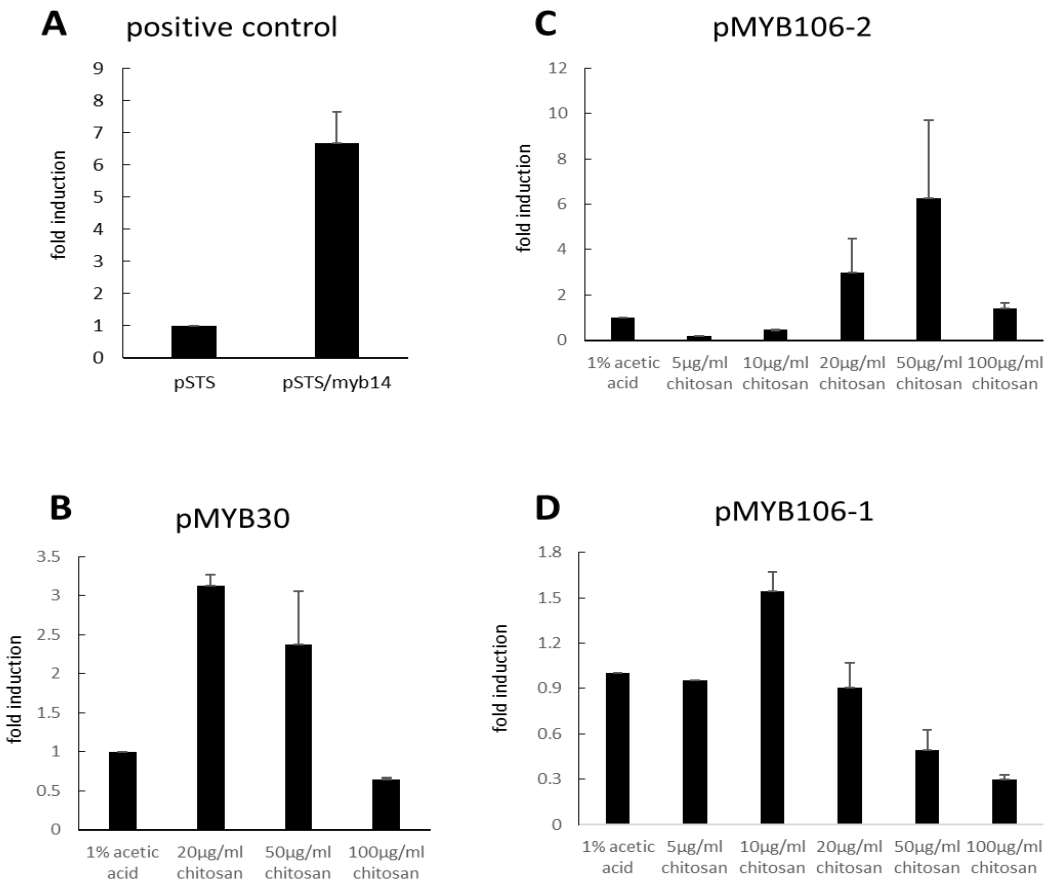

Supplementary Figure S9. The promoter activity of two alleles MYB106 and MYB30 in time course of chitosan treatment. **A** The fold induction of promoter activities STS with MYB14 as the positive control **B** the promoter of MYB30 activity after 1% acetic acid, 20μg/ml chitosan,50μg/ml chitosan, and 100μg/ml chitosan treatments. **C** pMYB106-1 promoter activity after 1% acetic acid, 5μg/ml chitosan,10μg/ml chitosan 20μg/ml chitosan,50μg/ml chitosan, and 100μg/ml chitosan treatments. **D** pMYB106-2 promoter activity after 1% acetic acid, 5μg/ml chitosan,10μg/ml chitosan 20μg/ml chitosan,50μg/ml chitosan, and 100μg/ml chitosan treatments. 1 independent experimental series.

D-MYB106 coding sequence variation in Ke114 and Ke35

Red labels show the SNP sites between the D type and S type of MYB106 in Ke114 and Ke35

>ATGGGAGGATCTCCCTGCTGCGACACCACCGCCTTGAAACGTGGCCCTTG
GAAGCCTGAAGAAGACCGAAAGCTCCTATCCTACATCCAAGAACACGGCC
ATGGGAGCTGGCGGTGCGTGCCCGAGAATGCTGGTCTTCAAAGGTGTGGG
AAGAGCTGCAGACTGAGATGGACGAACTACCTCAGACCTGATATCAAGAG
AGGCAAATTCAGCTTACGGGAAGAGCAGACCATTATTCAACTTCATGCTCT
TCTAGGCAACAGGTGGTCAGCTATAGCAACCCACTTACCAAATAGAACAGA
CAATGAGATCAAGAATTATTGGAACACACATCTCAAGAAAAGGTTGGCCAA
GATGGGAATAGACCCTGTAACTCATAAGCCCAGCCATGCCGTTCTAACCTC
CCCTAATGGTGACTCAAAGAACGCAGCTAACCTCAGCCACATGGCTCAATG
GGAGAGCGCCCGGCTCGAAGCCGAAGCCAGGCTGGTCAAAGATTCAAAA
CTCCGCCAAACTCAGCATGCCTCTGCTTCTGCTCCTGCTCCGGCTCAGCTG
CTTAACAAAATGGCTACTAGGCTTACACCTCCGCGTCGTCTTGACGTACTAA
ATGCATGGGAAAATGTGGGATCAAAATTGAAGATTGGCAGCAGCGGTAGTA
ACCGTGATATCCCATCACCAACCTCAACGTTGAGCTTCCTGGAAAACGTTT
CAACAATTTCAAGAGTGGAATCCTCTGAAATCACTGGAATTTTGGGCACGT
TAGGGACTGAAATCGACGCGTTTGGGACACAACAATGTGACATCAATATGA
CATGGACCATGGAATCTACTGATGAAAATGCGAATTTCGTTCATCTTCTTCT
TAGTAGGTCTGGTGACGGCATCCTCACCAACAACGGTGGAAGAGATGGTG
AAGAACTTGAAGACAACAAGAATTATTGGAATGACATTATGAATTTGATGA
CCTGCCAACCATCCCGTTCGCCCAACTTCTAA

S-MYB106 coding sequence variation in Ke114 and Ke35

Red labels show the SNP sites between the D type and S type of MYB106 in Ke114 and Ke35

>ATGGGAGGATCTCCCTGCTGCGACACCCCCGCCTTGAAACGTGGCCCTTG
GAAGCCTGAAGAAGACCGGAAGCTCCTAGCCTACATCCAAGAACACGGCC
ATGGGAGCTGGCGGTGCGTGCCCGAGAATGCTGGTCTTCAAAGGTGTGGG
AAGAGCTGCAGACTGAGATGGACGAACTACCTCAGACCTGATATCAAGAG
AGGCAAATTCAGCTTACGGGAAGAGCAGACCATTATTCAACTTCATGCTCT
TCTAGGCAACAGGTGGTCAGCTATAGCAACCCACTTACCAAATAGAACAGA
CAATGAGATCAAGAATTATTGGAACACACATCTCAAGAAAAGGTTGGCCAA
GATGGGAATAGACCCTGTAACTCATAAGCCCAGCCATGCCGTTCTAACCTC
CCCTAATGGTGACTCAAAGAACGCAGCTAACCTCAGCCACATGGCTCAATG
GGAGAGCGCCCGGCTCGAAGCCGAAGCCAGGCTGGTCAAAGATTCAAAA
CTCCGCCAAACTCAGCATGCCTCTGCTTCTGCTCCTGCTCCGGCTCAGCTG
CTTAACAAAATGGCTACTAGGCTTACACCTCCGCGTCGTCTTGACGTACTAA
ATGCATGGGAAAATGTGGGATCAAAATTGAAGAtTGGCAGCAGCGGTAgTA
ACCGTGAtATCCCATCACCAACCTCAACGTTGAgCTTCCTGGAAAACGTTTC
AACAATTTCAAGAGTGGAATCCTCTGAAATCACTGGAATTTTGGGCACGTT

AGGGACTGAAATCGACGCGTTTGGGACACAACAATGTGACATCAATATGAC
ATGGACCATGGAATCTACTGATGAAAATGCGAATTTCGTTCATCTTCTTCTT
AGTAGGTCTGGTGACGGCATCCTCACCAACAACGGTGGAAGAGATGGTGA
AGAACTTGAAGACAACAAGAATTATTGGAATGACATTATGAATTTGATGAC
CTGCCAACCATCCCGTTCGCCCAACCTCTAA

D-MYB30 coding sequence variation in Ke114 and Ke35

Red labels show the SNP sites between the D type and S type of MYB30 in Ke114 and Ke35

>ATGGGGAGGCCACCTTGCTGTGACAAGATCGGGGTGAAGAAAGGGCCAT
GGACTCCTGAAGAGGACATCATCTTGGTCTCTTACATTCAAGATCATGGTCC
AGGGAATTGGAGAGCAGTTCCTCCTAGCACAGGTCTGCTTAGATGCAGTAA
GAGTTGCAGGCTTAGATGGACTAATTATCTCCGCCCGGGTATCAAACGCGG
TAACTTTACTGATCAGGAGGAGAAGATGATAATCCACCTCCAGGCTCTTTTG
GGCAATAGATGGGCTGCCATAGCTTCTTATCTTCCTCAGAGAACGGACAAT
GATATAAAAAATTATTGGAACACCCATTTGAAAAAGAAGCTGAAGAAGTTT
CCCACAGGTGTAGATGACCATAATCAAGATGGGTTTTCAATCTCCAAAGGT
CAGTGGGAGAGAAGGCTTCAAACAGACATCCACATGGCTAAACAAGCGCT
ATGTGAGGCTTTGTCCATAGATACGTCAAGCTCGCTGCCTGACTTGAAGAG
CTCTAACGGCTACAACCCTAACACCAGACCTGTCCAAGCATCTACATATGC
ATCCAGTGCTGAAAACATAGCCAAATTGCTGGAAGGTTGGATGAGAAATTC
ACCAAAATCAACTCGAACGAATTCTGAAGCTACTCAGAACTCCAAAAACT
CCAGTGAAGGGGCAACTACACCAGATGCTCTTGACTCGTTGTTTAGCTTCA
ACTCTTCCAACTCTGATCTTTCTCTGTCTAATGATGAGACAGCAAATTTCAC
ACCCGAAACCATTCTCTTCCAAGATGAAAGCAAGCCAAATTTGGAGACTC
AAGTCCCTCTCACAATGATAGAGAAATGGCTCTTTGATGAAGGTGCTGCTA
CTCAAGAACAAGAAGACCTAATTGACATGTCACTAGAGGACACTGTTCAG
CTCTTCTAG

S-MYB30 coding sequence variation in Ke114 and Ke35

Red labels show the SNP sites between the D type and S type of MYB30 in Ke114 and Ke35

>ATGGGGAGGCCACCTTGCTGTGACAAGATCGGGGTGAAGAAAGGGCCAT
GGACTCCTGAAGAGGACATCATCTTGGTCTCTTACATTCAAGATCATGGTCC
AGGGAATTGGAGAGCAGTTCCTACTAGCACAGGTCTGCTTAGATGCAGTAA
GAGTTGCAGGCTTAGATGGACTAATTATCTCCGCCCGGGTATCAAACGCGG
TAACTTTACTGATCAGGAGGAGAAGATGATAATCCACCTCCAGGCTCTTTTG
GGCAATAGATGGGCTGCCATAGCTTCTTATCTTCCTCAGAGAACGGACAAT
GATATAAAAAATTATTGGAACACCCATTTGAAAAAGAAGCTGAAGAAGTTT
CCCACAGGTGTAGATGACCATAATCAAGATGGGTTTTCAATCTCCAAAGGT

CAGTGGGAGAGAAGGCTTCAAACAGACATCCACATGGCTAAACAAGCGCT
ATGTGAGGCTTTGTCCATAGATACGTCAAGCTCGCTGCCTGACTTGAAGAG
CTCTAACGGCTACAACCCTAACACCAGACCTGTCCAAGCATCTACATATGC
ATCCAGTGCTGAAAACATAGCCAAATTGCTGGAAGGTTGGATGAGAAATTC
ACCAAAATCAACTCGAACGAATTCTGAAGCTACTCAGAACTCCAAAAACT
CCAGTGAAGGGGCAACTACACCAGATGCTCTTGACTCGTTGTTTAGCTTCA
ACTCTTCCAACTCTGATCTTTCTCTGTCTAATGATGAGACAGCAAATTTCAC
ACCCGAAACCATTCTCTTCCAAGATGAAAGCAAGCCAAATTTGGAGACTC
AAGTCCCTCTCACAATGATAGAGAAATGGCTCTTTGATGAAGGTGCTGCTA
CTCAAGAACAAGAAGACCTAATTGACATGTCACTAGAGGACACTGCTCAG
CTCTTCTAG

D-MYB106 protein sequence variation in Ke114 and Ke35

Highlight parts show the amino acid differences between the D type and S type of MYB106 in Ke114 and Ke35

>MGGSPCCDTTALKRGPWKPEEDRKLLSYIQEHGHGSWRCVPENAGLQRCG
KSCRLRWTNYLRPDIKRGKFSLREEQTIIQLHALLGNRWSAIATHLPNRTDNEI
KNYWNTHLKKRLAKMGIDPVTHKPSHAVLTSPNGDSKNAANLSHMAQWES
ARLEAEARLVKDSKLRQTQHASASAPAPAQLLNKMATRLTPPRRLDVLNAW
ENVGSKLKIGSSGSNRDIPSPTSTLSFLENVSTISRVESSEITGILGTLGTEIDAFG
TQQCDINMTWTMESTDENANFVHLLLSRSGDGILTNNGGRDGEELEDNKNY
WNDIMNLMTCQPSRSPNF

S-MYB106 protein sequence variation in Ke114 and Ke35

Highlight parts show the amino acid differences between the D type and S type of MYB106 in Ke114 and Ke35

>MGGSPCCDTPALKRGPWKPEEDRKLLAYIQEHGHGSWRCVPENAGLQRCG
KSCRLRWTNYLRPDIKRGKFSLREEQTIIQLHALLGNRWSAIATHLPNRTDNEI
KNYWNTHLKKRLAKMGIDPVTHKPSHAVLTSPNGDSKNAANLSHMAQWES
ARLEAEARLVKDSKLRQTQHASASAPAPAQLLNKMATRLTPPRRLDVLNAW
ENVGSKLKIGSSGSNRDIPSPTSTLSFLENVSTISRVESSEITGILGTLGTEIDAFG
TQQCDINMTWTMESTDENANFVHLLLSRSGDGILTNNGGRDGEELEDNKNY
WNDIMNLMTCQPSRSPNL

D-MYB30 protein sequence variation in Ke114 and Ke35

Highlight parts show the amino acid differences between the D type and S type of MYB30 in Ke114 and Ke35

>MGRPPCCDKIGVKKGPWTPEEDIILVSYIQDHGPGNWRAVPPSTGLLRCSKS
CRLRWTNYLRPGIKRGNFTDQEEKMIIHLQALLGNRWAAIASYLPQRTDNDI
KNYWNTHLKKKLKKFPTGVDDHNQDGFSISKGQWERRLQTDIHMAKQALC
EALSIDTSSSLPDLKSSNGYNPNTRPVQASTYASSAENIAKLLEGWMRNSPKS
TRTNSEATQNSKNSSEGATTPDALDSLFSFNSSNSDLSLSNDETANFTPETILFQ
DESKPNLETQVPLTMIEKWLFDEGAATQEQEDLIDMSLEDTVQLF

S-MYB30 protein sequence variation in Ke114 and Ke35

Highlight parts show the amino acid differences between the D type and S type of MYB30 in Ke114 and Ke35

>MGRPPCCDKIGVKKGPWTPEEDIILVSYIQDHGPGNWRAVPTSTGLLRCSKS
CRLRWTNYLRPGIKRGNFTDQEEKMIIHLQALLGNRWAAIASYLPQRTDNDI
KNYWNTHLKKKLKKFPTGVDDHNQDGFSISKGQWERRLQTDIHMAKQALC
EALSIDTSSSLPDLKSSNGYNPNTRPVQASTYASSAENIAKLLEGWMRNSPKS
TRTNSEATQNSKNSSEGATTPDALDSLFSFNSSNSDLSLSNDETANFTPETILFQ

DESKPNLETQVPLTMIEKWLFDEGAATQEQEDLIDMSLEDTAQLF

Promoter sequence of MYB30 in Ke114 and Ke35

Highlight parts with different colors show the cis-acting regulatory elements (Lescot et al., 2002)

>TTTTCGGTATTTTTACTCGATTGTGATTCTCTTCTTATTTATGAAAATTTG
AATTTTAAAATTAATGTAAAAATAAATTTAAGACAAATTTTGGGACATATT
TTTTTATATATTTTTTTCTCAAAAAAGGAAAAACTTATGTTAAAGAAGAGT
TGCCAACGTATCCAAAAGGTTGCTAAAAATGAGGTATACAAACACAACTT
TTCCACTTCGGAAATATATATGTATATATTTTTTTTGCAAAAAAGACACAA
GCAAGAAAGAAAAAAAAAAACGCCCATCGTCCATATTCATTTTGTCTTCTA
CTGGGAACAATTAGAGGCATGAACAATGGGTAGATGACGAAAGGGGTAG
ATGCATTCACAGTATGGAGAGCATGTGTGCGTCCATATCAGCTTCTTTCCA
CCCAAGAAATTAAACAAAAACTGTGAAAGTGGACAATAGTCAAAAACAG
CGTGCTTATACATTTATGAATCCAACATCAAGTCTTCTCCCTTCTCCCTTCT
CTCTTCTCTCTTCTCTCTTCTCTCTTCTATGAGTCTTATCTTTTCTGTGTCTT
CTGTCTCGCTAACTGCTCATTAATCATCCACTACTGCGTATGTGTATGCAC
ACCTCACAGTCAATTAGTCATAGACTCGTAGATAAGTTTTGCAACCCTTCT
TACCCATGCAGGTCACAATCTTCTGACGCAGTTTTCAACCATCACCACGTA
TCAGTCTTTTGTACCTATCCCTTGTTTGTTAGGTTTTTATTTTCCATCCCTAT
AAATCCTCTTTCAAACTCTCACTGATTACTTTTCAAGGTGTTTGCATTCATA
CCCTAAAAGATTCTCTGGTAACTAAAGTGGATTTTTTTCTTTTTTTGAGGC
GGGGCTATGGTTGCCCATCATAGGGGGTGAATCCTGAAGGAACAAAGTAG
AGGCATTACTCAATTAAAAAAATGGGTTGGGATGATTTACAAGTTTTATAT
ATGGATTGAACTACAATGATCATGTTTCCTAATATGAACGCAATGAAAGT
AGACCACGGATGAGGGGCTCCACAGTCCTCACGGCTAAGCTAAGCTCTCA
TATTCCATCCTTTTCTGAATTGAATGATGGGCCCCTAACAAGCCTAATATG
GGGAGTCCTCCAAAGTAATCCTCTCTCCCTCTCCCTCTGTCTATTCAAAAT
TTCAAATTTTCCACACATTGAACGCTATCCACATCACCCCCTTCCCACGTC
GTGCACACAACCTCAGAATCAAAAGGTACCTGCCGACTCCGTTGTTTTTCT
AAAGCTAATAAATCTTCTGGAACATGCAATAGTATATTTCTTATGCAGCTA
GCCATGAAATCGGTTTTCAATTTCCACTGTTCACATTGATTTTCTGATGAA
TCTAGTTGTAATGCCGTAACGCACACAAACCCAATTTGTGACGCCTAGGG
CCACTGGCCAAATTGGAGATTCACAAAGTTGATAATTAGTGGTGTAGTTA
CACAAATTCTGAATAATTAATTCTAGGCTTCCCTCCTAACTATAGTAGTCA
CATGGTGTCTAAATCCAAATACATGCATATTGGCTACATGTATCACCTCTT
ATCTATTCCTAAATGAAGCCGTCCTTTCAGCCATTATAACTATGTGATGAA
TAACAATATTTTCATGGACAACGAGTGCCGTGTGGTTTCACTCGGTACAGC
TCTTTTCATGTACTCTTTCCCCCAGATGATGACTATGCTTGATGCATATATA
CATATATAGATATACGCACAACTATATTTCATGGTACCATAGAATATCAAT
TGGTAATTAAGTTGTTGATCTAGTAGTGGACATTAATATAGGTGAGGCAG
ACAACTGAGGAGTGGATTGTGAGTTGAGACAAACCCAACTTGGCCATAAC
CTCCATGGAATGGATCCACTTGGAATGCACGTATCACAAGTACCAAATCA
ATGTATTGCAAGGACGTACACTTCCATCTTCCGAAATTGGGTATGATCTGA
AATTCGTAATTAGAAGAATTAGATGGATCATGGACGGACACATTTTTTTTA

ATGTGCATGCACCTCTGTGTTCAATAATCACCACCACATGGGCAGCTTTGC
AGTATCCATGCAACGGAAGTTAAAAGAGCCTTTTAGCCCATAATAGAAAC
TCATCACTGTCAGGCGCACATTACCGGAATGGAGGCCTACTTGAATTTCA
AAACATCTAAGGGCTTGTGAAGTGTTTTTAGAAAACGGTTTTTGTACCATT
TTTCATCTTTCGAAACATGTTTGATAATTTATTTTAATTTTTTTTTTGGGAG
TAGGAGTAAGTAGAACCCTATTAAAAAACATGGTCCTCCCGACCTTACTA
AAATTGGGTTACTCACGAAAATATCAAGACTGTTACATGGTACTATACTTG
GATGCCATAAAATTATTGATTTGTCCATTTGACAGATTAATCTCTAATGGG
AAGCCCTCCCTAGAGAAAAAATGGCGTACTGATACCTAATCAATTCACCT
AAAGCAGTAAGGGGGAAGCAAGGGTTTTCGTTTTTTACTTTTCTGGGGAG
TGGGAGTAAGTGGAATTACCGTATTGAATGCGACGCGGTTTTGTGAGGTG
GAGAGAGGTGACACAAAGGAGAAGCTGACTTTTTGCAAGGGAAGAGTAA
ATGCATGCTGTACTGTTTTGACTCGTAAGAAAGAATCCATTTACCTCACTT
TGGTCAGCGTAGCCAGCCTATATATGCCCACCTGGACAAGGAAGCCCTTGC
CTTGGACGCTTGTCTCCACATTTCCAAAGTTGAAACGCTAAGGAAAAGAC
CTTTGTCTGGAAACCCTTCCACAACTCAGAGAGAGAGAGCGAAAAGC

BOX4 Function: part of a conserved DNA module involved in light responsiveness

CGTCA-motif and TGACG-motif Function: cis-acting regulatory element involved in the MeJA-responsiveness

GA motif ,I box, TCCC-motif and TCT-motif Function: part of a light responsive element

TCA-element Function: salicylic acid responsiveness

G-box Function: cis-acting regulatory element involved in light responsiveness

CAT-box Function: meristem expression

MBS Function: MYB binding site involved in drought-inducibility

LTR Function: low-temperature responsiveness

CCAAT-box MYBHv1 binding site

A-box Function: cis -acting regulatory element

TATA-box Function: corepromoterelementaround-30oftranscriptionstart

MYB recognition site

CAAT-box Function: common cis-acting element in promoter and enhancer regions

ABRE Function: cis-acting element involved in the abscisic acid responsiveness

MRE Function: MYB binding site involved in light responsiveness

P-box Function: gibberellin-responsive element

The first allele promoter sequence of MYB106 (named proMYB106-1) in Ke114 and Ke35

Highlight parts with different colors show the cis-acting regulatory elements (Lescot et al., 2002)

Red labels show the insert sites between the proMYB106-1 and prroMYB106-2

Orange labels show the SNP sites between the proMYB106-1 and prroMYB106-2

>ATCATTCCCGTGCCCCCAACGACTCTCTCTCTCTCTCTCAGTAGACAGTAC
CCTCTTCTTATGCCTATTTGTTTGCCATAGGGCATTGCCTTTTTTTGAGCACC
TCTATGGCTACCTTATATCTGCTCAATAAAGAAAAGTCTACGCCTCTCCTGG
CTCCTGGCTCCCGGCTTCCCTGGTAATTTGAGATAAGTCATTTATGTATCTAC
TTTGTTATCCTTCAAAATCATGCATAAGTCCCCTGTTGCCCGCAACGTTTAA
AATATAAAAAATATGACAATATCAATAATTGAATCTCATGGAAATATCCGATA
AAAATTTGAATAAACAATATCCATAAAGTAATCGATTAAAACTCATAAAATT
ATAAAAAAAAACCTTAAAAAAATAAAATAAATGATAATAAACAAATAAATT
GTTTTATTGAAGAAAATTATATATAACATTCCATATAATAATTGTAATATATGTA
TAATTATCATTTTTATTTGATTTTTTTAATCTTATTTATAAATTTATATTTCTTTT
GTATTATGTATTATATAAGATTCATGATTTTTGTATTTTTAATAAATGAAATTTG
AAGGGCCAAGTTCGGGCCTTTGATTGTATTTAAAATATATTTTATTGCATTAA
ATATTATAATAGTTAGTTTGAACATTATCTTGGAAGGGGATAATAATTTAATTA
TTATTTCATTTTTTATATAGATATAAAATTAAAACTTTAGGTTTAGAAGGCAA
ATAGAAAAAAGTACATATGGATGGTTTTATGTTATCAAATCCTAAATTACAA
GGCATGCATTGCTTGGCAGATAATAATGTTCAAACCCCAAGTCCTTGATGTG
AAGTTATAAAATGGCCAACGTATCTACCATTAATCTAAAAAATTGTGATAAA
TTCATGAAAAATTGGAGATATATTGTGGGCAATTCAAAGGTATTACGATAAA
TTAAATATAAAAAAAATATGATTTTGTTTTTTAAGATTACTAAAATATGACATAT
TGAGTAAAAATTCATAAAAAATAAATGGTTTTTTTAATCATTGGTTTTGTTTG
AATCATTTATAAGTTGTAGAATCTCCTTGATTCTTTTCCCTTTTGCATTGCTC
ATTTTATTGCATGTGGAGGGTGGTGAAATAACTCCTTGACTAATCTTGTCTA
ATCAGCCTCTAAGTCTTGTAATTTTTGGGCTAGTGCCTTACTTCTTTTGATCA
ATTCCTTCGTTCTCACAAGATCTCCTCCTATTCTTCACTTATCCTCTTCTCCA
TCGTGGTTATTTGCTCTTGTGGTTGTACCAAATGTGGAAGATCCTCTTACAT
TTGCCTACCATTTGTGTAAGTTTGCAGCATGACTATGTTTCAAGCTTTTCAAT
CATTCCCATAGGTTGCTCTAATAGGTTATGCTCTCTTCAAAAGACAACGAGT
TTATTCCATAATACAAACTTCTTTTGCAATATGGAAGATGACAATTAGAGTG
AGAAAGTTAGTTAGGTTGACAATCTTTCTTAGAGGATAAGTCAATCATATGG
AAGACATGAAAGATAATAGTTATAATGAAAACTTAAGCTACCAAAAATTGG
ACTATCACGAGAATGGTCTAACTTAAAAACTCAAGGGTACACAAAATTCAC
CTCACCTCAAAATAAGGATCATAGAAAGAGATAACGTCCTTGCAGGTTGAC
CTGACCAATTAACCCGCACCTAAAAAGATGAGTTTAACTGCTCTTATCCTCA
TATGCCCAAAAGTCAACAAAGTTTATAATAACCCGTAAAAAAAGTATGTCT
CTTTACGAGATTTACCTATATCTACAAAGGAAGAATGCTTAAAAAGGAAGT
CATAGACAATAAGAGAAGGTTTGGAAAGGGAAAATTAATAATTTTTAGTTAT

TCATGAAGATCTTTGAGCATCTTCAAAAACCATGGTTTTTAGATGTAAATTC
AAACCTTTTTTTTATAAAAATAAAAGATAAATGGCGAGACAAAATAACCATT
TTGAACCATTGTTTCAAAAGGTTACCACAATACCTTACCGTAGTGGTCAAG
TTGGAACCAAAACTCCATATTTTTCTCCAGCTTGTCAGAGTTAGTAGCCAG
AAATGAATAAAATGCCACCTAAATTGACTGGCAACATTTATCAGTATTGTAA
GATATGACATGACCGTGGAATTTATAATATTCGTCCTTGGTGGGTACCTTTCG
GGTCATGGGCTTAGGCTAAAATTTAAGAACAAGTTCAGAAAACTTATGAAT
TGGAGACTCTAGACCAAAATATTGGTACGGTAAGTAAGGGTCTATGACCTA
AACTTACTTCTTTGGGTCACCACCGATATTTTGCCCCTTTGGGTCATCACTG
ATAAAGTTAATTGCCAATCAATTACCATGCATACACGTAACGTTATTGTTCAT
GCATCAATGGGAGTCAGGGAGGTTCCTTTCAGAATCGGTCCCCTTGGTTAC
AGGAGCCATATTAATGGTGTACAATTAATGGATGGTGATGTGTTGTAGAGGA
ACTTACACTCTAAACAATTAAAAGCTGGGGTACGGGTTTTTCATAACCTTCA
TCCAGGACGGCACAGTGATTGGAACAAGCTATGGGAGACGAATTAACCAC
AGTAAAATGATAGGGAATGGTTGGACAGTGTAGCTGTGTAACAATGATTTAT
TTGCTATGTTCTAATCGCTTAATTTTAAAAATTAATGGGTGGATAAGTTCAGA
AGGATGTGTGTTTTTTTGGTTTAGATGAGGTAAAAATCTGTCTTCCATAAAG
AGCAGGGCAGGGGTAGGGGCAGTATGCCACTAATTACAGAGGTTTACACA
ATTTAATGGAATTCAATACTTTATCCCATAAATAGTGCTGATCGTTGCCCATT
TCTCTATCCTCTGGTGTCTCCCATTTTTCTAACAAACTCCCTTTCCATCTCCT
GATCATCATCATTCACCTCAAAGAAGCTTCTTATATCCAGCTGCCTCATTCTG
CTTTGCTCGCCGTGTCACTGGGCACTCCCTCAAA

A-box Function: cis -acting regulatory element

AACA motif Function: involved in endosperm-specific negative expression

ABRE Function: cis -acting element involved in the abscisic acid responsiveness

Box 4 motif and ATC motif Function: part of a conserved DNA module involved in light responsiveness

CAT-box Function: cis-acting regulatory element related to meristem expression

CAAT-box Function: common cis-acting element in promoter and enhancer regions

G Box, GT1-motif, GATA-motif, LAMP element and TCT-motif Function: part of a light responsive element

HD-Zip 1 Function: element involved in differentiation of the palisade mesophyll cells

LTR Function: low-temperature responsiveness

MYB binding site

MRE Function: MYB binding site involved in light responsiveness

P-box Function: gibberellin-responsive element

TATC-box Function: cis-acting element involved in gibberellin-responsiveness

TCA-element Function: cis-acting element involved in salicylic acid responsiveness

TGA-element Function: auxin-responsive element

TATA-box Function: core promoter element around -30 of transcription start

The second allele promoter sequence of MYB106 (named proMYB106-2) in Ke114 and Ke35

Highlight parts with different colors show the cis-acting regulatory elements (Lescot et al., 2002)

Red labels show the insert sites between the proMYB106-1 and prroMYB106-2

Orange labels show the SNP sites between the proMYB106-1 and prroMYB106-2

>ATCATTCCCGTGCCCCCAACGACTCTCTCTCTCTCTCTCTCAGTAGACAGT
ACCCTCTTCTTATGCCTATTTGTTTGCCATAGGGCATTGCCTTTTTTTGAGCA
CCTCTATGGCTACCTTATATCTGCTCAATAAAGAAAAGTCTACGCCTCTCCT
GGCTCCTGGCTCCCGGCTTCCCTGGTAATTTGAGATAAGTCATTTATGTATCT
ACTTTGTTATCCTTCAAAATCATGCATAAGTCCCCTGTTGCCCGCAACGTTT
AAAATATAAAAAATATGACAATATCAATAATTGAATCTCATGGAAATATCCGA
TAAAAATTTGAATAAACAATATCCATAAAGTAATCGATTAAAACTCATAAAA
TTATAAAAAAAAACCTTAAAAAAATAAAATAAATGATAATAAACAAATAAAT
TGTTTTATTGAAGAAAATTATATATAACATTCCATATAATAATTGTAATATATGT
ATAATTATCATTTTTATTTGATTTTTTTAATCTTATTTATAAATTTATATTTCTTT
TGTATTATGTATTATATAAGATTCATGATTTTTGTATTTTTAATAAATGAAATTT
GAAGGGCCAAGTTCGGGCCTTTGATTGTATTTAAAATATATTTTATTGCATTA
AATATTATAATAGTTAGTTTGAACATTATCTTGGAAGGGGATAATAATTTAAT
TATTATTTCATTTTTTATATAGATATAAAATTAAAACTTTAGGTTTAGAAGGCA
AATAGAAAAAAGTACATATGGATGGTTTTATGTTATCAAATCCTAAATTACA
AGGCATGCATTGCTTGGCAGATAATAGTGTTCAAACCCCAAGTCCTTGATGT
GAAGTTATAAAATGGCCAACGTATCTACCATTAATCTAAAAAATTGTAATAA
ATTCATGAAAAATTGGAGATATATTGTGGGCAATTCAAAGGTATTACGATAA
ATTAAATAAAAAAAATATGATTTTGTTTTTTAAGATTACTAAAATATGACACA
TTGAGTAAAAATTCATAAAAAATAAATGGTTTTTTTAATCATTGGTTTTGTTT
GAATCATTTATAAGTTGTAGAATCTCCTTGATTCTTTTCCCTTTTGCATTGCT
CATTTTATTGCATGTGGAGGGTGGTGAAATAACTCCTAGACTAATCTTGTCT
AATCAGCCTCTAAGTCTTGTAATTTTTGGGCTAGTGCCTTACTTCTTTTGATC
AATTCCTTCGTTCTCACAAGATCTCCTCCTATTCTTCACTTATCCTCTTCTCC
ATCGTGGTTATTTGCTCTTGTGGTTGTACCAAATGTGGAAGATCCTCTTACA
TTTGCCTACCATTTGTGTAAGTTTGCAGCATGACTATGTTTCAAGCTTTTCA
ATCATTCCCATAGGTTGCTCTAATAGGTTATGCTCTCTTCAAAAGACAACGA
GTTTATTCCATAATACAAACTTCTTTTGCAATATGGAAGATGACAATTAGAGT
GAGAAAGTTAGTTAGGTTGACAATCTTTCTTAGAGGATAAGTCAATCATATG
GAAGACATGAAAGATAATAGTTATAATGAAAACTTAAGCTACCAAAAATTG
GACTATCACGAGAATGGTCTAACTTAAAAACTCAAGGGTACACAAAATTCA
CCTCACCTCAAAATAAGGATCATAGAAAGAGATAACCTCCTTGCAGGTTGA
CCTGACCAATTAACCCGCACCTAAAAAGATGAGCTTAACTGCTCTTATCCTC
ATATGCCCAAAAGTCAACAAAGTTTATAATAACCCGTAAAAAAAGTATGTCT
CTTTACGAGATTTACCTATATCTACAAAGGAAGAATACCTAAAAAGGAAGTC
ATAGACAATAAGAGAAGGTTTGGAAAGGGAAAATTAATAATTTTTAGTTATT

CATGAAGATCTTTGAGCATCTTCAAAAACCATGGTTTTTAGATGTAAATTCA
AACCTTTTTTTTTATAAAAATAAAAGATAAATGGCGAGACAAAAATAACCAT
TTTGAACCATTGTTTCAAAAGGTTACCACAATACCTTACCGTAGTGGTCAA
GTTGGAACCAAAACTCCATATTTTTCTCCAGCTTGTCAGAGTTAGTAGCCA
GAAATGAATAAAATGCCACCTAAATTGACTGGCAACATTTATCAGTATTGTA
AGATATGACATGACCGTGGAATTTATAATATTCGTCCTTGGTGGGTACCTTTC
GGGTCATGGGCTTAGGCTAAAATTTAAGAACAAGTTCAGAAAAGTTATGAA
TTGGAGACTCTAGACCAAAATATTGGTACGGTAAGTAAGGGTCTATGACCT
AAACTTACTTCTTTGGGTCACCACCGATATTTTGCCCCTTTGGGTCATCACT
GATAAAGTTAATTGCCAATCAATTACCATGCATACACGTAACGTTATTGTTCA
TGCATCAATGGGAGTCAGGGAGGTTCCTTTCAGAATCGGTCCCCTTGGTTA
CAGGAGCCATATTAATGGTGTACAATTAATGGATGGTGATGTGTTGTAGAGG
AACTTACACTCTAAACAATTAAAAGCTGGGGTACGGGTTTTTCATAACCTTC
ATCCAGGACGGCACAGTGATTGGAACAAGCTATGGGAGACGAATTAACCA
CAGTAAAATGATAGGGAATGGTTGGACAGTGTAGCTGTGTAACAATGATTT
ATTTGCTATGTTATAATCGCTTAATTTTAAAAATTAATGGGTGGATAAGTTCA
GAAGGATGTGTGTTTTTTTGGTTTAGATGAGGTAAAAATCTGTCTTCCATAA
AGAGCAGGGCAGGGGTAGGGGCAGTATGCCACTAATTACAGAGGTTGACA
CAATTTAATGGAATTCAATACTTTATCCCATAAATAGTGCTGATCGTTGCCC
ATTTCTCTATCCTCTGGTGTCTCCCATTTTTCTAACAAACTCCCTTTCCATCT
CCTGATCATCATCATTCACCTCAAAGAAGCTTCTTATATCCAGCTGCCTCATT
CTGCTTTGCTCGCCGTGTCACTGGGCACTCCCTCAAA

A-box Function: cis -acting regulatory element

AACA motif Function: involved in endosperm-specific negative expression

ABRE Function: cis-acting element involved in the abscisic acid responsiveness

Box 4 motif and ATC motif Function: part of a conserved DNA module involved in light responsiveness

CAT-box Function: cis-acting regulatory element related to meristem expression

CAAT-box Function: common cis-acting element in promoter and enhancer regions

G Box, GT1-motif, GATA-motif, LAMP element and TCT-motif Function: part of a light responsive element

HD-Zip 1 Function: element involved in differentiation of the palisade mesophyll cells

LTR Function: low-temperature responsiveness

MYB binding site

MRE Function: MYB binding site involved in light responsiveness

P-box Function: gibberellin-responsive element

TATC-box Function: cis-acting element involved in gibberellin-responsiveness

TCA-element Function: cis-acting element involved in salicylic acid responsiveness

TGA-element Function: auxin-responsive element

TATA-box Function: core promoter element around -30 of transcription start

References

Alonso, J. M., Stepanova, A. N., Leisse, T. J., Kim, C. J., Chen, H., Shinn, P., … Joseph R. Ecker. (2003). Genome-Wide Insertional Mutagenesis of Arabidopsis thaliana. *Science*, *301*(5633), 653–657. https://doi.org/10.1126/science.1086391

Armijo, G., Schlechter, R., Agurto, M., Muñoz, D., Nuñez, C., & Arce-Johnson, P. (2016). Grapevine pathogenic microorganisms: Understanding infection strategies and host response scenarios. *Frontiers in Plant Science*, Vol. 7. https://doi.org/10.3389/fpls.2016.00382

Arnold, C., Schnitzler, A., Douard, A., Peter, R., & Gillet, F. (2005). Is there a future for wild grapevine (Vitis vinifera subsp. silvestris) in the Rhine Valley? *Biodiversity and Conservation*, Vol. 14, pp. 1507–1523. https://doi.org/10.1007/s10531-004-9789-9

Austin, C. N., & Wilcox, W. F. (2011). Effects of fruit-zone leaf removal, training systems, and irrigation on the development of grapevine powdery mildew. *American Journal of Enology and Viticulture*, *62*(2). https://doi.org/10.5344/ajev.2010.10084

Bach, L., Michaelson, L. V., Haslam, R., Bellec, Y., Gissot, L., Marion, J., … Faure, J. D. (2008). The very-long-chain hydroxy fatty acyl-CoA dehydratase PASTICCINO2 is essential and limiting for plant development. *Proceedings of the National Academy of Sciences of the United States of America*, *105*(38). https://doi.org/10.1073/pnas.0805089105

Barthlott, W., & Neinhuis, C. (1997). Purity of the sacred lotus, or escape from contamination in biological surfaces. *Planta*, *202*(1). https://doi.org/10.1007/s004250050096

Barthlott, Wilhelm, Neinhuis, C., Cutler, D., Ditsch, F., Meusel, I., Theisen, I., & Wilhelmi, H. (1998). Classification and terminology of plant epicuticular waxes. *Botanical Journal of the Linnean Society*, *126*(3). https://doi.org/10.1111/j.1095-8339.1998.tb02529.x

Beaudoin, F., Wu, X., Li, F., Haslam, R. P., Markham, J. E., Zheng, H., … Kunst, L. (2009). Functional characterization of the Arabidopsis β-ketoacyl-coenzyme a reductase candidates of the fatty acid elongase. *Plant Physiology*, *150*(3), 1174–1191. https://doi.org/10.1104/pp.109.137497

Beckett, A., & Read, N. D. (1986). Low-Temperature Scanning Electron Microscopy. In H. C. Aldrich & W. J. Todd (Eds.), *Ultrastructure Techniques for Microorganisms* (pp. 45–86). https://doi.org/10.1007/978-1-4684-5119-1_2

Bernard, A., Domergue, F., Pascal, S., Jetter, R., Renne, C., Faure, J. D., … Joubès, J. (2012). Reconstitution of plant alkane biosynthesis in yeast demonstrates that Arabidopsis ECERIFERUM1 and ECERIFERUM3 are core components of a very-long-chain alkane synthesis complex. *Plant Cell*, *24*(7). https://doi.org/10.1105/tpc.112.099796

Bernard, A., & Joubès, J. (2013, January). Arabidopsis cuticular waxes: Advances in synthesis, export and regulation. *Progress in Lipid Research*, Vol. 52, pp. 110–

129. https://doi.org/10.1016/j.plipres.2012.10.002

Bird, D. A. (2008). The role of ABC transporters in cuticular lipid secretion. *Plant Science*, Vol. 174. https://doi.org/10.1016/j.plantsci.2008.03.016

Bird, D., Beisson, F., Brigham, A., Shin, J., Greer, S., Jetter, R., … Samuels, L. (2007). Characterization of Arabidopsis ABCG11/WBC11, an ATP binding cassette (ABC) transporter that is required for cuticular lipid secretion. *Plant Journal*, *52*(3). https://doi.org/10.1111/j.1365-313X.2007.03252.x

Bonaventure, G., Salas, J. J., Pollard, M. R., & Ohlrogge, J. B. (2003). Disruption of the FATB gene in Arabidopsis demonstrates an essential role of saturated fatty acids in plant growth. *Plant Cell*, *15*(4). https://doi.org/10.1105/tpc.008946

Bourdenx, B., Bernard, A., Domergue, F., Pascal, S., Léger, A., Roby, D., … Joubès, J. (2011). Overexpression of Arabidopsis ECERIFERUM1 promotes wax very-long-chain alkane biosynthesis and influences plant response to biotic and abiotic stresses. *Plant Physiology*, *156*(1). https://doi.org/10.1104/pp.111.172320

Brewer, M. T., & Milgroom, M. G. (2010). Phylogeography and population structure of the grape powdery mildew fungus, Erysiphe necator, from diverse Vitis species. *BMC Evolutionary Biology*, *10*, 268. https://doi.org/10.1186/1471-2148-10-268

Burton, Z., & Bhushan, B. (2006). *Surface Characterization and Adhesion and Friction Properties of Hydrophobic Leaf Surfaces and Nanopatterned Polymers for Superhydrophobic Surfaces*. https://doi.org/10.1007/3-540-26910-x_3

Chen, N., Song, B., Tang, S., He, J., Zhou, Y., Feng, J., … Xu, X. (2018). Overexpression of the ABC transporter gene TsABCG11 increases cuticle lipids and abiotic stress tolerance in Arabidopsis. *Plant Biotechnology Reports*, *12*(5). https://doi.org/10.1007/s11816-018-0495-6

Chen, X., Goodwin, S. M., Boroff, V. L., Liu, X., & Jenks, M. A. (2003). Cloning and characterization of the WAX2 gene of Arabidopsis involved in cuticle membrane and wax production. *Plant Cell*, *15*(5). https://doi.org/10.1105/tpc.010926

Clark, J. B., & Lister, G. R. (1975). Photosynthetic Action Spectra of Trees: II. The Relationship of Cuticle Structure to the Visible and Ultraviolet Spectral Properties of Needles from Four Coniferous Species. *Plant Physiology*, *55*(2). https://doi.org/10.1104/pp.55.2.407

Clough, S. J., & Bent, A. F. (1998). Floral dip: A simplified method for Agrobacterium-mediated transformation of Arabidopsis thaliana. *Plant Journal*, *16*(6). https://doi.org/10.1046/j.1365-313X.1998.00343.x

Collinge, D. B. (2009). Cell wall appositions: The first line of defence. *Journal of Experimental Botany*, Vol. 60, pp. 351–352. https://doi.org/10.1093/jxb/erp001

Culberson, C. F., Martin, J. T., & Juniper, B. E. (1971). The Cuticles of Plants. *The Bryologist*, *74*(3). https://doi.org/10.2307/3241660

Czemmel, S., Stracke, R., Weisshaar, B., Cordon, N., Harris, N. N., Walker, A. R., … Bogs, J. (2009). The grapevine R2R3-MYB transcription factor VvMYBF1 regulates flavonol synthesis in developing grape berries. *Plant Physiology*, Vol. 151, pp. 1513–1530. https://doi.org/10.1104/pp.109.142059

Davies, B. H. (1980). Advances in the Biochemistry and Physiology of Plant Lipids.

Biochemical Society Transactions, *8*(2). https://doi.org/10.1042/bst0080236

DeBono, A. G. (2011). The role and behavior of Arabidopsis thaliana lipid transfer proteins during cuticular wax deposition. *UBC Thesis*, (November).

Delp, C. J. (1954). Effect of temperature and humidity on the Grape powdery mildew fungus. *Phytopathology*, *44*(11), 615-626 pp.

Doyle, J. ., & Doyle, J. . (1987). A rapid isolation procedure for small amounts of leaf tissue. *Phytochemical Bulletin*, *19*.

Duan, D., Fischer, S., Merz, P., Bogs, J., Riemann, M., & Nick, P. (2016). An ancestral allele of grapevine transcription factor MYB14 promotes plant defence. *Journal of Experimental Botany*, *67*(6), 1795–1804. https://doi.org/10.1093/jxb/erv569

Duan, D., Halter, D., Baltenweck, R., Tisch, C., Tröster, V., Kortekamp, A., … Nick, P. (2015). Genetic diversity of stilbene metabolism in Vitis sylvestris. *Journal of Experimental Botany*, *66*(11), 3243–3257. https://doi.org/10.1093/jxb/erv137

Dubos, C., Stracke, R., Grotewold, E., Weisshaar, B., Martin, C., & Lepiniec, L. (2010). MYB transcription factors in Arabidopsis. *Trends in Plant Science*, Vol. 15. https://doi.org/10.1016/j.tplants.2010.06.005

Edstam, M. M., Blomqvist, K., Eklöf, A., Wennergren, U., & Edqvist, J. (2013). Coexpression patterns indicate that GPI-anchored non-specific lipid transfer proteins are involved in accumulation of cuticular wax, suberin and sporopollenin. *Plant Molecular Biology*, *83*(6), 625–649. https://doi.org/10.1007/s11103-013-0113-5

Eigenbrode, S. D., & Espelie, K. E. (1995). Effects of plant epicuticular lipids on insect herbivores. *Annual Review of Entomology. Vol. 40*. https://doi.org/10.1146/annurev.ento.40.1.171

El-kenawy, M. (2017). Effect of Chitosan, Salicylic Acid and Fulvic Acid on Vegetative Growth, Yield and Fruit Quality of Thompson Seedless Grapevines. *Egyptian Journal of Horticulture*, *44*(1). https://doi.org/10.21608/ejoh.2017.1104.1007

Ellis, M. A. (2008). *Powdery Mildew of Grape*. 1–3.

English-Loeb, G., Norton, A. P., Gadoury, D. M., Seem, R. C., & Wilcox, W. F. (1999). Control of powdery mildew in wild and cultivated grapes by a tydeid mite. *Biological Control*, *14*(2). https://doi.org/10.1006/bcon.1998.0681

English-Loeb, G., Norton, A. P., Gadoury, D., Seem, R., & Wilcox, W. (2007). Biological control of grape powdery mildew using mycophagous mites. *Plant Disease*, *91*(4). https://doi.org/10.1094/PDIS-91-4-0421

Felsenstein, J. (1985). Confidence Limits on Phylogenies: An Approach Using the Bootstrap. *Evolution*, *39*(4). https://doi.org/10.2307/2408678

Fiebig, A., Mayfield, J. A., Miley, N. L., Chau, S., Fischer, R. L., & Preuss, D. (2000). Alterations in CER6, a gene identical to CUT1, differentially affect long-chain lipid content on the surface of pollen and stems. *Plant Cell*, *12*(10). https://doi.org/10.1105/tpc.12.10.2001

Franke, R., Höfer, R., Briesen, I., Emsermann, M., Efremova, N., Yephremov, A., & Schreiber, L. (2009). The DAISY gene from Arabidopsis encodes a fatty acid

elongase condensing enzyme involved in the biosynthesis of aliphatic suberin in roots and the chalaza-micropyle region of seeds. *Plant Journal*, *57*(1). https://doi.org/10.1111/j.1365-313X.2008.03674.x

Fulda, M., Shockey, J., Werber, M., Wolter, F. P., & Heinz, E. (2002). Two long-chain acyl-CoA synthetases from Arabidopsis thaliana involved in peroxisomal fatty acid β-oxidation. *Plant Journal*, *32*(1). https://doi.org/10.1046/j.1365-313X.2002.01405.x

Gadoury, D. M., Pearson, R. C., Riegel, D. G., Seem, R. C., Becker, C. M., & Pscheidt, J. W. (1994). Reduction of powdery mildew and other diseases by over-the-trellis applications of lime sulfur to dormant grapevines. *Plant Disease*, *78*(1). https://doi.org/10.1094/PD-78-0083

Gadoury, D. M., Seem, R. C., Pearson, R. C., & Wilcox, W. F. (2001). Effects of powdery mildew on vine growth, yield, and quality of Concord grapes. *Plant Disease*, *85*(2), 137–140. https://doi.org/10.1094/PDIS.2001.85.2.137

Gadoury, David M. (1990). Germination of Ascospores and Infection of Vitis by Uncinula necator. *Phytopathology*, *80*(11). https://doi.org/10.1094/phyto-80-1198

Gadoury, David M. (1991). Heterothallism and Pathogenic Specialization in Uncinula necator. *Phytopathology*, *81*(10). https://doi.org/10.1094/phyto-81-1287

Gadoury, David M., Cadle-Davidson, L., Wilcox, W. F., Dry, I. B., See, R. C., & Mil, M. G. (2012). *Grapevine powdery mildew (Erysiphe necator a fascinating.pdf* (pp. 1–16). pp. 1–16. https://doi.org/10.1111/J.1364-3703.2011.00728.X

Gadoury, David M., Cadle-Davidson, L., Wilcox, W. F., Dry, I. B., Seem, R. C., & Milgroom, M. G. (2012). Grapevine powdery mildew (Erysiphe necator): A fascinating system for the study of the biology, ecology and epidemiology of an obligate biotroph. *Molecular Plant Pathology*, *13*(1), 1–16. https://doi.org/10.1111/j.1364-3703.2011.00728.x

Gadoury, David M., Seem, R. C., Ficke, A., & Wilcox, W. F. (2003). Ontogenic resistance to powdery mildew in grape berries. *Phytopathology*, Vol. 93, pp. 547–555. https://doi.org/10.1094/PHYTO.2003.93.5.547

Gemmrich, A. R., & Seidel, M. (1996). Immunodetection of overwintering oidium mycelium in bud scales of Vitis vinifera. *Vitis*, *35*(1).

Gniwotta, F., Vogg, G., Gartmann, V., Carver, T. L. W., Riederer, M., & Jetter, R. (2005). What do microbes encounter at the plant surface? Chemical composition of pea leaf cuticular waxes. *Plant Physiology*, Vol. 139. https://doi.org/10.1104/pp.104.053579

Grabski, S., De Feijter, A. W., & Schindler, M. (1993). Endoplasmic Reticulum Forms a Dynamic Continuum for Lipid Diffusion between Contiguous Soybean Root Cells. *The Plant Cell*. https://doi.org/10.1105/tpc.5.1.25

Greer, S., Wen, M., Bird, D., Wu, X., Samuels, L., Kunst, L., & Jetter, R. (2007). The cytochrome P450 enzyme CYP96A15 is the midchain alkane hydroxylase responsible for formation of secondary alcohols and ketones in stem cuticular wax of arabidopsis. *Plant Physiology*, *145*(3). https://doi.org/10.1104/pp.107.107300

Guan, P., Terigele, Schmidt, F., Riemann, M., Fischer, J., Thines, E., & Nick, P. (2020). Hunting modulators of plant defence: The grapevine trunk disease fungus Eutypa lata secretes an amplifier for plant basal immunity. *Journal of Experimental Botany*, *71*(12). https://doi.org/10.1093/jxb/eraa152

Halleen, F., & Holz, G. (2017). An Overview of the Biology, Epidemiology and Control of Uncinula necator (Powdery Mildew) on Grapevine, with Ref ere nee to South Africa. *South African Journal of Enology & Viticulture*, *22*(2). https://doi.org/10.21548/22-2-2205

Hansjakob, A., Riederer, M., & Hildebrandt, U. (2011). Wax matters: Absence of very-long-chain aldehydes from the leaf cuticular wax of the glossy11 mutant of maize compromises the prepenetration processes of Blumeria graminis. *Plant Pathology*, Vol. 60, pp. 1151–1161. https://doi.org/10.1111/j.1365-3059.2011.02467.x

Heintz, C., & Blaich, R. (1990). Ultrastructural and histochemical studies on interactions between Vitis vinifera L. and Uncinula necator (Schw.) Burr. *New Phytologist*, Vol. 115, pp. 107–117. https://doi.org/10.1111/j.1469-8137.1990.tb00928.x

Holmes, M. G., & Keiller, D. R. (2002). Effects of pubescence and waxes on the reflectance of leaves in the ultraviolet and photosynthetic wavebands: A comparison of a range of species. *Plant, Cell and Environment*, *25*(1). https://doi.org/10.1046/j.1365-3040.2002.00779.x

Hooker, T. S., Lam, P., Zheng, H., & Kunst, L. (2007). A core subunit of the RNA-processing/degrading exosome specifically influences cuticular wax biosynthesis in Arabidopsis. *Plant Cell*, *19*(3). https://doi.org/10.1105/tpc.106.049304

Jakoby, M. J., Falkenhan, D., Mader, M. T., Brininstool, G., Wischnitzki, E., Platz, N., … Schnittger, A. (2008). Transcriptional profiling of mature Arabidopsis trichomes reveals that NOECK encodes the MIXTA-like transcriptional regulator MYB106. *Plant Physiology*, *148*(3). https://doi.org/10.1104/pp.108.126979

Jeffree, C. E. (2007). The Fine Structure of the Plant Cuticle. In *Annual Plant Reviews* (Vol. 23). https://doi.org/10.1002/9780470988718.ch2

Jenks, M. A., Rashotte, A. M., Tuttle, H. A., & Feldmann, K. A. (1996). Mutants in Arabidopsis thaliana altered in epicuticular wax and leaf morphology. *Plant Physiology*, *110*(2). https://doi.org/10.1104/pp.110.2.377

Jenks, M. A., Tuttle, H. A., Eigenbrode, S. D., & Feldmann, K. A. (1995). Leaf epicuticular waxes of the Eceriferum mutants in Arabidopsis. *Plant Physiology*, *108*(1). https://doi.org/10.1104/pp.108.1.369

Jetter, R. ., Kunst, L., & Samuels, A. L. (2008). Biology of the plant cuticle: Composition of plant cuticular waxes. In *Systematic Botany* (Vol. 33). https://doi.org/10.1600/036364408785679914

Jetter, R., Schäffer, S., & Riederer, M. (2000). Leaf cuticular waxes are arranged in chemically and mechanically distinct layers: Evidence from Prunus laurocerasus L. *Plant, Cell and Environment*, *23*(6). https://doi.org/10.1046/j.1365-3040.2000.00581.x

Jiao, Y., Xu, W., Duan, D., Wang, Y., & Nick, P. (2016). A stilbene synthase allele from a Chinese wild grapevine confers resistance to powdery mildew by recruiting salicylic acid signalling for efficient defence. *Journal of Experimental Botany*, *67*(19). https://doi.org/10.1093/jxb/erw351

Jones, L., Riaz, S., Morales-Cruz, A., Amrine, K. C. H., McGuire, B., Gubler, W. D., … Cantu, D. (2014). Adaptive genomic structural variation in the grape powdery mildew pathogen, Erysiphe necator. *BMC Genomics*, *15*(1). https://doi.org/10.1186/1471-2164-15-1081

Kannangara, R., Branigan, C., Liu, Y., Penfield, T., Rao, V., Mouille, G., … Broun, P. (2007). The transcription factor WIN1/SHN1 regulates cutin biosynthesis in Arabidopsis thaliana. *Plant Cell*, *19*(4). https://doi.org/10.1105/tpc.106.047076

Karimi, M., Inzé, D., & Depicker, A. (2002). GATEWAY vectors for Agrobacterium-mediated plant.pdf. *TRENDS in Plant Science*, Vol. 7, pp. 193–195. Retrieved from file:///C:/Users/Risa/Downloads/1-s2.0-S1360138502022513-main.pdf

Khattab, I. M., Sahi, V. P., Baltenweck, R., Maia-Grondard, A., Hugueney, P., Bieler, E., … Nick, P. (2020). Ancestral chemotypes of cultivated grapevine with resistance to Botryosphaeriaceae-related dieback allocate metabolism towards bioactive stilbenes. *New Phytologist*. https://doi.org/10.1111/nph.16919

Kim, H., Lee, S. B., Kim, H. J., Min, M. K., Hwang, I., & Suh, M. C. (2012). Characterization of glycosylphosphatidylinositol-anchored lipid transfer protein 2 (LTPG2) and overlapping function between LTPG/LTPG1 and LTPG2 in cuticular wax export or accumulation in arabidopsis thaliana. *Plant and Cell Physiology*, *53*(8). https://doi.org/10.1093/pcp/pcs083

Kim, H. U. (2020). Lipid metabolism in plants. *Plants*, Vol. 9. https://doi.org/10.3390/plants9070871

Kim, J., Jung, J. H., Lee, S. B., Go, Y. S., Kim, H. J., Cahoon, R., … Suh, M. C. (2013). Arabidopsis 3-ketoacyl-coenzyme a synthase9 is involved in the synthesis of tetracosanoic acids as precursors of cuticular waxes, suberins, sphingolipids, and phospholipids. *Plant Physiology*, *162*(2). https://doi.org/10.1104/pp.112.210450

Kircher, S., Kozma-Bognar, L., Kim, L., Adam, E., Harter, K., Schäfe, E., & Nagy, F. (1999). Light Quality–Dependent Nuclear Import of the Plant Photoreceptors Phytochrome A and B. *The Plant Cell*, *11*, 1445–1456.

Kleinboelting, N., Huep, G., Kloetgen, A., Viehoever, P., & Weisshaar, B. (2012). GABI-Kat SimpleSearch: New features of the Arabidopsis thaliana T-DNA mutant database. *Nucleic Acids Research*, Vol. 40. https://doi.org/10.1093/nar/gkr1047

Klotz, J., & Nick, P. (2012). A novel actin-microtubule cross-linking kinesin, NtKCH, functions in cell expansion and division. *New Phytologist*, Vol. 193, pp. 576–589. https://doi.org/10.1111/j.1469-8137.2011.03944.x

Koch, K., & Barthlott, W. (2006). Plant epicuticular waxes: Chemistry, form, self-Assembly and function. *Natural Product Communications*, *1*(11). https://doi.org/10.1177/1934578x0600101123

Koch, K., & Ensikat, H. J. (2008). The hydrophobic coatings of plant surfaces:

Epicuticular wax crystals and their morphologies, crystallinity and molecular self-assembly. *Micron*, Vol. 39. https://doi.org/10.1016/j.micron.2007.11.010

Koch, K., Neinhuis, C., Ensikat, H. J., & Barthlott, W. (2004). Self assembly of epicuticular waxes on living plant surfaces imaged by atomic force microscopy (AFM). *Journal of Experimental Botany*, *55*(397). https://doi.org/10.1093/jxb/erh077

Kumar, S., Stecher, G., & Tamura, K. (2016). MEGA7: Molecular Evolutionary Genetics Analysis Version 7.0 for Bigger Datasets. *Molecular Biology and Evolution*, *33*(7). https://doi.org/10.1093/molbev/msw054

Kunst, L., & Samuels, A. L. (2003). Biosynthesis and secretion of plant cuticular wax. *Progress in Lipid Research*, *42*(1), 51–80. https://doi.org/10.1016/S0163-7827(02)00045-0

Kunst, L, Taylor, D., & Underhill, E. (1992). Fatty acid elongation in developing seeds of Arabidopsis thaliana. *Plant Physiology and Biochemistry (Paris)*, *30*(4).

Kunst, Ljerka, & Samuels, L. (2009). Plant cuticles shine: advances in wax biosynthesis and export. *Current Opinion in Plant Biology*, Vol. 12. https://doi.org/10.1016/j.pbi.2009.09.009

Lacey Samuels, A., Mcfarlane, H. E., Shin, J. J. H., & Bird, D. A. (2010). Arabidopsis ABCG transporters, which are required for export of diverse cuticular lipids, dimerize in different combinations. *Plant Cell*, *22*(9). https://doi.org/10.1105/tpc.110.077974

Lange, C. (1996). Braun, U. 1995. The Powdery Mildews (Erysiphales) of Europe. *Nordic Journal of Botany*, *16*(2). https://doi.org/10.1111/j.1756-1051.1996.tb00953.x

Latchman, D. S. (1997). Transcription factors: An overview. *International Journal of Biochemistry and Cell Biology*, *29*(12). https://doi.org/10.1016/S1357-2725(97)00085-X

Lee, S. B., Go, Y. S., Bae, H. J., Park, J. H., Cho, S. H., Cho, H. J., … Suh, M. C. (2009). Disruption of glycosylphosphatidylinositol-anchored lipid transfer protein gene altered cuticular lipid composition, increased plastoglobules, and enhanced susceptibility to infection by the fungal pathogen alternaria brassicicola. *Plant Physiology*, *150*(1). https://doi.org/10.1104/pp.109.137745

Lee, S. B., & Suh, M. C. (2015). Advances in the understanding of cuticular waxes in Arabidopsis thaliana and crop species. *Plant Cell Reports*, *34*(4), 557–572. https://doi.org/10.1007/s00299-015-1772-2

Leinhos, G. m. E., Randall E. Gold, Düggelin, M., & Guggenheim, R. (1997). Development and morphology of Uncinula necator following treatment with the fungicides kresoxim-methyl and penconazole. *Mycological Research*, *101*(9), 1033–1046.

Lescot, M., Déhais, P., Thijs, G., Marchal, K., Moreau, Y., Van De Peer, Y., … Rombauts, S. (2002). PlantCARE, a database of plant cis-acting regulatory elements and a portal to tools for in silico analysis of promoter sequences. *Nucleic Acids Research*, *30*(1). https://doi.org/10.1093/nar/30.1.325

Leveau, J. H. J. (2018). Microbial Communities in the Phyllosphere. In *Annual Plant*

Reviews online. https://doi.org/10.1002/9781119312994.apr0239

Lewandowska, M., Keyl, A., & Feussner, I. (2020). Tansley review Wax biosynthesis in response to danger: its regulation upon abiotic and biotic stress. *New Phytologist*, *227*(698–713). https://doi.org/10.1111/nph.16571

Li-Beisson, Y., Shorrosh, B., Beisson, F., Andersson, M. X., Arondel, V., Bates, P. D., … Ohlrogge, J. (2013). Acyl-Lipid Metabolism. *The Arabidopsis Book*, *11*. https://doi.org/10.1199/tab.0161

Li, F., Wu, X., Lam, P., Bird, D., Zheng, H., Samuels, L., … Kunst, L. (2008). Identification of the wax ester synthase/acyl-coenzyme a:diacylglycerol acyltransferase WSD1 required for stem wax ester biosynthesis in Arabidopsis. *Plant Physiology*, *148*(1). https://doi.org/10.1104/pp.108.123471

Li, L., Yu, X., Thompson, A., Guo, M., Yoshida, S., Asami, T., … Yin, Y. (2009). Arabidopsis MYB30 is a direct target of BES1 and cooperates with BES1 to regulate brassinosteroid-induced gene expression. *Plant Journal*, *58*(2). https://doi.org/10.1111/j.1365-313X.2008.03778.x

Li, N., Xu, C., Li-Beisson, Y., & Philippar, K. (2016). Fatty Acid and Lipid Transport in Plant Cells. *Trends in Plant Science*, Vol. 21. https://doi.org/10.1016/j.tplants.2015.10.011

Liang, Z., Duan, S., Sheng, J., Zhu, S., Ni, X., Shao, J., … Dong, Y. (2019). Whole-genome resequencing of 472 Vitis accessions for grapevine diversity and demographic history analyses. *Nature Communications*, Vol. 10. https://doi.org/10.1038/s41467-019-09135-8

Liu, L., Zhang, J., Adrian, J., Gissot, L., Coupland, G., Yu, D., & Turck, F. (2014). Elevated levels of MYB30 in the phloem accelerate flowering in Arabidopsis through the regulation of FLOWERING LOCUS T. *PLoS ONE*, *9*(2). https://doi.org/10.1371/journal.pone.0089799

Livak, K. J., & Schmittgen, T. D. (2001). Analysis of relative gene expression data using real-time quantitative PCR and the 2-ΔΔCT method. *Methods*, *25*(4). https://doi.org/10.1006/meth.2001.1262

Logemann, E., Birkenbihl, R. P., Ülker, B., & Somssich, I. E. (2006). An improved method for preparing Agrobacterium cells that simplifies the Arabidopsis transformation protocol. *Plant Methods*, *2*(1). https://doi.org/10.1186/1746-4811-2-16

Mabuchi, K., Maki, H., Itaya, T., Suzuki, T., Nomoto, M., Sakaoka, S., … Tsukagoshi, H. (2018). MYB30 links ROS signaling, root cell elongation, and plant immune responses. *Proceedings of the National Academy of Sciences of the United States of America*, *115*(20). https://doi.org/10.1073/pnas.1804233115

Maisch, J., Fierová, J., Fischer, L., & Nick, P. (2009). Tobacco Arp3 is localized to actin-nucleating sites in vivo. *Journal of Experimental Botany*, *60*(2). https://doi.org/10.1093/jxb/ern307

Marcell, L. M., & Beattie, G. A. (2002). Effect of leaf surface waxes on leaf colonization by Pantoea agglomerans and Clavibacter michiganensis. *Molecular Plant-Microbe Interactions*, *15*(12). https://doi.org/10.1094/MPMI.2002.15.12.1236

Mazliak, P. (1973). Lipid Metabolism in Plants. *Annual Review of Plant Physiology*, *24*(1). https://doi.org/10.1146/annurev.pp.24.060173.001443

McDonald, K. (2007). Cryopreparation Methods for Electron Microscopy of Selected Model Systems. *Methods in Cell Biology*, *79*, 23–56. https://doi.org/10.1016/S0091-679X(06)79002-1

McDonald, K. L. (2009). A review of high-pressure freezing preparation techniques for correlative light and electron microscopy of the same cells and tissues. *Journal of Microscopy*, *235*(3), 273–281. https://doi.org/10.1111/j.1365-2818.2009.03218.x

McFarlane, H. E., Watanabe, Y., Yang, W., Huang, Y., Ohlrogge, J., & Samuels, A. L. (2014). Golgi- and trans-golgi network-mediated vesicle trafficking is required for wax secretion from epidermal cells. *Plant Physiology*, *164*(3). https://doi.org/10.1104/pp.113.234583

McNevin, J. P., Woodward, W., Hannoufa, A., Feldmann, K. A., & Lemieux, B. (1993). Isolation and characterization of eceriferum (cer) mutants induced by T-DNA insertions in Arabidopsis thaliana. *Genome*, *36*(3). https://doi.org/10.1139/g93-082

Metz, J. G., Pollard, M. R., Anderson, L., Hayes, T. R., & Lassner, M. W. (2000). Purification of a jojoba embryo fatty acyl-coenzyme A reductase and expression of its cDNA in high erucic acid rapeseed. *Plant Physiology*, *122*(3). https://doi.org/10.1104/pp.122.3.635

Millar, A. A., Clemens, S., Zachgo, S., Michael Giblin, E., Taylor, D. C., & Kunst, L. (1999). CUT1, an Arabidopsis gene required for cuticular wax biosynthesis and pollen fertility, encodes a very-long-chain fatty acid condensing enzyme. *Plant Cell*, *11*(5). https://doi.org/10.1105/tpc.11.5.825

Millar, A. A., Wrischer, M., & Kunst, L. (1998). Accumulation of very-long-chain fatty acids in membrane glycerolipids is associated with dramatic alterations in plant morphology. *Plant Cell*, *10*(11). https://doi.org/10.1105/tpc.10.11.1889

Moharramipour, S., Tsumuki, H., Sato, K., Murata, S., & Kanehisa, K. (1997). Effects of leaf color, epicuticular wax amount and gramine content in barley hybrids on cereal aphid populations. *Applied Entomology and Zoology*, *32*(1). https://doi.org/10.1303/aez.32.1

Nakagawa, T., Ishiguro, S., & Kimura, T. (2009). Gateway vectors for plant transformation. *Plant Biotechnology*, Vol. 26, pp. 275–284. https://doi.org/10.5511/plantbiotechnology.26.275

Ni, X., Quisenberry, S. S., Siegfried, B. D., & Lee, K. W. (1998). Influence of cereal leaf epicuticular wax on Diuraphis noxia probing behavior and nymphoposition. *Entomologia Experimentalis et Applicata*, *89*(2). https://doi.org/10.1046/j.1570-7458.1998.00389.x

Norton, A. P., English-Loeb, G., Gadoury, D., & Seem, R. C. (2000). Mycophagous mites and foliar pathogens: Leaf domatia mediate tritrophic interactions in grapes. *Ecology*, *81*(2), 490–499. https://doi.org/10.1890/0012-9658(2000)081[0490:MMAFPL]2.0.CO;2

Oshima, Y., Shikata, M., Koyama, T., Ohtsubo, N., Mitsuda, N., & Nobutaka

Mitsuda, M. O.-T. (2013). MIXTA-Like Transcription Factors and WAX INDUCER1/SHINE1 Coordinately Regulate Cuticle Development in Arabidopsis and Torenia fournieri. *The Plant Cell*, *25*, 1609–1624. Retrieved from Online version contains Web-only datwww.plantcell.org/cgi/doi/10.1105/tpc.113.110783

Panikashvili, D., Savaldi-Goldstein, S., Mandel, T., Yifhar, T., Franke, R. B., Höfer, R., … Aharoni, A. (2007). The arabidopsis DESPERADO/AtWBC11 transporter is required for cutin and wax secretion. *Plant Physiology*, *145*(4). https://doi.org/10.1104/pp.107.105676

Patwari, P., Salewski, V., Gutbrod, K., Kreszies, T., Dresen-Scholz, B., Peisker, H., … Dörmann, P. (2019). Surface wax esters contribute to drought tolerance in Arabidopsis. *Plant Journal*, *98*(4). https://doi.org/10.1111/tpj.14269

Pighin, J. A., Zheng, H., Balakshin, L. J., Goodman, J. P., Western, T. L., Jetter, R., … Samuels, A. L. (2004). Plant cuticular lipid export requires an ABC transporter. *Science*, *306*(5696). https://doi.org/10.1126/science.1102331

Portu, J., López, R., Baroja, E., Santamaría, P., & Garde-Cerdán, T. (2016). Improvement of grape and wine phenolic content by foliar application to grapevine of three different elicitors: Methyl jasmonate, chitosan, and yeast extract. *Food Chemistry*, *201*. https://doi.org/10.1016/j.foodchem.2016.01.086

Post-Beittenmiller, D. (1996). Biochemistry and molecular biology of wax production in plants. *Annual Review of Plant Physiology and Plant Molecular Biology*, *47*(1), 405–430. https://doi.org/10.1146/annurev.arplant.47.1.405

Premachandra, gnanasiri s., Saneoka, H., Fujita, K., & Ogata, S. (1992). Leaf Water Relations, Osmotic Adjustment, Cell Membrane Stability, Epicuticular Wax Load and Growth as Affected by Increasing Water Deficits in Sorghum. *Journal of Experimental Botany*, *43*(12). https://doi.org/10.1093/jxb/43.12.1569

Qiu, W., Feechan, A., & Dry, I. (2015). Current understanding of grapevine defense mechanisms against the biotrophic fungus (Erysiphe necator), the causal agent of powdery mildew disease. *Horticulture Research*, Vol. 2. https://doi.org/10.1038/hortres.2015.20

Racovita, R. C., Peng, C., Awakawa, T., Abe, I., & Jetter, R. (2015). Very-long-chain 3-hydroxy fatty acids, 3-hydroxy fatty acid methyl esters and 2-alkanols from cuticular waxes of Aloe arborescens leaves. *Phytochemistry*, *113*. https://doi.org/10.1016/j.phytochem.2014.08.005

Rashotte, A. M., & Feldmann, K. A. (1998). Correlations between epicuticular wax structures and chemical composition in Arabidopsis thaliana. *International Journal of Plant Sciences*, *159*(5). https://doi.org/10.1086/297596

Razeq, F. M., Kosma, D. K., Rowland, O., & Molina, I. (2014). Extracellular lipids of Camelina sativa: Characterization of chloroform-extractable waxes from aerial and subterranean surfaces. *Phytochemistry*, *106*. https://doi.org/10.1016/j.phytochem.2014.06.018

Reisberg, E. E., Hildebrandt, U., Riederer, M., & Hentschel, U. (2013). Distinct Phyllosphere Bacterial Communities on Arabidopsis Wax Mutant Leaves. *PLoS ONE*, *8*(11), e78613. https://doi.org/10.1371/journal.pone.0078613

Rhee, Y., Hlousek-Radojcic, A., Ponsamuel, J., Liu, D., & Post-Beittenmiller, D. (1998). Epicuticular Wax Accumulation and Fatty Acid Elongation Activities Are Induced during Leaf Development of Leeks. *Plant Physiology*, *116*(3). https://doi.org/10.1104/pp.116.3.901

Riechmann, J. L., Heard, J., Martin, G., Reuber, L., Jiang, C. Z., Keddie, J., … Yu, G. L. (2000). Arabidopsis transcription factors: Genome-wide comparative analysis among eukaryotes. *Science*, *290*(5499). https://doi.org/10.1126/science.290.5499.2105

Rosso, M. G., Li, Y., Strizhov, N., Reiss, B., Dekker, K., & Weisshaar, B. (2003). An Arabidopsis thaliana T-DNA mutagenized population (GABI-Kat) for flanking sequence tag-based reverse genetics. *Plant Molecular Biology*, Vol. 53, pp. 247–259. https://doi.org/10.1023/B:PLAN.0000009297.37235.4a

Rumbolz, J., Kassemeyer, H.-H., V Steinmetz, H. B. D., Mendgen, K., D Mathys, S. W., & Guggenheim, R. (2000). *Differentiation of infection structures of the powdery mildew fungus Uncinula necator and adhesion to the host cuticle* (pp. 409–421). pp. 409–421. Retrieved from https://doi.org/10.1139/b00-016

Rumbolz, J., Kassemeyer, H. H., Steinmetz, V., Deising, H. B., Mendgen, K., Mathys, D., … Guggenheim, R. (2000). Differentiation of infection structures of the powdery mildew fungus Uncinula necator and adhesion to the host cuticle. *Canadian Journal of Botany*, Vol. 78, pp. 409–421. https://doi.org/10.1139/cjb-78-7-984

Russell, P. E. (2005). A century of fungicide evolution. *Journal of Agricultural Science*, Vol. 143. https://doi.org/10.1017/S0021859605004971

Saitou, N., & Nei, M. (1987). The neighbor-joining method: a new method for reconstructing phylogenetic trees. *Molecular Biology and Evolution*, *4*(4). https://doi.org/10.1093/oxfordjournals.molbev.a040454

Salas, J. J., & Ohlrogge, J. B. (2002). Characterization of substrate specificity of plant FatA and FatB acyl-ACP thioesterases. *Archives of Biochemistry and Biophysics*, *403*(1). https://doi.org/10.1016/S0003-9861(02)00017-6

Sall, M. A. (1982). Perennation of Powdery Mildew in Buds of Grapevines. *Plant Disease*, *66*(1). https://doi.org/10.1094/pd-66-678

Samuels, L., Kunst, L., & Jetter, R. (2008). Sealing plant surfaces: Cuticular wax formation by epidermal cells. *Annual Review of Plant Biology*, Vol. 59. https://doi.org/10.1146/annurev.arplant.59.103006.093219

Schneider-Belhaddad, F., & Kolattukudy, P. (2000). Solubilization, partial purification, and characterization of a fatty aldehyde decarbonylase from a higher plant, Pisum sativum. *Archives of Biochemistry and Biophysics*, *377*(2). https://doi.org/10.1006/abbi.2000.1798

Schonherr, J., & Riederer, M. (1989). Foliar penetration and accumulation of organic chemicals in plant cuticles. *Reviews of Environmental Contamination and Toxicology*, *108*. https://doi.org/10.1007/978-1-4613-8850-0_1

Sharma, P., Kothari, S. L., Rathore, M. S., & Gour, V. S. (2018). Properties, variations, roles, and potential applications of epicuticular wax: A review. *Turkish Journal of Botany*, Vol. 42. https://doi.org/10.3906/bot-1702-25

Shetty, D. S., Narkar, S. P., Sawant, I. S., & Sawant, S. D. (2014). Efficacy of quinone outside inhibitors (QoI) and demethylation inhibitors (DMI) fungicides against grape anthracnose. *Indian Phytopathology*, *67*(2).

Shockey, J. M., Fulda, M. S., & Browse, J. A. (2002). Arabidopsis contains nine long-chain acyl-coenzyme A synthetase genes that participate in fatty acid and glycerolipid metabolism. *Plant Physiology*, *129*(4). https://doi.org/10.1104/pp.003269

Staehelin, L. A., & Chapman, R. L. (1987). Secretion and membrane recycling in plant cells: novel intermediary structures visualized in ultrarapidly frozen sycamore and carrot suspension-culture cells. *Planta*, *171*(1). https://doi.org/10.1007/BF00395066

Stolpe, T., Süßlin, C., Marrocco, K., Nick, P., Kretsch, T., & Kircher, S. (2005). In planta analysis of protein-protein interactions related to light signaling by bimolecular fluorescence complementation. *Protoplasma*, *226*(3–4), 137–146. https://doi.org/10.1007/s00709-005-0122-6

Suh, M. C., Samuels, A. L., Jetter, R., Kunst, L., Pollard, M., Ohlrogge, J., & Beisson, F. (2005). Cuticular lipid composition, surface structure, and gene expression in Arabidopsis stem epidermis. *Plant Physiology*, *139*(4). https://doi.org/10.1104/pp.105.070805

Svyatyna, K., Jikumaru, Y., Brendel, R., Reichelt, M., Mithöfer, A., Takano, M., … Riemann, M. (2014). Light induces jasmonate-isoleucine conjugation via OsJAR1-dependent and -independent pathways in rice. *Plant, Cell and Environment*, *37*(4). https://doi.org/10.1111/pce.12201

Tisch, C. (2017). *Biologie der schwarzfäule an reben und potentielle abwehrmechanismen bei der europäischen wildrebe und verschieden resistenten sorten*.

Todd, J., Post-Beittenmiller, D., & Jaworski, J. G. (1999). KCS1 encodes a fatty acid elongase 3-ketoacyl-CoA synthase affecting wax biosynthesis in Arabidopsis thaliana. *Plant Journal*, *17*(2). https://doi.org/10.1046/j.1365-313X.1999.00352.x

Tsuba, M., Katagiri, C., Takeuchi, Y., Takada, Y., & Yamaoka, N. (2002). Chemical factors of the leaf surface involved in the morphogenesis of Blumeria graminis. *Physiological and Molecular Plant Pathology*, *60*(2). https://doi.org/10.1006/pmpp.2002.0376

Vailleau, F., Daniel, X., Tronchet, M., Montillet, J. L., Triantaphylidès, C., & Roby, D. (2002). A R2R3-MYB gene, AtMYB30, acts as a positive regulator of the hypersensitive cell death program in plants in response to pathogen attack. *Proceedings of the National Academy of Sciences of the United States of America*, *99*(15). https://doi.org/10.1073/pnas.152047199

Vailleau, S. R. F., Le´ger, A., S, J. J., Miersch, O., Huard, C., Ble´e, E., … Dominique Roby. (2008). A MYB Transcription Factor Regulates Very-Long-Chain Fatty Acid Biosynthesis for Activation of the Hypersensitive Cell Death Response in Arabidopsis. *The Plant Cell*, *20*, 752–767. Retrieved from www.plantcell.org/cgi/doi/10.1105/tpc.107.054858

Von Wettstein-Knowles, P. M. (2018). Waxes, cutin, and suberin. In *Lipid Metabolism in Plants*. https://doi.org/10.1201/9781351074070

Wang, S., Duan, L., Eneji, A. E., & Li, Z. (2007). Variations in growth, photosynthesis and defense system among four weed species under increased UV-B radiation. *Journal of Integrative Plant Biology*, *49*(5). https://doi.org/10.1111/j.1744-7909.2007.00466.x

Wang, W., Zhang, Y., Xu, C., Ren, J., Liu, X., Black, K., … Ren, H. (2014). Cucumber ECERIFERUM1 (CsCER1), which influences the cuticle properties and drought tolerance of cucumber, plays a key role in VLC alkanes biosynthesis. *Plant Molecular Biology*, Vol. 87, pp. 219–233. https://doi.org/10.1007/s11103-014-0271-0

Wang, X., Kong, L., Zhi, P., & Chang, C. (2020). Update on cuticular wax biosynthesis and its roles in plant disease resistance. *International Journal of Molecular Sciences*, Vol. 21, pp. 1–15. https://doi.org/10.3390/ijms21155514

Welter, L. J., Tisch, C., Kortekamp, A., Töpfer, R., & Zyprian, E. (2017). *Powdery mildew responsive genes of resistant grapevine cultivar "Regent"* (pp. 181–188). pp. 181–188. https://doi.org/10.5073/vitis.2017.56.181-188

Weng, H., Molina, I., Shockey, J., & Browse, J. (2010). Organ fusion and defective cuticle function in a lacs1 lacs2 double mutant of Arabidopsis. *Planta*, *231*(5). https://doi.org/10.1007/s00425-010-1110-4

Wenping Qiu, A. F. and I. D. (2015). *Current understanding of grapevine defense mechanisms against the biotrophic.pdf* (pp. 2052–7276). pp. 2052–7276. https://doi.org/10.1038/hortres.2015.20

Wille, G., Hellal, J., Ollivier, P., Richard, A., Burel, A., Jolly, L., … Michel, C. (2017). Cryo-Scanning Electron Microscopy (SEM) and Scanning Transmission Electron Microscopy (STEM)-in-SEM for Bio- and Organo-Mineral Interface Characterization in the Environment. *Microscopy and Microanalysis*, *23*(6), 1159–1172. https://doi.org/10.1017/S143192761701265X

Williams, M. H., Rosenqvist, E., & Buchhave, M. (2000). The effect of reducing production water availability on the post-production quality of potted miniature roses (Rosa x hybrida). *Postharvest Biology and Technology*, *18*(2). https://doi.org/10.1016/S0925-5214(99)00076-9

Wollenweber, E., Kraut, L., & Mues, R. (1998). External accumulation of biflavonoids on gymnosperm leaves. *Zeitschrift Fur Naturforschung - Section C Journal of Biosciences*, *53*(11–12). https://doi.org/10.1515/znc-1998-11-1202

Wollenweber, Eckhard. (1978). The Distribution and Chemical Constituents of the Farinose Exudates in Gymnogrammoid Ferns. *American Fern Journal*, *68*(1). https://doi.org/10.2307/1546411

Wollenweber, Eckhard, & H. Dietz, V. (1981). Occurrence and distribution of free flavonoid aglycones in plants. *Phytochemistry*, Vol. 20. https://doi.org/10.1016/0031-9422(81)83001-4

Yeats, T. H., & Rose, J. K. C. (2013). The formation and function of plant cuticles. *Plant Physiology*, Vol. 163, pp. 5–20. https://doi.org/10.1104/pp.113.222737

Zeisler-Diehl, V. V., Barthlott, W., & Schreiber, L. (2018). Plant Cuticular Waxes:

Composition, Function, and Interactions with Microorganisms. In *Hydrocarbons, Oils and Lipids: Diversity, Origin, Chemistry and Fate*. https://doi.org/10.1007/978-3-319-54529-5_7-1

Zhang, X., Henriques, R., Lin, S. S., Niu, Q. W., & Chua, N. H. (2006). Agrobacterium-mediated transformation of Arabidopsis thaliana using the floral dip method. *Nature Protocols*, *1*(2), 641–646. https://doi.org/10.1038/nprot.2006.97

Zhang, Y.-L., Zhang, C.-L., Wang, G.-L., Wang, Y.-X., Qi, C.-H., Zhao, Q., … Hao, Y.-J. (2019). The R2R3 MYB transcription factor MdMYB30 modulates plant resistance against pathogens by regulating cuticular wax biosynthesis. *BMC Plant Biology*, *19*(362). https://doi.org/10.1186/s12870-019-1918-4

Zhao, Z., Yang, X., Lü, S., Fan, J., Opiyo, S., Yang, P., … Xia, Y. (2020). Deciphering the Novel Role of AtMIN7 in Cuticle Formation and Defense against the Bacterial Pathogen Infection. *International Journal of Molecular Sciences*, *21*(5547). https://doi.org/10.3390/ijms21155547

Zheng, H., Rowland, O., & Kunst, L. (2005). Disruptions of the Arabidopsis enoyl-CoA reductase gene reveal an essential role for very-long-chain fatty acid synthesis in cell expansion during plant morphogenesis. *Plant Cell*, *17*(5). https://doi.org/10.1105/tpc.104.030155

Zheng, Y., Schumaker, K. S., & Guo, Y. (2012). Sumoylation of transcription factor MYB30 by the small ubiquitin-like modifier E3 ligase SIZ1 mediates abscisic acid response in Arabidopsis thaliana. *Proceedings of the National Academy of Sciences of the United States of America*, *109*(31). https://doi.org/10.1073/pnas.1202630109

Zoecklein, B. W., Wolf, T. K., Duncan, N. W., Judge, J. M., & Cook, M. K. (1992). Effects of Fruit Zone Leaf Removal on Yield, Fruit Composition, and Fruit Rot Incidence of Chardonnay and White Riesling (Vitis vinifera L.) Grapes. *American Journal of Enology and Viticulture*, *43*(2).